December 2010

Cardiac Adaptation To Chronic Blockade Of Voltage-Gated, L-Type Calcium Channels In The Sarcolemma

Ji Zhou
The University of Western Ontario

Supervisor
Dr. Njanoor Narayanan
The University of Western Ontario

Joint Supervisor
Dr. Stephen M. Sims
The University of Western Ontario

Graduate Program in Physiology

A thesis submitted in partial fulfillment of the requirements for the degree in Doctor of Philosophy

© Ji Zhou 2010

Follow this and additional works at: https://ir.lib.uwo.ca/etd

 Part of the Cellular and Molecular Physiology Commons, and the Other Physiology Commons

Cardiac Adaptation to Chronic Blockade of Voltage-gated, L-type Calcium Channels in the Sarcolemma

(Thesis format: Integrated-Article)

by

Ji <u>Zhou</u>

Graduate Program in Physiology

Submitted in partial fulfillment

of the requirements for the degree of

Doctor of Philosophy

School of Graduate and Postdoctoral Studies

The University of Western Ontario

London, Ontario, Canada

THE UNIVERSITY OF WESTERN ONTARIO
SCHOOL OF GRADUATE AND POSTDOCTORAL STUDIES

CERTIFICATE OF EXAMINATION

Supervisor   Joint Supervisor

_____   _____

Dr. Njanoor Narayanan   Dr. Stephen M. Sims

Supervisory Committee   Examiners

_____
                                                _____
Dr. Douglas Jones (GSR)   Dr. Balwant Tuana

                                                _____
_____   Dr. Earl Noble
Dr. Qing ping Feng

                                                _____
                                                Dr. Donglin Bai

                                                _____
                                                Dr. Jeff Dixon

The thesis by

Ji <u>Zhou</u>

entitled:

**Cardiac Adaptation to Chronic Blockade of Voltage-gated, L-type Calcium
Channels in the Sarcolemma**

is accepted in partial fulfillment of the

requirements for the degree of

Doctor of Philosophy

Date_____   _____
                                                Chair of the Thesis Examination Board

ii

ABSTRACT

L-type Ca^{2+} channels (dihydropyridine receptors, DHPRs) in the sarcolemma are essential to cardiac excitation-contraction (E-C) coupling. Thus, Ca^{2+} influx through DHPRs upon cardiomyocyte excitation triggers Ca^{2+} release from the sarcoplasmic reticulum (SR) through ryanodine receptors (RyRs) to initiate myofilament activation and muscle contraction. Muscle relaxation occurs upon sequestration of Ca^{2+} back into the SR lumen by sarco/endoplasmic reticulum calcium-ATPase (SERCA) in the SR. As a treatment option for hypertension, long-term use of DHPR blockers is associated with increased risk of heart failure, but the underlying mechanisms are unknown. This research used male Wistar rats treated with verapamil (subcutaneously, 625 µg/h/kg for 4 weeks) to determine the impact of chronic DHPR blockade *in vivo*, on E-C coupling events and heart function at all levels ranging from molecules to whole organism. The results presented in chapter 2 demonstrate that chronic DHPR blockade caused functional remodeling of RyRs and spatio-temporal dyssynchrony of E-C coupling events, resulting in systolic dysfunction and enhanced susceptibility to arrhythmia. Findings in chapter 3 reveal that chronic DHPR blockade was accompanied by depressed SERCA function, abnormal cardiomyocyte Ca^{2+} handling, and diastolic dysfunction. Results in chapter 4 reveal adaptational changes in protein phosphorylation-dependent regulation of SR/cardiomyocyte Ca^{2+} cycling due to chronic DHPR blockade. These include over-expression of Ca^{2+}/calmodulin-dependent protein kinases II (CaMKII), hyper-phosphorylation of SR Ca^{2+} cycling proteins by CaMKII and cAMP-dependent protein kinase (PKA), paradoxically diminished SR Ca^{2+} content and contractile reserve, and blunted inotropic response to β–adrenergic stimulation. The above adaptations to chronic

DHPR blockade occurred in the absence of cardiac hypertrophy or fibrosis. Thus, molecular remodeling may invoke cardiac pathology and heart failure without microscopic structural changes in cardiomyocytes. The findings from this thesis reveal, for the first time, integrated mechanisms underlying the increased risk of heart failure associated with chronic DHPR blockade. In addition to urging caution in the conventional clinical use of DHPR blockers, the novel mechanistic events and molecular remodeling revealed here imply that manipulation of the stoichiometry of molecular players in E-C coupling demand critical attention and careful scrutiny in the design and deployment of therapeutic approaches for heart diseases.

CO-AUTHORSHIP

Chapter 2, entitled "Chronic L-type Calcium Channel Blockade with Verapamil Causes Cardiac Ryanodine Receptor Remodeling and Predisposition to Heart Failure in the Rat", was written by J. Zhou with suggestions from Drs. D.L. Jones, S.M. Sims and N. Narayanan. A. Xu performed Western blot analysis shown in Figure 2.1. Dr. M. Jiang performed patch clamping to examine DHPR Ca^{2+} currents (I_{Ca}) in cardiomyocytes shown in Figure 2.2. Electrophysiological experiments were done with Dr. D.L Jones. All other studies were performed by J. Zhou who also prepared all the data figures. All experiments were carried out in the laboratories of Drs. D. L. Jones, S.M. Sims and N. Narayanan.

Chapter 3, entitled "Remodeling of Cardiac Sarcoplasmic Reticulum Calcium Pump and Diastolic Dysfunction Ensue Chronic L-type Calcium Channel Blockade with Verapamil in the Rat", was written by J. Zhou with suggestions from Drs. D.L. Jones, S.M. Sims and N. Narayanan. All the studies were performed by J. Zhou who also prepared all the data figures. Experiments were carried out in the laboratories of Drs. D. L. Jones, S.M. Sims and N. Narayanan.

Chapter 4, entitled "Impact of Chronic L-type Calcium Channel Blockade on Phosphorylation-dependent Regulation of Cardiac Sarcoplasmic Reticulum Function in the Rat", was written by J. Zhou with suggestions from Drs. D. L. Jones, S.M. Sims and N. Narayanan. A. Xu performed CaMKII- and PKA-mediated phosphorylation of Ca^{2+}-cycling proteins in cardiac SR vesicles shown in Figure 4.3 and Figure 4.4. Dr. Subrata Chakrabarti contributed to Fig.4.9 and assessed histological slides for cardiac hypertrophy and fibrosis. All other studies were performed by J. Zhou who also prepared

all the data figures. Experiments were carried out in the laboratories of Drs. D. L. Jones,

S.M. Sims and N. Narayanan.

ACKNOWLEDGEMENTS

his valuable advice. This thesis benefits from his impressive set of expertise in the field of cardiac electrophysiology. I am grateful in every possible way for his precious times to read my research proposal and this thesis and gave his critical comments.

I am grateful to have known and worked with many wonderful colleagues. Many thanks go in particular to Ann Xu, Dr. Mao Jiang, and Dr. Venkatachalem Sathish for their advice and their willingness to share their bright thoughts with me. I benefited by outstanding works from them. Most of this thesis would not have been existed if they did not teach me the techniques properly. This thesis benefits from the exceptional skills and work of Ann Xu. The scientific atmosphere created from my closest colleagues in the laboratories always kept me motivated.

I wish to express my warm and sincere thanks to Dr. Peter Chidiac who read my research proposal and gave me constructive comments on my research. At my difficult times, Dr. Chidiac gave me his valuable advice and unflinching encouragement. I greatly appreciate Jari Tuomi, Jason Moreau and Jeff Turner for all the emotional support, camaraderie, entertainment, and caring they provided at my difficult times. This thesis also benefited from Dr. Qinping Feng's critical comments on research during committee meetings.

I will never find the words to thank for my parents who are always behind me and silently support me. They taught me to be humble and grateful and their words and love guided me through this most challenging time in my life.

Finally, I would like to thank everybody who was important to the successful realization of thesis, as well as expressing my apology that I could not mention personally one by one. I am grateful of the help of many terrific people for the

TABLE OF CONTENTS

CHAPTER FOUR— IMPACT OF CHRONIC L-TYPE CALCIUM CHANNEL BLOCKADE ON PHOSPHORYLATION-DEPENDENT REGULATION OF CARDIAC SARCOPLASMIC RETICULUM FUNCTION IN THE RAT

LIST OF TABLES

LIST OF FIGURES

LIST OF APPENDICES

LIST OF ABBREVIATIONS

αKAP: α kinase anchoring protein

AV node: atrioventricular node

B_{max}: the maximum binding sites

Ca^{2+}: the calcium ion

Ca^{2+}/CaM: Ca^{2+}-bound calmodulin

$[Ca^{2+}]_i$: cytosolic free Ca^{2+} concentration

$[Ca^{2+}]_{SR}$: Ca^{2+} concentration in the SR lumen

CaM: calmodulin

CaM BP: calmodulin binding peptide

CaMKII: Ca^{2+}/calmodulin-dependent protein kinase II

CICR: calcium-induced calcium release

cSNRT: sinus node recovery time corrected for spontaneous sinus cycle length

CSQ: calsequestrin

DHPR: dihydropyridine receptor (L-type, voltage-dependent calcium channel)

DHPR blockers: compounds that block the DHPRs, also called calcium channel blockers

DP: developed pressure

dp/dt: rate of change of left ventricular pressure

E-C coupling: cardiac excitation-contraction coupling

EDP: end diastolic pressure

FDAR: frequency-dependent acceleration of relaxation

FKBP12.6: protein FK 506-binding protein 12.6

HPLC: high performance liquid chromatography

I_{Ca}: DHPR Ca^{2+} influx or L-type Ca^{2+} current

Iso: isoproterenol

LV: left ventricle

PKA: cyclic-AMP-dependent protein kinase

PLN: phospholamban

P_o: channel open probability

RV: right ventricle

RyRs: ryanodine receptors (ryanodine-sensitive Ca^{2+} release channels)

SERCA: sarco/endoplasmic reticulum calcium-ATPase

SNRT: sinus node recovery time

SR: sarcoplasmic reticulum

τ: time constant of decay of $[Ca^{2+}]_i$ transient

Tau: time constant of relaxation

V_{max} : maximum velocity of SR Ca^{2+} pumping

VPL: verapamil-treated group

VT: ventricular tachycardia

WCL: Wenckebach cycle length

CHAPTER ONE

INTRODUCTION

1.1.   Chapter Summary

Known as dihydropyridine receptors (DHPRs), voltage-gated, L-type Ca^{2+} channels in the sarcolemma convert the electrical signal into the Ca^{2+} signal thereby enabling the cardiac excitation-contraction coupling (E-C coupling) and consequently the heart beat [1-5]. During cardiac E-C coupling, the action potential causes the sarcolemma to depolarize which activates the voltage-gated DHPRs. This opening of DHPRs permits a small amount of Ca^{2+} to enter the cardiomyocyte and triggers a large amount of Ca^{2+} release from the sarcoplasmic reticulum (SR) through ion channels known as ryanodine receptors (RyRs). The resulting rise in cytoplasmic Ca^{2+} activates myofilaments to produce a muscle contraction [3-6]. Subsequent muscle relaxation occurs upon lowering of cytoplasmic Ca^{2+} through sequestration of Ca^{2+} back into the SR lumen by a Ca^{2+}-pumping ATPase (SERCA) [4, 7, 8] and extrusion of Ca^{2+} out of the cell via Na^{2+}/Ca^{2+} exchanger [4, 9-12].

The DHPR is vital for the cardiac cycle since complete blockade of DHPRs turns off E-C coupling and causes immediate cessation of the heart beat [4, 13]. Intriguingly, DHPR blockers are frequently prescribed for long-term treatment of cardiovascular disease such as hypertension and angina pectoris [14, 15]. Presumably, DHPRs are only partially blocked by DHPR blockers at doses routinely employed clinically. However, the long-term effects of partial blockade of DHPR on cardiac E-C coupling events and contractile function are not yet understood. Moreover, recent large scale clinical trials have suggested that long-term use of DHPR blockers increases the risk of heart failure,

cardiac arrhythmias and myocardial infarction. However, the underlying mechanisms are not known[14, 16-18].

The SR Ca^{2+} cycling apparatus is immediately downstream of the DHPR in the E-C coupling process, and pivotal to enable the contraction-relaxation cycle. The crosstalk between the DHPR and SR Ca^{2+} cycling proteins is central to the maintenance of cellular Ca^{2+} homeostasis, cardiac contraction, and heart rhythm [4]. During cardiac E-C coupling, the magnitude and duration of Ca^{2+} influx via DHPR tightly controls the rate and amount of Ca^{2+} release from SR. On the other hand, Ca^{2+} release from the SR feeds back to alter DHPR function [19-21]. Close spatial proximity between the DHPR and the RyR (~10 nm) is a critical factor that ensures the stability and fidelity of intermolecular Ca^{2+} signaling between the DHPR and its molecular partners (RyR, SERCA) in the SR Ca^{2+} cycling apparatus [2, 3]. Little is known about the impact of chronic inhibition of DHPRs on the expression and function of SR Ca^{2+} cycling proteins and the molecular events governing cardiac E-C coupling. In this thesis, I provide a comprehensive assessment of the cardiac E-C coupling adaption to chronic, partial DHPR blockade. This chapter provides a brief review of the pertinent literature and outlines the rationale, objectives and hypotheses of the research.

1.2.   Cardiac E-C coupling.

1.2.1   Ca^{2+} Cycling During E-C Coupling

Cardiac excitation–contraction coupling (E-C coupling) is the process from electrical excitation of the cardiomyocyte to contraction. The calcium ion (Ca^{2+}) is crucial to this process and Ca^{2+} cycling during E-C coupling has been well established [4] (Fig.1-1). During the cardiac action potential, L-type Ca^{2+} channels (DHPRs) in the sarcolemma are activated and Ca^{2+} enters the cell as inward Ca^{2+} current (DHPR Ca^{2+} current, I_{Ca}). This DHPR Ca^{2+} influx triggers Ca^{2+} release from the sarcoplasmic reticulum (SR) through ion
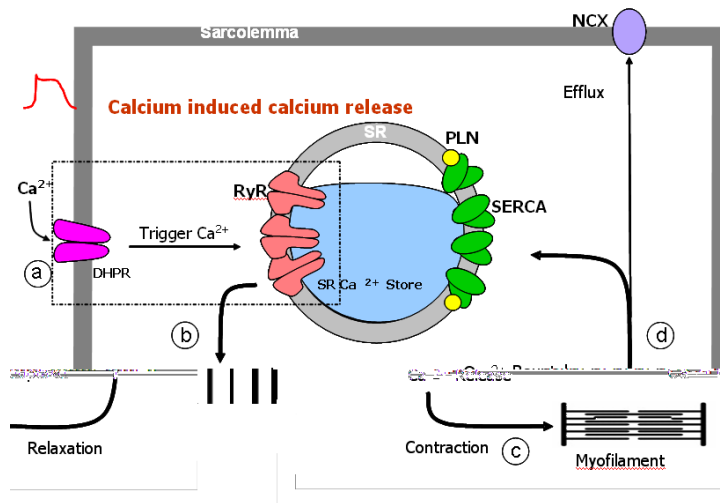
Figure 1.1 Schematic of cardiac excitation contraction coupling.

channels known as ryanodine receptors (RyRs) by the mechanism known as "Ca^{2+} induced Ca^{2+} release" (CICR) [4, 22]. The consequent rise in cytosolic free Ca^{2+} causes myofilament activation and contraction by Ca^{2+} binding to the thin-filament protein troponin C. For relaxation and diastolic filling of cardiac chambers to occur, the added Ca^{2+} must be removed from the cytosol such that Ca^{2+} dissociates from troponin C to turn off the contractile machinery. This requires Ca^{2+} transport out of the cytosol by four pathways involving SR Ca^{2+}-ATPase (SERCA), sarcolemmal Na$^+$/Ca^{2+} exchanger (NCX), sarcolemmal Ca^{2+}-ATPase and mitochondrial Ca^{2+} uniport. The relative contributions of

these four Ca^{2+} transport pathways dependent on the species. In rats, 92% of the Ca^{2+} is taken up (and released) by the SR, and only 7% is extruded by NCX (most of which enters via DHPR), showing that E-C coupling is highly SR-dependent [4, 23]. In rabbits and humans, ~70% of the cytosolic Ca^{2+} is taken up by the SR, whereas 28% is transported through NCX [4]. Ca^{2+} that is recycled to the SR lumen is stored as a complex predominantly with an abundant resident Ca^{2+} binding protein, calsequestrin (CSQ).

1.2.2 Local Control Mechanism of E-C Coupling

The understanding of E-C coupling has changed dramatically over the past few years from the old, "common-pool" theories to a new "local-control" mechanism of E-C coupling [24]. The essence of this mechanism is that: 1) Ca^{2+} entry via DHPRs in the sarcolemma is the predominant stimulus for CICR and initiates E-C coupling, and 2) the rate and amount of Ca^{2+} released from the SR is tightly and locally controlled by the magnitude and duration of the DHPR Ca^{2+} current [25]. The co-localization and functional coupling of DHPRs and RyRs are the cornerstones of the modern local control theory of cardiac E-C coupling [26]. Immunolabeling with specific antibodies and ultrastructural analysis using transmission electron microscopy have established that DHPRs and RyRs are co-localized at cardiac intracellular junctions called dyads, where SR terminal cisternae are apposed to the plasmalemmal T tubules [27]. At dyads, dozens of DHPRs co-localize with hundreds of RyRs and functionally group as a local SR Ca^{2+}-release unit called a couplon [26]. In a dyadic junction or "a couplon" of the cardiomyocytes, DHPRs open and close stochastically upon depolarization, delivering a train of local Ca^{2+} pulses (Ca^{2+} sparklets) to RyRs in the abutting SR terminal cisternae [28]. The stochastic

activation of a cluster of RyRs from different couplons discharges Ca^{2+} sparks which are the fundamental units of SR Ca^{2+} release produced at a couplon and reflect the concerted activation of a cluster of RyRs [4]. During cardiac myoctyte E-C coupling, thousands of Ca^{2+} sparks from ~10,000 discrete couplons in a ventricular myocyte are synchronized by the opening of DHPRs upon action potential activation and summate into a whole-cell Ca^{2+} transient that evokes contraction [4, 19, 28].

The stability and fidelity of intermolecular Ca^{2+} signaling between DHPRs and RyRs in a couplon are essential for the maintenance of normal heart rhythm and contractile function [27]. The discovery of structure and disposition of couplons by electron micrographs provides a structural base for the local control mechanism [29]. In a couplon, DHPRs and RyRs are juxtaposed across a dyadic cleft of ~10 nm [2, 3, 27 30]. This restricted cytoplasmic space and close proximity facilitates the stability and fidelity of Ca^{2+} signaling between DHPRs and RyRs.

It is estimated that a dyad has over 100 RyRs arranged in large organized arrays up to 200 nm in diameter [27] and every DHPR couples 5-10 RyRs [27]. A Ca^{2+} spark reflects the nearly synchronous activation of a cluster of about 6–20 RyRs at a dyad [3, 27]. The space between dyads ensures Ca^{2+} sparks are recruited under the tight control of the DHPR Ca^{2+}current (Ica). Resting Ca^{2+} sparks are normally rare and isolated by the space between couplons. But when cellular and SR Ca^{2+} load rise, the exclusively local stochastic cluster behavior is overcome and Ca^{2+} released at one couplon can activate a neighbouring couplon (partially owing to higher SR content and $[Ca^{2+}]_i$) and generate propagated Ca^{2+} waves and oscillations [4, 31].

1.3.   DHPRs

1.3.1   Structure and Function of DHPRs

DHPRs participate in a wide range of functions, but their central role in the heart is to provide the Ca^{2+} trigger for E-C coupling. DHPR Ca^{2+} influx (I_{ca}) is essential to excitability as it shapes the long plateau phase of the cardiac action potential that is unique to cardiac ventricular myocytes. Most of the Ca^{2+} for cross-bridge formation and myocyte contraction comes from the SR intracellular Ca^{2+} store, and I_{Ca} serves to trigger release of this Ca^{2+} by activating the RyR [4, 32].

DHPRs are heterotetrameric polypeptide complexes comprised of α_1, $\alpha2/\delta$, β, and γ subunits that allow depolarization-induced Ca^{2+} influx into the cytosol. The α_1 subunit forms the ion conducting pore while the accessory subunits ($\alpha2/\delta$, β, and γ) are tightly bound to the α_1 subunit and modulate biophysical properties of the α_1 subunit [33]. In all excitable tissues, Ca^{2+} channels invariably contain α_1, α_2/δ, and β subunits. These are considered the functional minimum core for Ca^{2+} channel assembly. Since the γ subunit does not appear to be expressed in heart, it is not discussed further here.

α_1 subunit The L-type Ca^{2+} channel α_1 subunit (170–240 kDa) consists of 4 homologous motifs (I–IV), each composed of 6 membrane-spanning α-helices (termed S1 to S6) linked by variable cytoplasmic loops between the S5 and S6 segments. To date, 10 α_1 subunit genes have been identified and separated into 4 classes: $Ca_v 1.1$, 1.2, 1.3 , and 1.4 . Only the $Ca_v 1.2$ subunit is expressed in high levels in cardiac muscle. The Cav1.2 gene encodes for the typical I_{Ca} in ventricular myocytes [5]. Cav1.3 is mainly expressed in atrioventricular and sinus nodes. No function for Cav1.1 and 1.4 has yet been reported in

the heart [1].   The α_1 subunit harbors the ion-selective pore, voltage sensor, gating machinery, and the binding sites for channel-modulating drugs [1] and is autoregulatory. The pore is asymmetric, with conserved glutamate residues (EEEE) comprising the ion-selectivity filter(s) [1]. The cytoplasmic C terminus is a region richly endowed with motifs and consensus sites for cell membrane targeting, phosphorylation, and Ca^{2+}-dependent signal transduction [34].

α_2/δ subunits The α_2/δ subunits are closely associated with the α_1 subunit by surface interaction. The α_2 subunit is entirely extracellular, and the δ subunit has a single transmembrane region with a very short intracellular part. The α_2/δ subunit affects α_1 function by increasing channel density, charge movement, and B_{max} of drug binding (e.g., isradipine, a DHPR blocker) [1]. The α_2/δ_1 subunit possesses a high-affinity binding site for certain GABA-antagonists which are used to treat paroxysmal neurological conditions such as epilepsy and pain disorders [35]. The α_2/δ_2 subunit also binds gabapentin, but at low affinity. Mice deficient in α_2/δ_2 exhibit enhanced seizure susceptibility and a tendency to develop bradycardia [36].

β subunits Together with α_2/δ, β subunits modulate the biophysical properties of the DHPR α_1 subunit and are an essential part of functional DHPRs. β subunits are reported to initiate trafficking α_1 subunits from the endoplasmic reticulum to the plasma membrane [37]. As shown in β subunit knock-out mice, the β subunit is crucial to maintain normal E-C coupling. β subunit knock-out mice suffer from impaired E-C coupling and early lethality [38]. The exact mechanism for the defect of E-C coupling is not known, but it is possible that the deficiency in β subunits results in the degradation of the α_1 subunit.

Moreover, with unchanged α_1 subunit levels, reduction in β subunit expression paralleled a reduction in I_{Ca} [1].

1.3.2   Regulations of DHPRs

β_1-adrenergic stimulation is one of the best-characterized signaling pathways that modulate I_{Ca} [5]. β-adrenergic stimulation increases peak I_{Ca}, slows channel inactivation, and augments the channel's open probability (P_o).   Th e effects o f β_1-adrenergic stimulation on I_{Ca} are important in the mammalian heart which leads to an increase in contractility.   This stimulation of I_{Ca} is through PKA–mediated phosphorylation of DHPRs. PKA catalyzes phosphorylation of amino acid Ser 1928 on the α-subunit and two amino acids on the β subunit that cause increased channel openings [1, 5, 39].

Similar to PKA, activation of CaMKII also promotes I_{Ca} facilitation (i.e. activation of CaMKII augments peak I_{Ca} and slows channel inactivation)[1, 39].   Like PKA, CaMKII can also phosphorylate DHPR α subunits. However, in contrast to PKA, the critical amino acid for CaMKII action is not yet identified[1, 39].   CaMKII is primarily activated by Ca^{2+} released from intracellular SR Ca^{2+} stores, rather than by I_{Ca}. I_{Ca} does not occur when SR Ca^{2+} release is eliminated [40]. Moreover, CaMKII is most effective for increasing I_{Ca} during the cardiomyocyte action potential plateau [41]. Thus SR Ca^{2+} release is essential for CaMKII-mediated I_{Ca} facilitation. Excessive CaMKII activity has the potential to trigger arrhythmias by further enhancing DHPR reopening during the action potential plateau (further discussed in section of " DHPRs and heart diseases").

Besides PKA and CaMKII, I_{Ca} is also regulated by many other factors, such as calmodulin (CaM), cytoskeleton, sorcin, protein phosphatases etc. [1, 5, 39]. For example,

the Ca^{2+}-binding protein CaM is a critical sensor in mediating Ca^{2+}-dependent inactivation of DHPRs. The cardiac DHPRs display long-lasting openings and minor voltage-dependent inactivation components. In the heart, Ca^{2+}-dependent inactivation is compatible with the length of the Ca^{2+}-mediated plateau phase in the action potential. Therefore, Ca^{2+}-induced inhibition of the DHPRs plays a critical role in controlling Ca^{2+} entry and downstream signal transduction. In the C terminal tail of the α_1 subunit, there is a Ca^{2+}-dependent CaM-binding motif that has been implicated in autoregulation. It is suggested that α_1 binding to CaM is essential to promote Ca^{2+}-dependent inactivation [5].

1.3.3   DHPRs and Heart Diseases

There is overwhelming evidence that cardiac E-C coupling depends on DHPR function [1-5]. Because I_{Ca} constitutes the main trigger for E-C coupling, it has drawn a lot of attention in human and experimental heart failure. Most investigators found that the expression of DHPRs is up-regulated in hypertrophied hearts [42], but unchanged or down-regulated in the end-stage of heart failure [1, 5, 39, 43]. In allografts from hearts with diastolic heart failure, the transcript and protein expression levels of the β subunit were decreased while the expression levels of other subunits were unchanged [44]. At the functional level, most of the analyses have shown that the density and activity of whole-cell I_{Ca} were unchanged in the failing heart [1, 45, 46] but open probability (P_o) and availability were paradoxically enhanced at single channel level [1, 45, 47]. Such a paradox might be explained by the hypothesis that the cardiomyocytes from these failing hearts expressed fewer but more active DHPRs than normal. This hypothesis would be consistent with the finding of a decrease in T-tubule density in human and experimental heart failure [48], and

could account for the observed decrease in E-C coupling gain or CICR efficiency [49, 50].

Moreover, the increased single channel P_o has been suggested to result from an increase in PKA-dependent phosphorylation of the α_1 unit in the failing heart [46]. CaMKII may also play a role because CaMKII-mediated hyperphosphorylation of DHPRs was found in a mice model of pressure-overload heart failure [51]. Another possibility to account for the increased single channel activity is an overexpression of β subunits [47]. In fact, human failing heart samples have shown increased levels of β subunits [47].

DHPRs also play a role in the pathogenesis of arrhythmias. In chronic human atrial fibrillation, I_{Ca} was down-regulated accompanied by reduced protein expression of the α_1 subunit and increased P_o [52]. The Timothy syndrome is a rare, variant of the long QT syndrome characterized by severe arrhythmic profiles, structural heart anomalies, syncope, and sudden death. Now the pathogenesis of the Timothy syndrome has been identified as a mutation of α_1 subunit of DHPRs [5, 39]. I_{Ca} is suggested to be a major determinant of the QT interval [5]. Although QT prolongation has long been known to increase the risk of sudden cardiac death and overall cardiac mortality among patients with a variety of underlying etiologies, a shorter than normal QT interval could also be detrimental, leading to the concept of a new clinical entity, the short QT syndrome [53]. Recently, novel mutations of DHPRs were reported to reduce I_{Ca} amplitude, shorten the QT interval, and lead to sudden cardiac death, atrial fibrillation and a Brugada type I ECG pattern [54].

Long-term enhancement of DHPR Ca^{2+} signaling by over-expressing DHPR in transgenic mice triggers Ca^{2+} imbalance and induces cardiac hypertrophy and dilatory remodeling [55]. The chronic inhibition of DHPR Ca^{2+} signals either by DHPR blockers [14,

[17, 18, 56] or by DHPR mutation [54] is reported to increase the risk of heart failure, promote

sudden death, and lead to arrhythmia (short QT syndrome, artial fibrillation, and Brugada

syndrome) [54].

1.4.   SR Ca^{2+} Cycling Apparatus In Cardiac E-C Coupling

Downstream of the DHPR, the SR Ca^{2+} cycling apparatus plays a pivotal role in the E-C coupling to enable the cardiac cycle [57]. The major proteins of the SR Ca^{2+}-cycling apparatus include RyRs and SERCA which maintain the basic SR function of release and uptake of Ca^{2+} respectively [57]. Alterations in the expression and function of SR Ca^{2+} transport proteins significantly affect cardiac performance.

1.4.1   Structure and Function of RyRs.

RyRs were first observed in the 1970s in electron micrographs of striated muscle [58] and subsequently were isolated as integral SR membrane proteins and their role as the Ca^{2+} release channel demonstrated [59]. The complementary DNA encoding three distinct RyR channels was cloned and the corresponding gene sequences obtained for three isoforms: RyR1, RyR2, and RyR3. RyR2 is the predominant isoform present in the cardiac muscle [60, 61]. As one of the largest proteins identified to date, RyR2 is a tetramer with each monomer being 565 KD [60, 61]. RyR2 channels are organized in regular arrays such that neighboring channels are in physical contact with each other. Physical and functional association among RyR2 channels results in coordinated gating behavior termed coupled gating that allows clusters of channels to function as "Ca^{2+} release units" [61].

1.4.2   Regulation of RyRs

RyR2 does not exist in isolation, but is coupled to other proteins which can modulate its P_o [62]. These endogenous regulatory proteins include FK-506 binding protein 12.6 (FKBP 12.6), calmodulin, junctin, triadin and CSQ etc. [60, 62, 63]. Among them, the modulation of RyR2 Ca^{2+} release property by FKBP 12.6 is well established [64, 65 63]. Each single FKBP12.6 molecule binds to a monomer of RyR2 and keeps the channel in a stable closed state at rest, thereby preventing diastolic Ca^{2+} leak [65, 66]. It has been suggested that phosphorylation of RyR2 dissociates FKBP12.6 from RyR2, resulting in increased channel activity (i.e., P_o) [65-67]. Dissociation of FKBP12.6 from RyR2 channels also results in functional but not physical uncoupling of adjacent RyR2 channels [68]. Coupled gating of RyR2 channels describes the simultaneous opening and closing of groups of channels as opposed to stochastic and independent gating of individual channels. Functional uncoupling of adjacent RyR2 channels can decrease E-C coupling gain and destabilize single RyR2 channels, thereby promoting diastolic Ca^{2+} leak [61].

In addition to FKBP12.6, Ca^{2+} concentration in the SR lumen ($[Ca^{2+}]_{SR}$) and CSQ also play important roles in influencing the functional activity of RyR2 [69]. RyR2 P_o changes as a monotonic function of $[Ca^{2+}]_{SR}$ with an EC_{50} around1 mM [70]. Since resting $[Ca^{2+}]_{SR}$ is ~1 mM, a decline in $[Ca^{2+}]_{SR}$ reduces RyR2 activity and forces CICR to terminate upon reaching a critical level of $[Ca^{2+}]_{SR}$. This mechanism, termed luminal Ca^{2+}–dependent deactivation [71] leaves the Ca^{2+} store in a temporarily unresponsive, refractory state, preventing untimely SR Ca^{2+} release before the next cardiac cycle. Mechanistically, luminal Ca^{2+} seems to act on RyR2 by allosterically affecting RyR2's

sensitivity to cytosolic Ca^{2+}. Consequently, lowering $[Ca^{2+}]_{SR}$ reduces the sensitivity of

RyR2 to activation by cytosolic Ca^{2+} whereas increasing $[Ca^{2+}]_{SR}$ sensitizes the RyR2 [69].

Thus, the functional status of RyR2 at any time is determined by combined inputs from

cytosolic and luminal Ca^{2+}.

Being Ca^{2+} dependent and strategically localized at the points of SR Ca^{2+} release,

CSQ presents itself as a putative luminal Ca^{2+} sensor for the RyR2. As suggested by

crosslinking studies, CSQ exists in the junctional SR as a mixture of monomers, dimers

and multimers [72]. While the multimeric form of CSQ functions as a Ca^{2+} buffer, the

monomers appear to be responsible for the regulatory function of the protein. Consistent

with its regulatory role, CSQ inhibits RyR2 activity at low $[Ca^{2+}]_{SR}$ and this inhibition is

relieved at elevated $[Ca^{2+}]_{SR}$ in reconstitution studies [70]. Although direct effects of CSQ

on RyR2 have been described, according to most reports, Ca^{2+}-dependent interactions of

CSQ2 with RyR2 are mediated by the integral membrane proteins triadin and/or junctin.

CSQ is thought to modulate RyR2 function in the following manner: when $[Ca^{2+}]_{SR}$ is

low, CSQ2 is bound to triadin and/or junctin and inhibits the activity of RyR2; with SR

Ca^{2+} load restored, increased $[Ca^{2+}]$ inhibits binding of CSQ to triadin and/or junctin,

thereby relieving the inhibitory action of CSQ on the RyR2 channel activity. This Ca^{2+}-

dependent modulation of RyR2 by CSQ has been suggested as the molecular basis for

deactivation of RyR2 and store refractoriness following SR Ca^{2+} release [70].

1.4.3   Structure and Function of SERCA

The cardiac SR vesicles were first identified as "Relaxing Factor" in 1960s since

preparations of cardiac SR vesicles prevented contraction of native actomyosin

(containing myosin, actin, and the troponin complex) upon addition of ATP [73]. It was soon established that this effect was produced by ATP–dependent sequestration of Ca^{2+} by the vesicles due to the Ca^{2+} activated SERCA. In humans, 3 genes (ATP2A1-3) generate multiple isoforms (SERCAla,b, SERCA2a-c, SERCA3a-f) by developmental or tissue-specific alternative splicing with SERCA2 the dominant isoform in the heart [74]. SERCA2 is a single polypeptide with 993 amino acids of 110kDa [63] and is one of the P-type ion motive ATPases, as it transfers phosphate from ATP to an aspartate residue during its catalytic cycle [63, 74]. A substantial portion of the ATPase molecule is on the cytoplasmic side of the SR membrane where it has the ATP binding and phosphorylation domains. The Ca^{2+}-binding sites are located within the ion channel formed by the transmembrane segments M4, M5, M6 and M8 [7, 63, 74]. Activated by Ca^{2+}, SERCA2 pumps Ca^{2+} from the cytosol to the SR lumen against a concentration gradient at the expense of ATP hydrolysis [7, 63]. In the Ca^{2+} transport cycle, the SERCA2 alternates between two major conformational states, E1 and E2, in heart muscle by cytosolic proteins and calmodulin. The cycle begins with the binding of two moles of Ca^{2+} and one mole of ATP to the E1 conformation to form an enzyme-Ca^{2+}-ATP complex. The binding of Ca^{2+} and ATP induces a conformational change in the ATPase resulting in translocation of Ca^{2+} to the inside and the simultaneous formation of a phosphorylated intermediate with Ca^{2+} still bound to the complex. The final step involves release of Ca^{2+} into the lumen of the SR and the simultaneous decomposition of the phosphorylated intermediate into ADP and inorganic phosphates both of which are released into the cytoplasm [7, 75] (Fig.1.2). SERCA2 accounts for 70–80% of Ca^{2+} removal from the cytoplasm during cardiac muscle relaxation in higher mammalian species and human

myocardium [4, 76, 77]. Therefore, the rate of muscle relaxation is largely determined by the reuptake of Ca^{2+} into the SR by SERCA2 [78].

b Phosphorylation

$$E_1 \cdot ATP \cdot 2Ca^{2+} \longleftrightarrow E_1 \cdot P(Ca^{2+})_2$$

a Ca^{2+} binding   **c Ca^{2+} release**

$$E_2 + P_i \longleftrightarrow E_2 \cdot P + 2Ca^{2+}$$
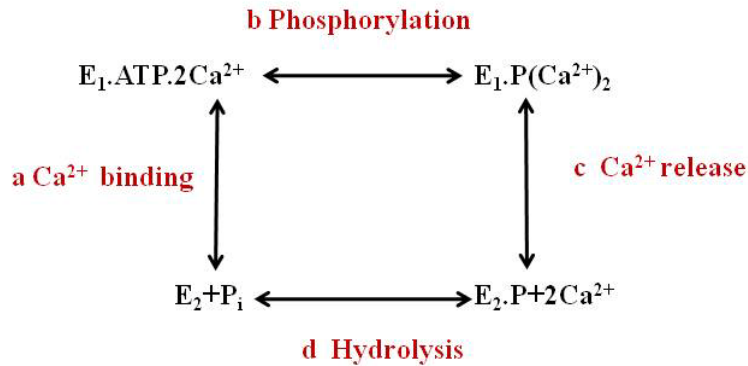
d Hydrolysis

Figure 1.2 Ca^{2+} transport by SERCA. Powered by ATP hydrolysis, massive conformational changes of SERCA drives Ca^{2+} transport and are induced as discrete steps by Ca^{2+} binding (part a), phosphoenzyme formation (part b), Ca^{2+} release (part c) and dephosphorylation (part d).

1.4.4   Regulation of SERCA

A physiological mechanism for the regulation of cardiac SERCA involves phosphorylation of the intrinsic SR protein, phospholamban (PLN) [7, 63, 79, 80]. PLN is a 52-amino-acid transmembrane protein of the SR and is expressed mainly in cardiac but also in smooth and slow-twitch skeletal muscles [81]. PLN is proposed to have a pentameric tertiary structure [7]. Detailed cross-linking and site-directed mutagenesis studies have demonstrated that residues in PLN can interact directly with SERCA2 [82]. In its dephosphorylated state, PLN interacts with the SERCA2 and exerts an inhibitory effect manifested as a decrease in SERCA's affinity for Ca^{2+}. Phosphorylation of PLN by cAMP-dependent protein kinase (PKA) or Ca^{2+}/calmodulin-dependent protein kinase (CaMK) leads to a removal of the inhibition of PLN on SERCA2, resulting in enhanced affinity of the SERCA2 for Ca^{2+} and increased Ca^{2+} transport to the SR lumen [7] (Fig.1.3).
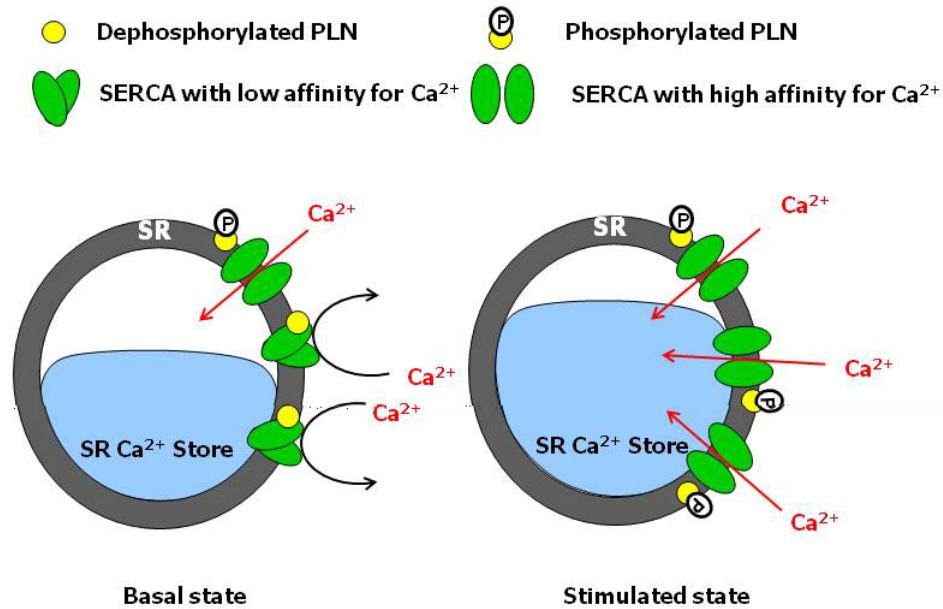
Figure 1.3 Role of PLN-SERCA interactions in physiological cardiac function. Under basal conditions, dephosphorylated PLN interacts with SERCA and decreases Ca^{2+} pump activity. Phosphorylation of PLN leads to functional dissociation of the PLN-SERCA complex and an increase in Ca^{2+} transport into the SR lumen. As more Ca^{2+} is accumulated in the SR lumen, a greater SR Ca^{2+} store is available for release in a subsequent beat, resulting in enhanced contractile force. (This figure is adapted from MacLennan DH & Kranias EG. Phospholamban: a crucial regulator of cardiac contractility. Nat Rev Mol Cell Biol 4, 566-577, 2003)

As the classic mechanistic concept, phosphorylation of PLN is thought to dissociate the inhibited PLN–SERCA2 complex [7]. However, this long-standing view has been questioned by a study from Dr. MacLennan group which reported that phosphorylation of PLN does not cause the disruption of the physical interaction between the SERCA and PLN but Ca^{2+} ions does [83]. Interestingly, the recent findings from our laboratory showed that the SR-associated CaM mediates the disruption of SERCA-PLN interaction in a Ca^{2+}-dependent manner, and triggers Ca^{2+} pumping [84,85]. Moreover, increasing evidence rising from our laboratory suggests that it is the Ca^{2+}-dependent CaM that controls the PLN-SERCA2 interaction as well as SERCA2 phosphorylation by CaMKII. Our laboratory discovered that cardiac SR contains tightly-bound CaM [84] and

demonstrated a critical role for CaM in controlling SERCA2 Ca^{2+} pump function and cardiac muscle relaxation [84, 86, 87]. A synthetic CaM-binding peptide (CaM BP) strongly inhibits SR Ca^{2+} uptake by SERCA, promotes SR Ca^{2+} release, and lowers CaMK-mediated protein phosphorylation in cardiac SR [84, 86, 87]. These effects of CaM BP are prevented and reversed by exogenous CaM [84, 86, 87]. Furthermore, endogenous CaM triggers SR Ca^{2+} pump function by dissociating SERCA2 from PLN with accelerating phosphoenzyme decomposition [84] and CaM BP inhibition of SERCA2 is observed only in the presence of PLN in the SR [88]. These demonstrate that Ca^{2+}-dependent CaM plays a critical role in the PLN-SERCA2 interaction and SERCA2 phosphorylation by CaMKII.

Three naturally occurring PLN mutations (L39stop, R9C, R14Del) have been identified in humans and all of them were associated with lethal heart failure [89-91]. Down-regulation of SERCA2 and PLN are observed in animal models of heart failure [78, 92, 93]. These observations reinforce the essential role of PLN in the regulation of physiological and diseased cardiac function.

1.5.   Phosphorylation-dependent Regulation of SR Function by Protein Kinases

The physiological regulation of SR function is achieved mainly through phosphorylation of SR Ca^{2+} cycling proteins [7]. In addition, the interactions among

molecular partners (e.g. SERCA-PLN, SERCA-CaM, RyR-FKBP12.6) are phosphorylation status dependent and likely govern the conformation and function of both the
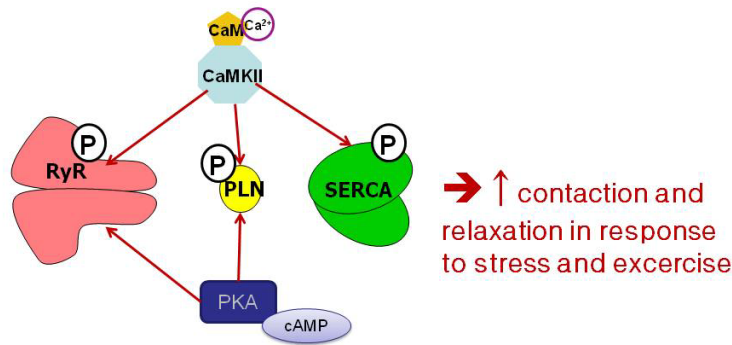
Figure 1.4 The phosphorylation targets of CaMKII and PKA in regulation of RyR/SERCA function .

RyR and SERCA [94].

Present in the cytosol, nucleus and SR [95-98], CaMKII plays a central role in controlling RyR and SERCA function by its ability to phosphorylate the RyR, SERCA and PLN (Fig.1.4). CaMKII has four different isoforms (α, β, δ, and γ) which are expressed in a tissue-specific manner [96, 99]. In cardiac tissue, the predominant isoform is CaMKIIδ [96, 99]. Experimental evidence obtained from our laboratory suggested that the "open state" but not the "closed state", of cardiac RyR undergoes phosphorylation by CaMKII [98]. The RyR and PLN (but not SERCA) are also regulated by cytosolic PKA through the phosphorylation [100] (Fig. 1.4). Clearly, CaMKII and PKA are two major protein kinase pathways that regulate the phosphorylation status of SR proteins, the intermolecular interactions and intramolecular events that govern SR Ca^{2+} cycling.

Phosphorylation of RyR2 is a key mechanism for regulating channel Ca^{2+} release function [62, 101]. RyR2 can be phosphorylated by CamKII and PKA [65, 66, 102, 103]. So far

three phosphorylation sites have been identified. In human and rodents, they are serine-(S) 2808 (S2809 in rabbit), S2814 (S2815 in rabbit), and S2030 (S2031 in rabbit) [104]. RyR2 S2808/S2809 can be phosphorylated by both CaMKII and PKA [104]; whereas S2814/S2815 has been implicated only being phosphorylated by CaMKII [100] and S2030/S2031 only by PKA [105]. Phosphorylation of the channel is generally regarded as an important regulatory mechanism, but the exact effects on channel function remain controversial as both stimulatory and inhibitory effects have been reported [102, 103, 106 104]. Differences in opinion have arisen over the importance assigned to specific phosphorylation sites on RyR2 but it has been speculated that different phosphorylation sites distinctly modify RyR2 function [101, 104].

Hyperphosphorylation of RyR by PKA and CaMK has been implicated in RyR dysfunction and heart failure [26, 66, 107]. However, several studies have questioned RyR hyperphosphorylation in heart failure [108, 109], and the functional consequence of RyR phosphorylation remains controversial [110]. But more and more evidence supports the suggestion that RyR phosphorylation by CaMKII results in increased RyR P_o and SR Ca^{2+} leak [66 101, 111, 112] which can lead to heart failure [66] and arrhythmias [111]. The PKA-mediated enhancement in SR Ca^{2+} leak is CaMKII-dependent [101]. This increased "leakiness" of the SR could underlie the increased propensity for arrhythmias in heart failure and eventually contribute to decreased contractility by reducing SR Ca^{2+} load.

PLN phosphorylation has been suggested as the primary mechanism for β-adrenergic stimulation in the heart [80]. The phosphorylation of PLN is thought to release the inhibition of PLN on SERCA2 and restore SERCA2 affinity for Ca^{2+} [4, 6, 7]. On the other hand, dephosphorylated PLN inhibits V_{max} of Ca^{2+} transport and lower the affinity

of SERCA2 for calcium [7]. Studies have shown that dephosphorylation of PLN acts as a brake on the SERCA2 pump whereas phosphorylation releases the "brake" and substantially increases Ca^{2+} transport activity and relaxation rate [81]. The PLN can be phosphorylated at serine 16 by PKA and threonine 17 by CaMKII [6, 80, 113]. A recent study from Dr. Tuana group suggested that CaMKII-medicated phosphorylation of PLN at threonine 17 is modulated by α kinase anchoring protein (αKAP) [96]. As a membrane protein, αKAP is found to interact with SERCA2 on the one hand and CaMKII on the other at the SR. In the presence of αKAP, CaMKII−medicated phosphorylation of PLN was markedly inhibited by the presence of αKAP [96]. Thus, a model of a CaMKII-αKAP-SERCA2-PLN complex at the SR membrane is proposed, where αKAP acts as a scaffold and an adaptor to promote the spatial positioning among these proteins to modulate PLN phosphorylation by CaMKII at the SR [96].

Our laboratory discovered a direct phosphorylation of SERCA2 at serine 38 by CaMKII, and consequent activation of Ca^{2+} transport through an increase in V_{max} [114]. This phenomenon, unique to the SERCA2 isoform of the Ca^{2+} pump expressed in the heart and slow-twitch skeletal muscle, has been confirmed by studies in other laboratories [88, 115]. All together these studies demonstrate that the CaM/CaMK/PLN pathway plays a central role in regulation of SR function.

1.6   DHPR Blockers

1.6.1   DHPR Blocker Treatment is Associated With Increased Risk of Heart Failure

Although chemically diverse, calcium channel blockers (DHPR blockers) share a common property of blocking I_{Ca} through DHPRs in the sarcolemma. Since their introduction nearly two decades ago, DHPR blockers have been shown to be effective in controlling blood pressure and anginal symptoms [14]. They were the most frequently prescribed antihypertensive drugs in the United States as recently as 1993 [116]. In the past a few years, however, the long-term safety of DHPR blockers has been questioned, owing to an association with development of cardiovascular events. Recent large clinical studies report that the use of DHPR blockers, particularly in high doses, was associated with an increased risk of adverse cardiovascular events, especially myocardial infarction and heart failure [14]. In 1995, a population-based case-control study of 2655 patients on anti-hypertensive treatment found that the use of short-acting DHPR blockers were associated with a 58% increased risk of myocardial infarction compared to the use of diuretics [17]. In 2000, a large meta-analysis, which included nine published trials, eight calcium channel blockers, and a total of 27,743 patients, found that the use of DHPR blockers was associated with a significantly higher risk of myocardial infarction, heart failure, and other major cardiovascular events [56]. In 2002, the ALLHAT Trial (Antihypertensive and Lipid-Lowering Treatment to Prevent Heart Attack Trial), a randomized double-blind trial involved 33,357 subjects aged 55 years or older, also found the patients on long-term treatment with amlodipine (a DHPR blocker) had a 38% higher

risk of heart failure and a 35% higher risk of hospitalization/fatal heart failure as compared to patients on chlorthalidone (a diuretic) [117]. Similarly, in 2003, the CONVINCE trial (the Controlled Onset Verapamil Investigation of Cardiovascular End Points Trial), which enrolled 16,602 patients, reports long-term using of extended-release verapamil was associated with an increased risk of heart failure compared with atenolol (a β-adrenergic blocker) or hydrochlorothiazide (a diuretic) [18]. Not known are the mechanisms that underlie the increased risk of heart failure associated with chronic treatment with DHPR blockers.

1.6.2   Deferent Classes of DHPR Blockers Exert Different Pharmacological Effects on Hearts

DHPR blockers are categorized into five classes according to their chemical structure: phenylalkylamines, dihydropyridines, benzothiazepines, diphenylpiperazines, and diarylaminopropylamines [14, 118]. Although all five classes work by blocking DHPRs, each structurally different class binds at a unique location on DHPRs and varies in tissue selectivity [14, 118, 119]. Among them, phenylalkylamines are the most cardiac selective as they preferentially block DHPRs in the myocardium [118, 120]. In contrast, dihydropyridines preferentially bind vascular smooth muscle L-type channels and produce the most potent vasodilatory effects of the DHPR blockers thereby indirectly affecting cardiac function by the sympathetic reflex (Table 1.1) [118-120]. Verapamil and nifedipine are the prototypes of phenylalkylamines and dihydropyridines respectively. Their tissue selectivity, pharmacological effects and clinical applications are discussed further below.

Table 1.1 Comparison of cardiovascular effects of nifedipine and verapamil *in vivo* [118, 120]

	Nifedipine (vascular selective)	*Verapamil (cardiac selective)*
Heart		
1. suppression of cardiac contractility	0/+	+++
2. suppression of conduction (AV node)	0	+++
3. suppression of automaticity (SA node)	0	+++
4. suppression of heart rate	0	++
5. cause reflex tachycardia	Yes	No
6. prescribed for ventricular tachycardia	No	Yes
Vessel		
1. vasodilatation of peripheral vessel	+++	+
2. vasodilatation of coronary vessel	+++	++

0, no effect; +, mild; ++, moderate; +++, pronounced.

Compared to nifedipine, verapamil preferentially blocks DHPRs in cardiac cells. At clinically used doses, nifedipine does not block DHPRs in the myocardium but verapamil does and produces inotropic and chronotropic effects on the heart *in vivo* [118, 120]. In contrast, the negative inotropic effect is rarely, if ever, seen in intact animals or patients with nifedipine treatment. Probably because of sympathetic reflex responses to its potent vasodilating effects, hemodynamic studies of the immediate release nifedipine formulation in patients with normal ventricular function have generally found a small increase in cardiac index without major effects on ejection fraction, left ventricular end-diastolic pressure or volume (From Drug Information issued by US Food and Drug Administration; available at http://dailymed.nlm.nih.gov/dailymed/drugInfo.cfm?id=726).

Verapamil is an antiarrhythmic drug which is the treatment of choice for idiopathic left ventricular tachycardia (also known as verapamil-sensitive VT) [121], and the

next treatment of choice for terminating sinus node, atrioventricular (AV) node reentry tachycardia after simple vagal maneuvers and adenosine [15]. The antiarrhythmic effect is partially due to the ability of verapamil to prolong the effective refractory period within the AV node and slow AV nodal conduction in a rate-related manner *in vivo* [118]. In contrast, nifedipine is not an antiarrhythmic drug [120]. In patients with normal conduction systems, nifedipine administered as the immediate release capsule had no tendency to prolong AV nodal conduction or sinus node recovery time, or to slow sinus rate [118]. Nifedipine is commonly prescribed to control high blood pressure and angina symptoms due to its preferential blockade of DHPRs in vascular smooth muscle.

Verapamil is thought to access cardiac DHPRs from the intracellular side and bind to open, depolarized channels [122]. One planar bilayer study reported that verapamil also can directly bind to RyRs *in vitro* and inhibit the Ca^{2+} release from the cardiac SR [123]. As verapamil is one of the most cardiac selective DHPR blockers [118]. Thus treatment with verapamil, but not nifedipine, provides an approach to build up an animal model for chronic and partial blockade of cardiac DHPRs *in vivo*.

1.7   Rationale, hypotheses, objectives, and significance of the research

1.7.1   Rationale and Hypothesis

As shown in Figure 1.1, the DHPR initiates cardiac E-C coupling and locally controls SR Ca^{2+} cycling through CICR. The close proximity of the SR and T-tubules facilitates the fidelity and stability of communication between the DHPR and SR Ca^{2+} cycling apparatus to ensure Ca^{2+} homeostasis and proper contraction. However, the impact of chronic, partial DHPR blockade on cardiac SR Ca^{2+} cycling function is not clear. Though used to control high blood pressure in patients [15], the long-term safety of DHPR blockers has been questioned as recent large scale clinical trials suggested long-term use of DHPR blockers increases the risk of heart failure and incidence of cardiac arrhythmias [14]. The mechanisms underlying this pathological phenomenon are not well known. Given the essential interplay of DHPR-RyR signaling in E-C coupling, I chose to address the impact of chronic DHPR blockade on heart function by investigating the following hypothesis. **Chronic, partial blockade of DHPRs *in vivo* will provoke remodeling of the SR Ca^{2+} cycling apparatus, leading to impaired cardiomyocyte Ca^{2+} homeostasis and heart dysfunction.** The investigation of this hypothesis can provide insights of the mechanistic basis for cardiac adaptation, and help clinicians to better understand and manage the risk of long-term treatment with DHPR blockers.

1.7.2   Objectives, Experimental Approaches, and Significance

The overall objective of this research is to determine the mechanisms of cardiac adaptation to chronic and partial DHPR blockade *in vivo*. **Specific aims** of these studies are identified as below.

Aim 1: To determine whether chronic DHPR blockade alters the expression and function of RyRs and DHPRs.

Aim 2: To determine whether chronic DHPR blockade alters the expression and function of cardiac SR Ca^{2+} pump.

Aim 3: To determine whether chronic DHPR blockade alters protein phosphorylation-dependent regulation of SR/cardiomyocyte Ca^{2+} cycling

Figure 1.5 shows the conceptual frame work of my research aims.
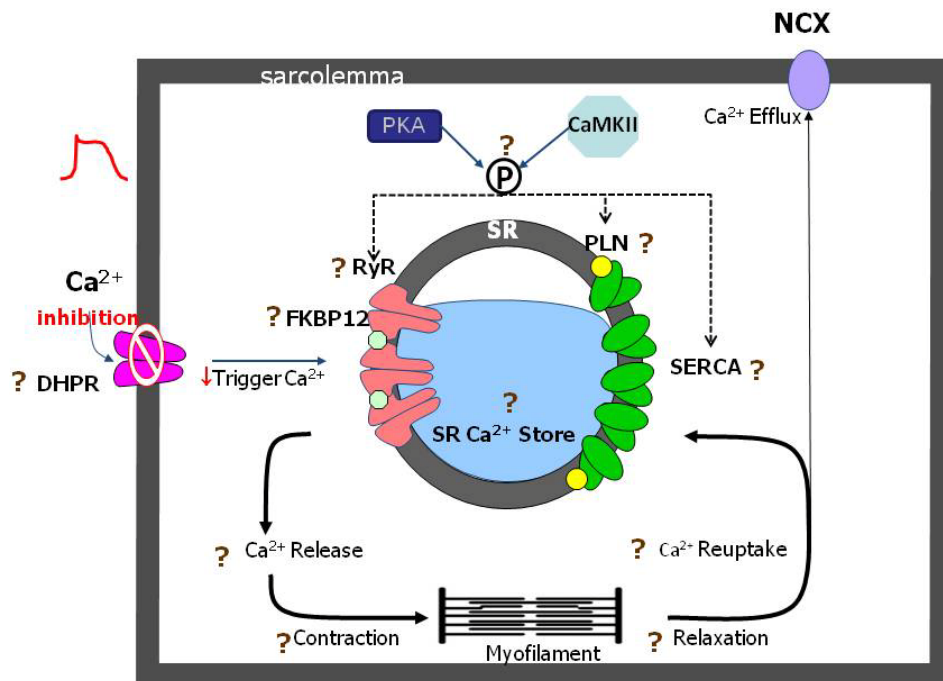
Figure 1.5 The conceptual framework of research aims. Question marks "?" indentify the target E-C coupling events or molecular players whose changes after chronic DHPR inhibition are not known and therefore are explored in this thesis.

Experimental approaches involve administration of verapamil (DHPR blocker) to adult rats at a rate of 625 ug/h/kg for 4 weeks via subcutaneously implanted osmotic mini pumps and assessment of: 1) expression and function of SR Ca^{2+} cycling proteins and the DHPR; 2) the kinetics of myocyte Ca^{2+} sparks, Ca^{2+} waves, and Ca^{2+} transients; 3) phosphorylation-dependent regulation of SR Ca^{2+} cycling; and 4) contractile function in isolated cardiomyocytes, perfused hearts and in whole animals. All procedures, assessment parameters and criteria for these studies are similar to those reported previously from this laboratory [84, 114, 124]. These experimental approaches enable assessment of SR/cardiomyocyte Ca^{2+} cycling and heart function in response to chronic DHPR blockade at all levels of organizations from intramolecular, intermolecular, molecular, cellular, organ, to the whole animal levels.

The significance of the proposed studies are: 1) to increase our understanding of the molecular mechanisms for the delicate communication among Ca^{2+} cycling proteins in cardiac E-C coupling, and 2) to identify the long-term risks of DHPR blockers by unraveling their underlying mechanisms.

1.8   **References**

1.   Benitah JP, Alvarez JL, Gomez AM. L-type Ca^{2+} current in ventricular cardiomyocytes. *J Mol Cell Cardiol*. 2010;48:26-36

2.   Sobie EA, Guatimosim S, Gomez-Viquez L, Song LS, Hartmann H, Saleet Jafri M, Lederer WJ. The Ca^{2+} leak paradox and rogue ryanodine receptors: SR Ca^{2+} efflux theory and practice. *Prog Biophys Mol Biol*. 2006;90:172-185

3.   Wang SQ, Song LS, Lakatta EG, Cheng H. Ca^{2+} signalling between single L-type Ca^{2+} channels and ryanodine receptors in heart cells. *Nature*. 2001;410:592-596

4.   Bers DM. Cardiac excitation-contraction coupling. *Nature*. 2002;415:198-205

5.   Bodi I, Mikala G, Koch SE, Akhter SA, Schwartz A. The L-type calcium channel in the heart: the beat goes on. *J Clin Invest*. 2005;115:3306-3317

6.   Kadambi VJ, Kranias EG. Phospholamban: a protein coming of age. *Biochem Biophys Res Commun*. 1997;239:1-5

7.   MacLennan DH, Kranias EG. Phospholamban: a crucial regulator of cardiac contractility. *Nat Rev Mol Cell Biol*. 2003;4:566-577

8.   Xu A, Narayanan N. Ca^{2+}/calmodulin-dependent phosphorylation of the Ca^{2+}-ATPase, uncoupled from phospholamban, stimulates Ca^{2+}-pumping in native cardiac sarcoplasmic reticulum. *Biochem Biophys Res Commun*. 1999;258:66-72

9.   Ruknudin AM, Lakatta EG. The regulation of the Na^{+}/Ca^{2+} exchanger and plasmalemmal Ca^{2+} ATPase by other proteins. *Ann N Y Acad Sci*. 2007;1099:86-102

10. Ottolia M, John S, Xie Y, Ren X, Philipson KD. Shedding light on the Na^+/Ca^{2+} exchanger. *Ann N Y Acad Sci*. 2007;1099:78-85

11. Larbig R, Torres N, Bridge JH, Goldhaber JI, Philipson KD. Activation of reverse Na^+-Ca^{2+} exchange by the Na^+ current augments the cardiac Ca^{2+} transient: evidence from NCX knockout mice. *J Physiol*. 2010;588:3267-3276

12. Philipson KD, Nicoll DA. Sodium-calcium exchange: a molecular perspective. *Annu Rev Physiol*. 2000;62:111-133

13. McCall D. Effect of verapamil and of extracellular Ca^{2+} and Na^+ on contraction frequency of cultured heart cells. *J Gen Physiol*. 1976;68:537-549

14. Eisenberg MJ, Brox A, Bestawros AN. Calcium channel blockers: an update. *Am J Med*. 2004;116:35-43

15. Libby P, Bonow R, Mann D, Zipes D, Braunwald E. *Braunwald's Heart Disease: A Textbook of Cardiovascular Medicine*. Natasha Andjelkovic; 2008.

16. Abernethy DR, Schwartz JB. Calcium-antagonist drugs. *N Engl J Med*. 1999;341:1447-1457

17. Psaty BM, Heckbert SR, Koepsell TD, Siscovick DS, Raghunathan TE, Weiss NS, Rosendaal FR, Lemaitre RN, Smith NL, Wahl PW, et al. The risk of myocardial infarction associated with antihypertensive drug therapies. *Jama*. 1995;274:620-625

18. Black HR, Elliott WJ, Grandits G, Grambsch P, Lucente T, White WB, Neaton JD, Grimm RH, Jr., Hansson L, Lacourciere Y, Muller J, Sleight P, Weber MA, Williams G, Wittes J, Zanchetti A, Anders RJ. Principal results of the Controlled Onset Verapamil Investigation of Cardiovascular End Points (CONVINCE) trial. *Jama*. 2003;289:2073-2082

19.   Wier WG, Balke CW. Ca^{2+} release mechanisms, Ca^{2+} sparks, and local control of excitation-contraction coupling in normal heart muscle. *Circ Res*. 1999;85:770-776

20.   Rios E, Stern MD. Calcium in close quarters: microdomain feedback in excitation-contraction coupling and other cell biological phenomena. *Annu Rev Biophys Biomol Struct*. 1997;26:47-82

21.   Kamp TJ, He JQ. L-type Ca^{2+} channels gaining respect in heart failure. *Circ Res*. 2002;91:451-453

22.   Fabiato A. Time and calcium dependence of activation and inactivation of calcium-induced release of calcium from the sarcoplasmic reticulum of a skinned canine cardiac Purkinje cell. *J Gen Physiol*. 1985;85:247-289

23.   Maier LS, Bers DM. Calcium, calmodulin, and calcium-calmodulin kinase II: heartbeat to heartbeat and beyond. *J Mol Cell Cardiol*. 2002;34:919-939

24.   Yue DT. Quenching the spark in the heart. *Science*. 1997;276:755-756

25.   Stern MD, Song LS, Cheng H, Sham JS, Yang HT, Boheler KR, Rios E. Local control models of cardiac excitation-contraction coupling. A possible role for allosteric interactions between ryanodine receptors. *J Gen Physiol*. 1999;113:469-489

26.   Bers DM. Macromolecular complexes regulating cardiac ryanodine receptor function. *J Mol Cell Cardiol*. 2004;37:417-429

27.   Wehrens XH, Lehnart SE, Marks AR. Intracellular calcium release and cardiac disease. *Annu Rev Physiol*. 2005;67:69-98

28.   Cheng H, Wang SQ. Calcium signaling between sarcolemmal calcium channels and ryanodine receptors in heart cells. *Front Biosci*. 2002;7:d1867-1878

29.   Franzini-Armstrong C, Protasi F, Ramesh V. Shape, size, and distribution of Ca^{2+} release units and couplons in skeletal and cardiac muscles. *Biophys J*. 1999;77:1528-1539

30.   Muller FU, Kirchhefer U, Begrow F, Reinke U, Neumann J, Schmitz W. Junctional sarcoplasmic reticulum transmembrane proteins in the heart. *Basic Res Cardiol*. 2002;97 Suppl 1:I52-55

31.   Cheng H, Lederer WJ. Calcium sparks. *Physiol Rev*. 2008;88:1491-1545

32.   Sun XH, Protasi F, Takahashi M, Takeshima H, Ferguson DG, Franzini-Armstrong C. Molecular architecture of membranes involved in excitation-contraction coupling of cardiac muscle. *J Cell Biol*. 1995;129:659-671

33.   Dolphin AC. A short history of voltage-gated calcium channels. *Br J Pharmacol*. 2006;147 Suppl 1:S56-62

34.   Gao T, Bunemann M, Gerhardstein BL, Ma H, Hosey MM. Role of the C terminus of the alpha 1C (CaV1.2) subunit in membrane targeting of cardiac L-type calcium channels. *J Biol Chem*. 2000;275:25436-25444

35.   Sutton KG, Martin DJ, Pinnock RD, Lee K, Scott RH. Gabapentin inhibits high-threshold calcium channel currents in cultured rat dorsal root ganglion neurones. *Br J Pharmacol*. 2002;135:257-265

36.   Ivanov SV, Ward JM, Tessarollo L, McAreavey D, Sachdev V, Fananapazir L, Banks MK, Morris N, Djurickovic D, Devor-Henneman DE, Wei MH, Alvord GW, Gao B, Richardson JA, Minna JD, Rogawski MA, Lerman MI. Cerebellar

ataxia, seizures, premature death, and cardiac abnormalities in mice with targeted disruption of the Cacna2d2 gene. *Am J Pathol*. 2004;165:1007-1018

37.   Yamaguchi H, Hara M, Strobeck M, Fukasawa K, Schwartz A, Varadi G. Multiple modulation pathways of calcium channel activity by a beta subunit. Direct evidence of beta subunit participation in membrane trafficking of the alpha1C subunit. *J Biol Chem*. 1998;273:19348-19356

38.   Gregg RG, Messing A, Strube C, Beurg M, Moss R, Behan M, Sukhareva M, Haynes S, Powell JA, Coronado R, Powers PA. Absence of the beta subunit (cchb1) of the skeletal muscle dihydropyridine receptor alters expression of the alpha 1 subunit and eliminates excitation-contraction coupling. *Proc Natl Acad Sci U S A*. 1996;93:13961-13966

39.   Anderson ME. Calmodulin kinase and L-type calcium channels; a recipe for arrhythmias? *Trends Cardiovasc Med*. 2004;14:152-161

40.   Wu Y, MacMillan LB, McNeill RB, Colbran RJ, Anderson ME. CaM kinase augments cardiac L-type Ca^{2+} current: a cellular mechanism for long Q-T arrhythmias. *Am J Physiol*. 1999;276:H2168-2178

41.   Wu Y, Kimbrough JT, Colbran RJ, Anderson ME. Calmodulin kinase is functionally targeted to the action potential plateau for regulation of L-type Ca^{2+} current in rabbit cardiomyocytes. *J Physiol*. 2004;554:145-155

42.   Haase H, Kresse A, Hohaus A, Schulte HD, Maier M, Osterziel KJ, Lange PE, Morano I. Expression of calcium channel subunits in the normal and diseased human myocardium. *J Mol Med*. 1996;74:99-104

43.   Yang Y, Chen X, Margulies K, Jeevanandam V, Pollack P, Bailey BA, Houser SR. L-type Ca^{2+} channel alpha 1c subunit isoform switching in failing human ventricular myocardium. *J Mol Cell Cardiol*. 2000;32:973-984

44.   Hullin R, Asmus F, Ludwig A, Hersel J, Boekstegers P. Subunit expression of the cardiac L-type calcium channel is differentially regulated in diastolic heart failure of the cardiac allograft. *Circulation*. 1999;100:155-163

45.   Benitah JP, Gomez AM, Fauconnier J, Kerfant BG, Perrier E, Vassort G, Richard S. Voltage-gated Ca^{2+} currents in the human pathophysiologic heart: a review. *Basic Res Cardiol*. 2002;97 Suppl 1:I11-18

46.   Schroder F, Handrock R, Beuckelmann DJ, Hirt S, Hullin R, Priebe L, Schwinger RH, Weil J, Herzig S. Increased availability and open probability of single L-type calcium channels from failing compared with nonfailing human ventricle. *Circulation*. 1998;98:969-976

47.   Hullin R, Matthes J, von Vietinghoff S, Bodi I, Rubio M, D'Souza K, Friedrich Khan I, Rottlander D, Hoppe UC, Mohacsi P, Schmitteckert E, Gilsbach R, Bunemann M, Hein L, Schwartz A, Herzig S. Increased expression of the auxiliary beta2-subunit of ventricular L-type Ca^{2+} channels leads to single-channel activity characteristic of heart failure. *PLoS One*. 2007;2:e292

48.   Louch WE, Bito V, Heinzel FR, Macianskiene R, Vanhaecke J, Flameng W, Mubagwa K, Sipido KR. Reduced synchrony of Ca^{2+} release with loss of T-tubules-a comparison to Ca^{2+} release in human failing cardiomyocytes. *Cardiovasc Res*. 2004;62:63-73

49.   Gomez AM, Valdivia HH, Cheng H, Lederer MR, Santana LF, Cannell MB, McCune SA, Altschuld RA, Lederer WJ. Defective excitation-contraction coupling in experimental cardiac hypertrophy and heart failure. *Science*. 1997;276:800-806

50.   Benitah JP, Kerfant BG, Vassort G, Richard S, Gomez AM. Altered communication between L-type calcium channels and ryanodine receptors in heart failure. *Front Biosci*. 2002;7:e263-275

51.   Wang Y, Tandan S, Cheng J, Yang C, Nguyen L, Sugianto J, Johnstone JL, Sun Y, Hill JA. Ca^{2+}/calmodulin-dependent protein kinase II-dependent remodeling of Ca^{2+} current in pressure overload heart failure. *J Biol Chem*. 2008;283:25524-25532

52.   Christ T, Boknik P, Wohrl S, Wettwer E, Graf EM, Bosch RF, Knaut M, Schmitz W, Ravens U, Dobrev D. L-type Ca^{2+} current downregulation in chronic human atrial fibrillation is associated with increased activity of protein phosphatases. *Circulation*. 2004;110:2651-2657

53.   Gussak I, Brugada P, Brugada J, Wright RS, Kopecky SL, Chaitman BR, Bjerregaard P. Idiopathic short QT interval: a new clinical syndrome? *Cardiology*. 2000;94:99-102

54.   Antzelevitch C, Pollevick GD, Cordeiro JM, Casis O, Sanguinetti MC, Aizawa Y, Guerchicoff A, Pfeiffer R, Oliva A, Wollnik B, Gelber P, Bonaros EP, Jr., Burashnikov E, Wu Y, Sargent JD, Schickel S, Oberheiden R, Bhatia A, Hsu LF, Haissaguerre M, Schimpf R, Borggrefe M, Wolpert C. Loss-of-function mutations in the cardiac calcium channel underlie a new clinical entity characterized by ST-segment elevation, short QT intervals, and sudden cardiac death. *Circulation*. 2007;115:442-449

55.   Muth JN, Bodi I, Lewis W, Varadi G, Schwartz A. A Ca^{2+}-dependent transgenic model of cardiac hypertrophy: A role for protein kinase Calpha. *Circulation*. 2001;103:140-147

56.   Pahor M, Psaty BM, Alderman MH, Applegate WB, Williamson JD, Cavazzini C, Furberg CD. Health outcomes associated with calcium antagonists compared with other first-line antihypertensive therapies: a meta-analysis of randomised controlled trials. *Lancet*. 2000;356:1949-1954

57.   Kaplan P, Lehotsky J, Racay P. Role of sarcoplasmic reticulum in the contractile dysfunction during myocardial ischaemia and reperfusion. *Physiol Res*. 1997;46:333-339

58.   Franzini-Armstrong C. STUDIES OF THE TRIAD : I. Structure of the Junction in Frog Twitch Fibers. *J Cell Biol*. 1970;47:488-499

59.   Lai FA, Anderson K, Rousseau E, Liu QY, Meissner G. Evidence for a Ca^{2+} channel within the ryanodine receptor complex from cardiac sarcoplasmic reticulum. *Biochem Biophys Res Commun*. 1988;151:441-449

60.   Blayney LM, Lai FA. Ryanodine receptor-mediated arrhythmias and sudden cardiac death. *Pharmacol Ther*. 2009;123:151-177

61.   Marx SO, Gaburjakova J, Gaburjakova M, Henrikson C, Ondrias K, Marks AR. Coupled gating between cardiac calcium release channels (ryanodine receptors). *Circ Res*. 2001;88:1151-1158

62.   Eisner DA, Kashimura T, O'Neill SC, Venetucci LA, Trafford AW. What role does modulation of the ryanodine receptor play in cardiac inotropy and arrhythmogenesis? *J Mol Cell Cardiol*. 2009;46:474-481

63.   MacLennan DH, Abu-Abed M, Kang C. Structure-function relationships in Ca^{2+} cycling proteins. *J Mol Cell Cardiol*. 2002;34:897-918

64.   Gomez AM, Rueda A, Sainte-Marie Y, Pereira L, Zissimopoulos S, Zhu X, Schaub R, Perrier E, Perrier R, Latouche C, Richard S, Picot MC, Jaisser F, Lai FA, Valdivia HH, Benitah JP. Mineralocorticoid modulation of cardiac ryanodine receptor activity is associated with downregulation of FK506-binding proteins. *Circulation*. 2009;119:2179-2187

65.   Wehrens XH, Lehnart SE, Huang F, Vest JA, Reiken SR, Mohler PJ, Sun J, Guatimosim S, Song LS, Rosemblit N, D'Armiento JM, Napolitano C, Memmi M, Priori SG, Lederer WJ, Marks AR. FKBP12.6 deficiency and defective calcium release channel (ryanodine receptor) function linked to exercise-induced sudden cardiac death. *Cell*. 2003;113:829-840

66.   Marx SO, Reiken S, Hisamatsu Y, Jayaraman T, Burkhoff D, Rosemblit N, Marks AR. PKA phosphorylation dissociates FKBP12.6 from the calcium release channel (ryanodine receptor): defective regulation in failing hearts. *Cell*. 2000;101:365-376

67.   Brillantes AB, Ondrias K, Scott A, Kobrinsky E, Ondriasova E, Moschella MC, Jayaraman T, Landers M, Ehrlich BE, Marks AR. Stabilization of calcium release channel (ryanodine receptor) function by FK506-binding protein. *Cell*. 1994;77:513-523

68.   Lehnart SE, Huang F, Marx SO, Marks AR. Immunophilins and coupled gating of ryanodine receptors. *Curr Top Med Chem*. 2003;3:1383-1391

69.   Gyorke S, Stevens SC, Terentyev D. Cardiac calsequestrin: quest inside the SR. *J Physiol*. 2009;587:3091-3094

70.   Gyorke S, Terentyev D. Modulation of ryanodine receptor by luminal calcium and accessory proteins in health and cardiac disease. *Cardiovasc Res*. 2008;77:245-255

71.   Terentyev D, Viatchenko-Karpinski S, Valdivia HH, Escobar AL, Gyorke S. Luminal Ca^{2+} controls termination and refractory behavior of Ca^{2+}-induced Ca^{2+} release in cardiac myocytes. *Circ Res*. 2002;91:414-420

72.   Froemming GR, Ohlendieck K. Oligomerisation of Ca^{2+}-regulatory membrane components involved in the excitation-contraction-relaxation cycle during

postnatal development of rabbit skeletal muscle. *Biochim Biophys Acta*. 1998;1387:226-238

73.   Inesi G, Ebashi S, Watanabe S. Preparation of Vesicular Relaxing Factor from Bovine Heart Tissue. *Am J Physiol*. 1964;207:1339-1344

74.   Hovnanian A. SERCA pumps and human diseases. *Subcell Biochem*. 2007;45:337-363

75.   Inesi G, Prasad AM, Pilankatta R. The Ca^{2+} ATPase of cardiac sarcoplasmic reticulum: Physiological role and relevance to diseases. *Biochem Biophys Res Commun*. 2008;369:182-187

76.   Bers DM, Bassani JW, Bassani RA. Na^{+}-Ca^{2+} exchange and Ca^{2+} fluxes during contraction and relaxation in mammalian ventricular muscle. *Ann N Y Acad Sci*. 1996;779:430-442

77.   Bers DM, Eisner DA, Valdivia HH. Sarcoplasmic reticulum Ca^{2+} and heart failure: roles of diastolic leak and Ca^{2+} transport. *Circ Res*. 2003;93:487-490

78.   Periasamy M, Bhupathy P, Babu GJ. Regulation of sarcoplasmic reticulum Ca^{2+} ATPase pump expression and its relevance to cardiac muscle physiology and pathology. *Cardiovasc Res*. 2008;77:265-273

79.   MacLennan DH, Toyofuku T, Kimura Y. Sites of regulatory interaction between calcium ATPases and phospholamban. *Basic Res Cardiol*. 1997;92 Suppl 1:11-15

80.   Vafiadaki E, Papalouka V, Arvanitis DA, Kranias EG, Sanoudou D. The role of SERCA2a/PLN complex, Ca^{2+} homeostasis, and anti-apoptotic proteins in determining cell fate. *Pflugers Arch*. 2009;457:687-700

81.   Simmerman HK, Jones LR. Phospholamban: protein structure, mechanism of action, and role in cardiac function. *Physiol Rev*. 1998;78:921-947

82.   James P, Inui M, Tada M, Chiesi M, Carafoli E. Nature and site of phospholamban regulation of the Ca^{2+} pump of sarcoplasmic reticulum. *Nature*. 1989;342:90-92

83.   Asahi M, McKenna E, Kurzydlowski K, Tada M, MacLennan DH. Physical interactions between phospholamban and sarco(endo)plasmic reticulum Ca^{2+}-ATPases are dissociated by elevated Ca^{2+}, but not by phospholamban phosphorylation, vanadate, or thapsigargin, and are enhanced by ATP. *J Biol Chem*. 2000;275:15034-15038

84.   Xu A, Narayanan N. Reversible inhibition of the calcium-pumping ATPase in native cardiac sarcoplasmic reticulum by a calmodulin-binding peptide. Evidence for calmodulin-dependent regulation of the V(max) of calcium transport. *J Biol Chem*. 2000;275:4407-4416

85.   Narayanan N, Xu A, Virdee I. Interplay of Phospholamban in Calmodulin Control of Sarcoplasmic Reticulum Calcium Pump Function. *J Mol Cell Cardiol*. 2007;42:s37

86.   Xu A, Narayanan N. Purification, amino-terminal sequence and functional properties of a 64 kDa cytosolic protein from heart muscle capable of modulating calcium transport across the sarcoplasmic reticulum in vitro. *Mol Cell Biochem*. 1994;132:7-14

87.   Xu A, Hawkins C, Narayanan N. Phosphorylation and activation of the Ca^{2+}-pumping ATPase of cardiac sarcoplasmic reticulum by Ca^{2+}/calmodulin-dependent protein kinase. *J Biol Chem*. 1993;268:8394-8397

88.   Damiani E, Sacchetto R, Margreth A. Variation of phospholamban in slow-twitch muscle sarcoplasmic reticulum between mammalian species and a link to the substrate specificity of endogenous Ca^{2+}-calmodulin-dependent protein kinase. *Biochim Biophys Acta*. 2000;1464:231-241

89.   Schmitt JP, Kamisago M, Asahi M, Li GH, Ahmad F, Mende U, Kranias EG, MacLennan DH, Seidman JG, Seidman CE. Dilated cardiomyopathy and heart failure caused by a mutation in phospholamban. *Science*. 2003;299:1410-1413

90.   Haghighi K, Kolokathis F, Pater L, Lynch RA, Asahi M, Gramolini AO, Fan GC, Tsiapras D, Hahn HS, Adamopoulos S, Liggett SB, Dorn GW, 2nd, MacLennan DH, Kremastinos DT, Kranias EG. Human phospholamban null results in lethal dilated cardiomyopathy revealing a critical difference between mouse and human. *J Clin Invest*. 2003;111:869-876

91.   Haghighi K, Kolokathis F, Gramolini AO, Waggoner JR, Pater L, Lynch RA, Fan GC, Tsiapras D, Parekh RR, Dorn GW, 2nd, MacLennan DH, Kremastinos DT, Kranias EG. A mutation in the human phospholamban gene, deleting arginine 14, results in lethal, hereditary cardiomyopathy. *Proc Natl Acad Sci U S A*. 2006;103:1388-1393

92.   Periasamy M, Huke S. SERCA pump level is a critical determinant of Ca^{2+} homeostasis and cardiac contractility. *J Mol Cell Cardiol*. 2001;33:1053-1063

93.   Phillips RM, Narayan P, Gomez AM, Dilly K, Jones LR, Lederer WJ, Altschuld RA. Sarcoplasmic reticulum in heart failure: central player or bystander? *Cardiovasc Res*. 1998;37:346-351

94.   Narayanan N, Xu A. Phosphorylation and regulation of the Ca^{2+}-pumping ATPase in cardiac sarcoplasmic reticulum by calcium/calmodulin-dependent protein kinase. *Basic Res Cardiol*. 1997;92 Suppl 1:25-35

95.   Edman CF, Schulman H. Identification and characterization of delta B-CaM kinase and delta C-CaM kinase from rat heart, two new multifunctional Ca^{2+}/calmodulin-dependent protein kinase isoforms. *Biochim Biophys Acta*. 1994;1221:89-101

96.   Singh P, Salih M, Tuana BS. Alpha-kinase anchoring protein alphaKAP interacts with SERCA2A to spatially position Ca^{2+}/calmodulin-dependent protein kinase II and modulate phospholamban phosphorylation. *J Biol Chem*. 2009;284:28212-28221

97.   Maier LS, Zhang T, Chen L, DeSantiago J, Brown JH, Bers DM. Transgenic CaMKIIdeltaC overexpression uniquely alters cardiac myocyte Ca^{2+} handling: reduced SR Ca^{2+} load and activated SR Ca^{2+} release. *Circ Res*. 2003;92:904-911

98.   Netticadan T, Xu A, Narayanan N. Divergent effects of ruthenium red and ryanodine on Ca^{2+}/calmodulin-dependent phosphorylation of the Ca^{2+} release channel (ryanodine receptor) in cardiac sarcoplasmic reticulum. *Arch Biochem Biophys*. 1996;333:368-376

99.   Zhang T, Kohlhaas M, Backs J, Mishra S, Phillips W, Dybkova N, Chang S, Ling H, Bers DM, Maier LS, Olson EN, Brown JH. CaMKIIdelta isoforms differentially affect calcium handling but similarly regulate HDAC/MEF2 transcriptional responses. *J Biol Chem*. 2007;282:35078-35087

100.   Wehrens XH, Lehnart SE, Reiken SR, Marks AR. Ca^{2+}/calmodulin-dependent protein kinase II phosphorylation regulates the cardiac ryanodine receptor. *Circ Res*. 2004;94:e61-70

101.   Currie S. Cardiac ryanodine receptor phosphorylation by CaM Kinase II: keeping the balance right. *Front Biosci*. 2009;14:5134-5156

102.   Coronado R, Morrissette J, Sukhareva M, Vaughan DM. Structure and function of ryanodine receptors. *Am J Physiol*. 1994;266:C1485-1504

103.   Meissner G. Ryanodine receptor/Ca^{2+} release channels and their regulation by endogenous effectors. *Annu Rev Physiol*. 1994;56:485-508

104.   Huke S, Bers DM. Ryanodine receptor phosphorylation at Serine 2030, 2808 and 2814 in rat cardiomyocytes. *Biochem Biophys Res Commun*. 2008;376:80-85

105.   Xiao B, Zhong G, Obayashi M, Yang D, Chen K, Walsh MP, Shimoni Y, Cheng H, Ter Keurs H, Chen SR. Ser-2030, but not Ser-2808, is the major phosphorylation site in cardiac ryanodine receptors responding to protein kinase A activation upon beta-adrenergic stimulation in normal and failing hearts. *Biochem J*. 2006;396:7-16

106.   Wehrens XH, Marks AR. Altered function and regulation of cardiac ryanodine receptors in cardiac disease. *Trends Biochem Sci*. 2003;28:671-678

107.   Ikeda Y, Hoshijima M, Chien KR. Toward biologically targeted therapy of calcium cycling defects in heart failure. *Physiology (Bethesda)*. 2008;23:6-16

108.   Xiao B, Jiang MT, Zhao M, Yang D, Sutherland C, Lai FA, Walsh MP, Warltier DC, Cheng H, Chen SR. Characterization of a novel PKA phosphorylation site, serine-2030, reveals no PKA hyperphosphorylation of the cardiac ryanodine receptor in canine heart failure. *Circ Res*. 2005;96:847-855

109.   Yang D, Zhu WZ, Xiao B, Brochet DX, Chen SR, Lakatta EG, Xiao RP, Cheng H. Ca^{2+}/calmodulin kinase II-dependent phosphorylation of ryanodine receptors suppresses Ca^{2+} sparks and Ca^{2+} waves in cardiac myocytes. *Circ Res*. 2007;100:399-407

110.   Seidler T, Hasenfuss G, Maier LS. Targeting altered calcium physiology in the heart: translational approaches to excitation, contraction, and transcription. *Physiology (Bethesda)*. 2007;22:328-334

111.   Ai X, Curran JW, Shannon TR, Bers DM, Pogwizd SM. Ca^{2+}/calmodulin-dependent protein kinase modulates cardiac ryanodine receptor phosphorylation and sarcoplasmic reticulum Ca^{2+} leak in heart failure. *Circ Res*. 2005;97:1314-1322

112.   Yano M, Ono K, Ohkusa T, Suetsugu M, Kohno M, Hisaoka T, Kobayashi S, Hisamatsu Y, Yamamoto T, Noguchi N, Takasawa S, Okamoto H, Matsuzaki M. Altered stoichiometry of FKBP12.6 versus ryanodine receptor as a cause of abnormal Ca^{2+} leak through ryanodine receptor in heart failure. *Circulation*. 2000;102:2131-2136

113.   Wegener AD, Simmerman HK, Lindemann JP, Jones LR. Phospholamban phosphorylation in intact ventricles. Phosphorylation of serine 16 and threonine 17 in response to beta-adrenergic stimulation. *J Biol Chem*. 1989;264:11468-11474

114.   Xu A, Netticadan T, Jones DL, Narayanan N. Serine phosphorylation of the sarcoplasmic reticulum Ca^{2+}-ATPase in the intact beating rabbit heart. *Biochem Biophys Res Commun*. 1999;264:241-246

115.   Netticadan T, Temsah RM, Kawabata K, Dhalla NS. Sarcoplasmic reticulum Ca^{2+}/Calmodulin-dependent protein kinase is altered in heart failure. *Circ Res*. 2000;86:596-605

116.   Manolio TA, Cutler JA, Furberg CD, Psaty BM, Whelton PK, Applegate WB. Trends in pharmacologic management of hypertension in the United States. *Arch Intern Med*. 1995;155:829-837

117.   Group TAOaCftACR. Major outcomes in high-risk hypertensive patients randomized to angiotensin-converting enzyme inhibitor or calcium channel blocker vs diuretic: The Antihypertensive and Lipid-Lowering Treatment to Prevent Heart Attack Trial (ALLHAT). *Jama*. 2002;288:2981-2997

118.   Goodman LS, Gilman AG, Hardman JG, Limbird LE. *Goodman & Gilman's the pharmacological basis of therapeutics*. New York ; London: McGraw-Hill Medical Publishing Division; 2001.

119.   Arroyo AM, Kao LW. Calcium channel blocker toxicity. *Pediatr Emerg Care*. 2009;25:532-538; quiz 539-540

120.   Theodore M. *Human Pharmacology, molecular to clinical*. 1998.

121.   Thomos Andreoli CC, Robert Griggers, and Ivor Benjamin. Andreoli and Carpenter's Cecil essentials of medicine. 2007

122.   Hockerman GH, Peterson BZ, Johnson BD, Catterall WA. Molecular determinants of drug binding and action on L-type calcium channels. *Annu Rev Pharmacol Toxicol*. 1997;37:361-396

123.   Valdivia HH, Valdivia C, Ma J, Coronado R. Direct binding of verapamil to the ryanodine receptor channel of sarcoplasmic reticulum. *Biophys J*. 1990;58:471-481

124.   Sathish V, Xu A, Karmazyn M, Sims SM, Narayanan N. Mechanistic basis of differences in Ca^{2+}-handling properties of sarcoplasmic reticulum in right and left ventricles of normal rat myocardium. *Am J Physiol Heart Circ Physiol*. 2006;291:H88-96

CHAPTER TWO

CHRONIC L-TYPE CALCIUM CHANNEL BLOCKADE WITH VERAPAMIL CAUSES CARDIAC RYANODINE RECEPTOR REMODELING AND PREDISPOSITION TO HEART FAILURE IN THE RAT

2.1   Chapter Summary

Ca^{2+} influx into cardiomyocytes via L-type, dihydropyridine receptor (DHPR)-Ca^{2+} channels, is crucial for ryanodine receptor (RyR2)-mediated sarcoplasmic reticulum (SR) Ca^{2+} release and muscle contraction. DHPR blockers are frequently prescribed for cardiovascular disorders. However, patients on chronic DHPR blockade with verapamil have increased heart failure risk and the underlying mechanism is unknown. We investigated whether chronic DHPR blockade-induced changes in the expression and function of cardiac RyR2 and excitation-contraction (E-C) coupling contribute to cardiac pathogenesis. Adult rats received verapamil, 625 µg/h/kg, or vehicle for 4 weeks via implanted osmotic mini-pumps. Western blots of SR/heart homogenates showed significantly increased DHPR (~45%) and diminished RyR2 (~50%) protein levels in the verapamil-treated (VPL) group versus control (P<0.05). Cardiomyocyte Ca^{2+} imaging revealed >2-fold higher diastolic Ca^{2+} spark frequency, Ca^{2+} spark sites/cell, and diastolic Ca^{2+} wave incidence in VPL group. Depolarization-induced I_{Ca} was unchanged whereas the speeds of contraction and relaxation were diminished 30%-45% in cardiomyocytes from VPL rats. P-R intervals were prolonged and extra-systoles were more frequent in VPL rats. Ventricular arrhythmia thresholds were 15 times lower in perfused hearts and arrhythmias were inducible in 50% of VPL group versus 0% in control.   Chronic verapamil treatment elicits DHPR and RyR2 remodeling with impaired Ca^{2+}signalling, diastolic SR Ca^{2+} leak, breakdown of spatiotemporal synchrony and fidelity of E-C coupling, arrhythmogenesis and abnormal contractility. These findings reveal, for the first time, integrated mechanisms underlying cardiac abnormalities and heart failure due to chronic DHPR blockade.

2.2   Introduction

In the heart, L-type Ca^{2+} channels in the sarcolemma, known as "dihydropyridine receptors" (DHPRs), play a central role in initiating the molecular events underlying excitation-contraction (E-C) coupling giving rise to the heart beat. Cardiac E-C coupling begins with voltage activation and opening of DHPRs permitting the entry of small amount of Ca^{2+} into the cardiomyocytes. This Ca^{2+} entry triggers a large amount of Ca^{2+} release from sarcoplasmic reticulum (SR) through ryanodine receptors (RyRs) by a process known as "Ca^{2+}-induced Ca^{2+} release" (CICR).   The consequent rise in cytoplasmic Ca^{2+} activates the myofilaments and evokes muscle contraction [1]. Recent advances have provided great insights into the mechanistic framework and molecular events underlying Ca^{2+} signaling between the DHPR and RyR. The RyR is the crucial downstream Ca^{2+} signaling molecule most proximal to the DHPR in the cardiac E-C coupling process. In the heart, RyR activation is tightly controlled by DHPRs, where SR Ca^{2+} release is graded by the magnitude and duration of the DHPR current [2]. This RyR functional coupling to the DHPR via CICR is the cornerstone of the modern local control theory of cardiac E-C coupling [3].   In a dyadic junction or "a couplon" of the cardiomyocytes, DHPRs open and close stochastically upon depolarization, delivering a train of local Ca^{2+} pulses (Ca^{2+} sparklets) to the RyRs in the abutting SR terminal cisternae.   The stochastic activation of a cluster of RyRs from different couplons discharges Ca^{2+} sparks which represent the elementary Ca^{2+} release events. The Ca^{2+} sparks summate into a whole-cell Ca^{2+} transient that evokes contraction [1,4-6]. The fidelity

of intermolecular Ca^{2+} signaling between DHPRs and RyRs is essential for the maintenance of normal heart rhythm and contractile function [7, 8].

Given the crucial importance of DHPR-RyR communication in the cardiac E-C coupling process, it is not surprising that complete DHPR blockade is accompanied by immediate cessation of the heart beat[9]. Intriguingly, DHPR blockers are frequently prescribed for long-term treatment of cardiovascular disease such as hypertension, angina pectoris and arrhythmias [10-12]. Presumably, the DHPR current is only partially blocked by DHPR blockers in clinically used dose, which may cause an acute decrease in cardiac contractility by reducing the amount of CICR and Ca^{2+} transient. However, the long-term effects of partial blockade of DHPR Ca^{2+} signals on cardiac E-C coupling and contractile function are not yet understood. Moreover, recent large-scale clinical trials have suggested long-term treatment with DHPR blockers increases the risk of heart failure and incidence of cardiac arrhythmias [10]. The mechanisms underlying these pathogenic phenomena are not known. The present study was undertaken to investigate the impact of chronic, yet partial DHPR blockade using the cardiac selective DHPR blocker, verapamil, on E-C coupling events in the rat heart. Our findings show that derangement of RyR/DHPR stoichiometry and ensuing alterations in intermolecular Ca^{2+} signaling and functional properties of the RyR underlie the increased risk of heart failure and arrhythmia observed following long-term verapamil treatment.

2.3   Methods

An expanded methods section is available at appendix B.

2.3.1   Animals

Male Wistar rats weighing 190 to 210 g were randomly assigned to control and verapamil-treated (VPL) groups.   Verapamil was dissolved in distilled water and administrated at a rate of 625 µg/h/kg for 4 weeks via subcutaneously implanted osmotic mini-pumps (Model 2ML4; ALZET, Cupertino, CA).   Control rats received vehicle solution in similar manner.   Following 4-week verapamil treatment, the animals were sacrificed and the ventricular myocardium was used for experiments.   All procedures were approved by the Animal Use and Care Committee of The University of Western Ontario and followed the Guidelines for the Care and Use of Experimental Animals of the Canadian Council on Animal Care.

2.3.2   Western Immunoblotting and [³H] Ryanodine Binding Assay

The protein levels of DHPR (α1 subunit), RyR2, and its accessory protein FKBP12.6, as well as calsequestrin (SR Ca^{2+} storage protein) were determined by western immunoblotting utilizing specific antibodies as described previously [13, 14]. The Ca^{2+}-dependent, high-affinity [³H] ryanodine binding assay was performed as described by Jiang et al. [13]

2.3.3 Imaging of Ca^{2+} Sparks and Assessment of Contractile Function in Cardiomyocytes

Ventricluar myocytes from control and VPL rats were isolated as previously described [15]. Isolated cardiomyocytes were loaded with the Ca^{2+} indicator dye, fluo-4-AM and a wide-field digital fluorescence imaging system was used to image Ca^{2+} sparks following procedures described previously [16]. Steady-state Ca^{2+} transients were established by field stimulation of cardiomyocytes at 0.5 Hz. Subsequently, the stimulation was stopped to observe Ca^{2+} sparks and waves. The acquired images were Gaussian filtered using three-by-three pixels and baseline Ca^{2+} images were subtracted pixel by pixel using the equation $\Delta F/Fo$ (%) = 100 x [F(x,y,t) - Fo(x,y)]/ Fo(x,y), where F(x,y,t) was the fluorescence at each pixel in the time series and Fo was an image of the "baseline" level given by the average of ~50 consecutive images of the cell at rest in the absence of sparks. To assess contraction, bright field images of cardiomyocytes were acquired at 67 frames/s (Cascade Photometrics 650 CCD camera, Roper Scientific Inc., Tucson, Arizona). Off line analysis was used to determine cell length and the rate of contraction and relaxation (ImageMaster Software, version 5; Photon Technology International, New Jersey).

2.3.4 Measurement of L-type Ca^{2+} Current (I$_{Ca}$)

L-type Ca^{2+} current was recorded in isolated ventricular myocytes using the nystatin (300 μg/ml) perforated patch configuration. Patch pipettes were prepared on a Sutter Instrument Co. puller (Model P-87, CA) with an initial resistance of 2-3 MΩ. Currents were recorded at room temperature (21-24°C) using an Axopatch 200A

amplifier, with data filtered at 1 kHz and sampled at 5 kHz using pCLAMP 6.0.4 software. Cells were held at -40 mV to inactivate voltage-dependent Na^+ channels. Voltage-dependent Ca^{2+} currents were corrected assuming linear leak. Capacitance was determined for each cell by integrating the current elicited by a 10-mV hyperpolarizing command, and currents were normalized to cell capacitance (pA/pF). Test potentials were adjusted to account for series resistance error.

2.3.5   Cardiac Electrophysiological Studies

Standard six limb lead ECG recordings were obtained from anesthetized rats for a 10-minute period. Subsequently, the hearts were removed and mounted on a Langendorff apparatus and perfused with Tyrodes solution at 35±1°C. A fluid-filled, balloon-tipped catheter was inserted through the left atrium into the left ventricle to measure pressure. Bipolar silver electrodes were placed on the right atrial appendage and ventricular apex to record epicardial electrocardiograms. The atrioventricular (AV) interval, Wenckebach cycle length (WCL) and stimulation threshold to induce ventricular arrhythmias were determined, as described previously [17]. WCL was defined as the minimum cycle length that failed to conduct 1:1 through the AV node. Ventricular arrhythmias were identified as premature, wide QRS complexes with concomitant decreases in ventricular pressure.

2.3.6   Data Analysis

Data are presented as means ± SEM. Statistical significance was evaluated by the Student's t-test and Chi square test with $P<0.05$ indicating a significant difference.

2.4   Results

2.4.1   Chronic Verapamil Treatment of Rats Alters DHPR/RyR2 Stoichiometry in the Heart

Western blotting experiments using heart ventricular homogenates as well as isolated SR vesicles showed ~50% decrease in RyR2 protein levels in VPL rats, compared to control (Fig. 2.1A and Fig.2.1B). A similar decrease (~ 45%) in FKBP 12.6 protein level, an accessory protein of RyR2, in VPL compared to control rats was also observed (Fig. 2.1C). In contrast, DHPR protein level was increased significantly by ~45% in VPL compared to control rats (Fig.2.1D). A recent report also showed a similar increase in DHPR protein level in the mouse heart following verapamil treatment [18]. The relative amount of SR Ca^{2+} binding protein, calsequestrin, did not differ significantly between VPL rats (89±6 arbitrary units, n=9) versus control rats (76±7 arbitrary units, n=9). Therefore, calsequestrin served as an internal protein loading control in western blotting experiments. The above findings reflect a dramatic ~3 fold increase in the DHPR: RyR2 stoichiometry in the VPL group. No significant change was evident in the RyR2: FKBP 12.6 stoichiometry following VPL treatment.
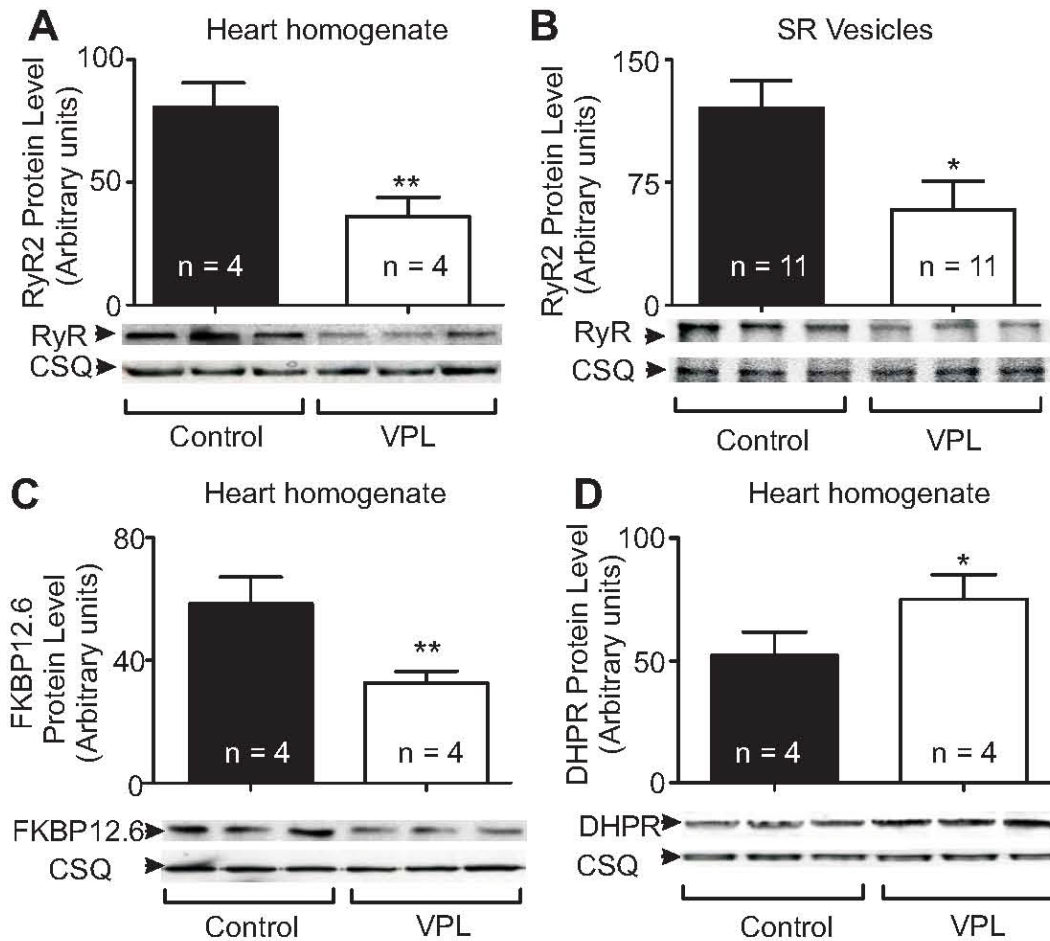
Fig. 2.1 Chronic verapamil treatment leads to alterations in the protein levels of cardiac RyR2, FKBP12.6 and DHPR. Identical amounts of ventricular homogenates (25 μg protein) and SR vesicles (25 μg protein) derived from control and verapamil-treated (VPL) rats were subjected to Western immunoblotting analysis. Bar graphs depict the relative amount of immunoreactive protein as determined by densitometry of Western blots, with n indicating the number of independent preparations. Representative immunoblots from three separate preparations each from control and VPL groups are shown at the bottom of the panels. Also shown are Western blots obtained by stripping and reprobing the same membrane for calsequestrin (CSQ), which served as an internal standard for equivalent protein loading. A, B, Immunoblotting for RyR2 of both purified SR vesicles and heart homogenate revealed that verapamil treatment caused significant decrease in RyR2. C, D, Levels of FKBP 12.6 were significantly decreased in VPL rats (C), whereas levels of DHPR were increased (D). Data represent means ± SEM. *$P<0.05$;**$P<0.01$ VPL *vs*. control. Note that the relative amount of CSQ did not differ between control and VPL rats (89±6 *vs*. 76±7 arbitrary unit, n=9 rats/group), validating this as an internal standard for equivalent protein loading.

2.4.2   Chronic Verapamil Treatment Alters [³H]-Ryanodine Binding to RyR2 in Cardiac SR Vesicles but Not Voltage-activated I_{Ca} in Cardiomyocytes

The plant alkaloid, ryanodine, binds preferentially to RyRs that are open, and changes in [³H]-ryanodine binding are thought to reflect changes in gating properties of RyRs [6, 12, 19, 20]. We examined the impact of altered DHPR:RyR2 stoichiometry on the gating properties of RyR2 at the subcellular level by determining Ca^{2+}-dependent, high affinity [³H]-ryanodine binding to RyR2 in isolated cardiac SR vesicles from VPL and control rats. Fig. 2.2A shows [³H]-ryanodine binding to RyR2 in SR vesicles from control and VPL rats as function of varying concentrations of ryanodine measured at saturating concentration of free Ca^{2+} (6.1 µmol/L). The level of specific [³H]-ryanodine binding was lower in VPL, compared with control. Scatchard plots of the data showed a homogenous population of binding sites; the maximum binding sites were significantly lower by ~35% in VPL group [B_{max} (fmol/mg protein): control 1284±128, VPL 846±80; $P<0.05$; n=7 rats /group]. This is consistent with the diminished RyR2 protein level observed (Fig. 2.1A and Fig. 2.1B). The dissociation constant (Kd) for [³H]-ryanodine binding was reduced significantly from 12.8±1.4 nmol/L in control to 7.7±1.3 nmol/L in the VPL group (n=7 rats /group, $P<0.01$). Thus, ryanodine binds to RyRs with apparently higher affinity in the VPL rats, suggesting increased RyR channel open probability. Analysis of Ca^{2+} dependence of [³H]-ryanodine binding to RyR2 at a saturating ryanodine concentration (25 nmol/L) showed no significant difference in the Ca^{2+} sensitivity of RyR2 in the control verses VPL [Fig. 2.2B; EC_{50} (µmol/L): control 0.22±0.03, VPL 0.27±0.05; n=8 rats /group].

Since chronic DHPR blockade in VPL rats was accompanied by increased DHPR protein expression in the heart, we directly measured L-type Ca^{2+} current (I_{Ca}) in cardiomyoctes isolated from VPL and control rats using the nystatin perforated configuration of patch clamp. Cells were held at -40 mV to inactvate Na^+ currents and stepped to various potentials. Depolarization initiated transient inward I_{Ca} that exhibited similar amplitudes and time courses in control and VPL myocytes (Fig. 2.2C). When peak current amplitude was corrected for cell capacitance to reveal current density, the current–voltage relationships of I_{Ca} were similar in control and VPL myocytes (Fig. 2.2D). Currents were corrected off-line for series resistance, accounting for the range of voltages within groups of cells. There was no significant difference in the peak inward current between the two groups. We confirmed that the voltage-activated currents were blocked in a concentration dependent manner by verapamil (not shown). Thus, the depolarization-induced I_{Ca} was not significantly altered in cardiomyocytes following chronic verapamil treatment of rats.
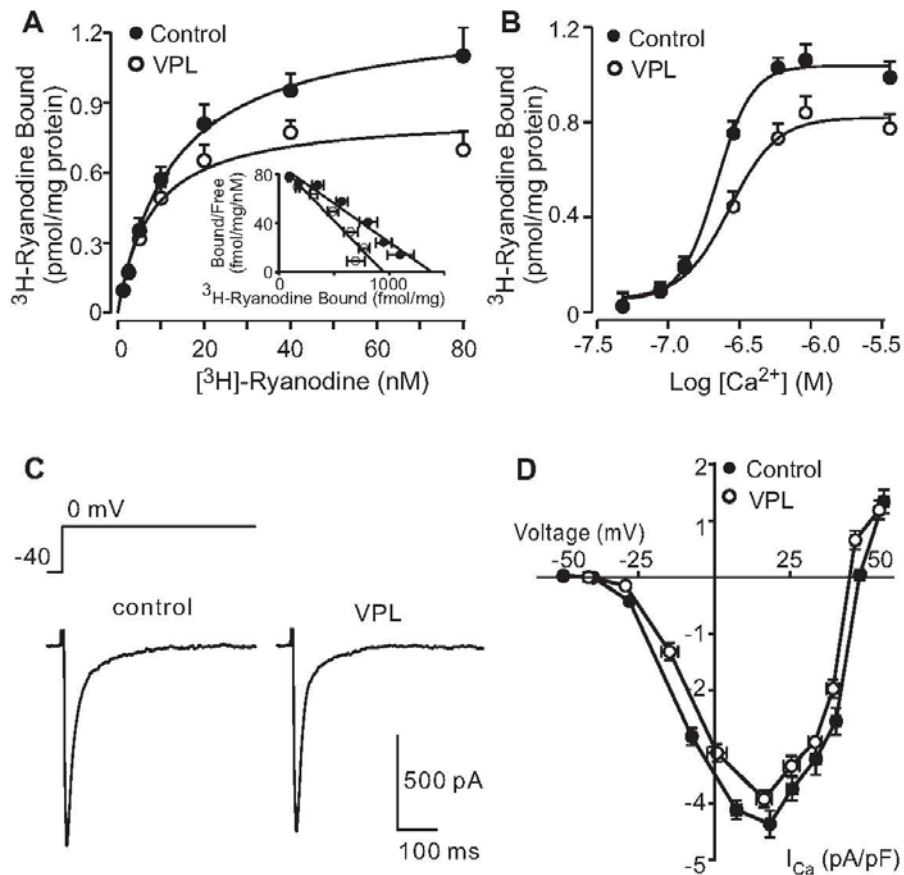
Fig.2.2 Chronic verapamil treatment alters high-affinity [³H]-ryanodine binding to cardiac RyRs but does not change DHPR Ca²⁺ currents. [³H]-ryanodine binding was evaluated in cardiac SR from control and VPL rats. DHPR Ca²⁺ currents (I_{Ca}) were examined in cardiomyocytes isolated from control and VPL rats using voltage-clamp in the perforated patch configuration. A, Saturation binding curves were generated in the presence of 6 µmol/L free Ca²⁺ at varying concentrations of [³H]-ryanodine. The data represent mean ± SEM with 7 separate SR preparations each from control and VPL rats. The decrease in Bmax in VPL rats is consistent with down-regulation of RyR. Inset: Linear scatchard plots of data indicate a homogenous population of binding sites (correlation coefficient: control, 0.99; VPL, 0.96) and increased binding affinity in VPL rats. B, Saturation binding curves generated in the presence of 25 nmol/L [³H]-ryanodine at varying free Ca²⁺ concentrations. There was a decrease in Bmax but no change apparent in EC_{50}. Data are means ± SEM of experiments using 8 separate SR preparations each from control and VPL rats. Smooth lines represent best fit using GraphPad Prism 4.0 software. C, Cells were held at -40 mV to inactivate Na⁺ currents. Depolarization initiated transient inward current that was similar in myocytes from control and VPL rats. D, Peak current amplitude was corrected for cell capacitance to reveal current density. The current-voltage relationships of calcium current in control cardiomyocytes (9 cells from 3 different preparations) and cardiomyocytes from VPL rats (9 cells from 2 different preparations) were similar. Currents were corrected off-line for series resistance, accounting for the range of voltages for groups of cells. There was no significant difference in the peak inward current between the two groups.

2.4.3   Chronic Verapamil Treatment Enhances Diastolic Ca^{2+} Spark Activity.

The ryanodine binding studies indicated altered RyR2 gating properties. To investigate the manifestation of these at the cellular level, we examined Ca^{2+} sparks by high speed fluorescence imaging of freshly isolated cardiomyocytes. Ca^{2+} sparks are the fundamental Ca^{2+} release events of RyRs and reveal Ca^{2+} release properties in situ [4-6]. Myocytes were field stimulated at 0.5 Hz until evoked Ca^{2+} transients had reached a steady state, which was evident as large, uniform changes in fluorescence intensity, illustrated as $\Delta F/Fo$ (%) (Fig. 2.3A,B, at left). Field stimulation was then stopped and Ca^{2+} levels were monitored for the next 20 to 23 s to reveal resting (diastolic) Ca^{2+} sparks, which are more apparent in the expanded traces at right (Fig. 2.3A, B). Ca^{2+} sparks in myocytes from control rats are infrequent, but did occur in spatially restricted regions as random, transient elevations of Ca^{2+} concentration. These are shown for three distinct spark sites in each cell, indicated in the bright field images of the myocytes at right for areas of interest of 10×10 pixels, 3.6 μm^2. Ca^{2+} sparks were defined as increases in $\Delta F/Fo$ (%) of greater than 5 % and duration of at least 5 frames (79 ms). The solitary nature of the Ca^{2+} sparks in control myocytes is evident in supplemental movie 1 in appendix C.

However, when this same protocol was applied to cardiomyocytes isolated from VPL rats, the number and amplitude of Ca^{2+} sparks during the rest period was markedly increased (Fig. 2.3B). The expanded traces illustrate three spark-active sites that show spontaneous Ca^{2+} sparks. Moreover, in the cell illustrated, a spontaneous Ca^{2+} wave arose (arrow in Fig. 2.3B, left; Ca^{2+} waves are considered in more detail in Fig. 6 below).

The marked increase in spark sites and spark frequency in myocytes of VPL rats is evident in supplemental movie 2 in appendix D. Ca^{2+} spark incidence was quantified from multiple cells from 3 rats in each group. The results summarized in Fig. 2.3C demonstrate that the number of spark sites per cell and the frequency of sparks per site per cell were significantly increased in VPL myocytes (Fig. 2.3C). Thus, live-cell imaging confirms the ryanodine binding data shown above, and provides complementary evidence for increased RyR open probability in VPL rats.

In addition to increased frequency, changes in the amplitude and kinetics of Ca^{2+} sparks were apparent in myocytes from VPL rats (Fig. 2.4). A typical spark observed in a control myocyte (Fig. 2.4A top) was brief and of relatively low amplitude. In contrast, the typical spark in a myocyte from a VPL rat (Fig. 2.4B top) was of longer duration and greater amplitude. Ca^{2+} fluorescence surface plots of whole cell (Fig. 2.4 bottom) show that sparks were spatially restricted and independent of each another. The typical spark of VPL rats spread further than that in control myocytes (Fig. 2.4, A2, B2). For the cell from the VPL rat illustrated, 4 sparks were observed during just one second of recording (panel 4B), whereas only 1 spark was ever detected in the control cell (Fig. 2.4A). We quantified these kinetic features from analyses of multiple cells from 3 rats from each group, and the mean values are summarized in Fig. 2.5. Spark amplitude was significantly higher in myocytes from VPL rats compared to control. In addition, the rate of rise and the time constant of decay were both increased in myocytes from VPL rats compared to control. Taking these features together, we determined the area under the curve (AUC) for diastolic Ca^{2+} sparks and found an increase of 380% in myocytes from VPL compared to those of control rats, indicating increased diastolic Ca^{2+} leak per spark.

While the mean data describing kinetic parameters showed significant changes, these parameters also markedly differed in their frequency distributions, with sparks of VPL rats exhibiting a broader distribution than sparks from control myocytes (supplemental Fig. 2.1). This indicates greater heterogeneity of RyR Ca^{2+} signaling in myocytes from VPL rats.
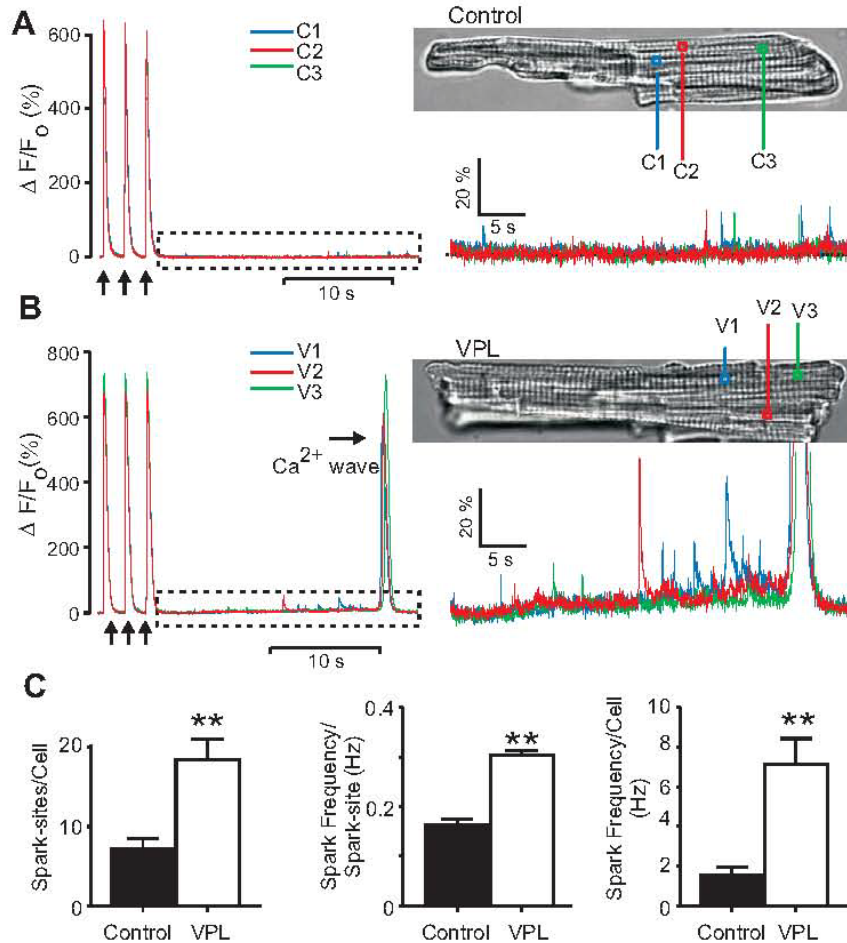
Fig. 2.3 Chronic verapamil treatment increases the frequency of Ca^{2+} sparks in resting cardiomyocytes. Myocytes were loaded with fluo-4 dye and observed using high-speed digital fluorescence imaging (Methods). A, B, Myocytes were stimulated at 0.5 Hz to elicit steady-state global Ca^{2+} transients (arrows below traces). Upon cessation of stimulation, Ca^{2+} sparks and waves were monitored. Fluorescence images of entire cells were collected at 67 frames per second. At left, the time course of fluorescence intensity of 3 active Ca^{2+} spark-sites, each shown in a different color, from a representative myocyte, each from a control (A) and a VPL rat (B). Spark sites (areas of interest of 10×10 pixels, 3.6 µm^2) are shown at right for each myocyte with bright field images. The recording areas were 127 x 24 µm. Ca^{2+} traces indicated by dashed rectangles are expanded at right, revealing the Ca^{2+} sparks that were spatially restricted. Control myocytes typically showed infrequent and small Ca^{2+} sparks, rising from stable baselines of Ca^{2+}. In contrast, myocytes from VPL rats exhibited greater spark frequency and amplitude, often accompanied by gradual rise in basal Ca^{2+} levels at spark sites. Ca^{2+} waves were also more frequently observed in myocytes of VPL rats compared to control (B, see right side of trace). C, Quantification of the number of spark-sites per myocyte, spark frequency corrected for number of spark sites, and spark frequency per myocyte in control and verapamil-treated (VPL) rats. Data are means ± SEM for 18 cells from 3 control rats, and 36 cells from 3 VPL rats. **$P < 0.01$ VPL *vs.* control.
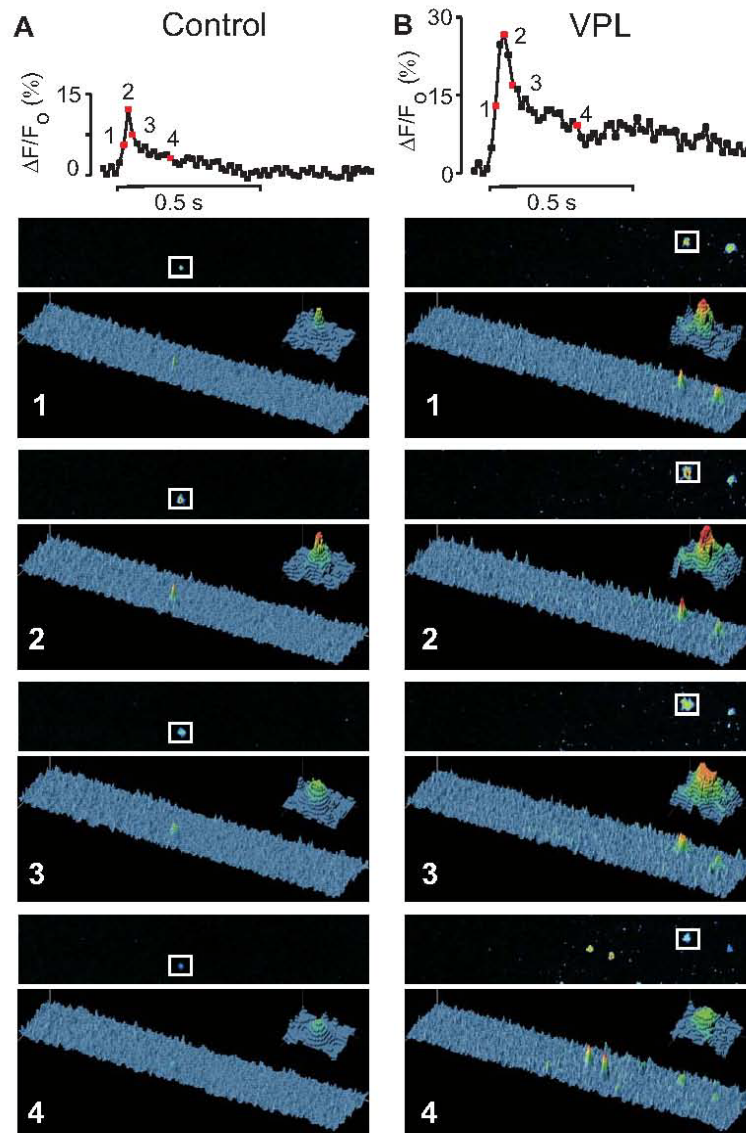
Fig. 2.4 High speed imaging of myocytes reveals the life time and spread of Ca^{2+} sparks. Typical Ca^{2+} sparks recorded from cardiomyocytes of control (A) and VPL (B) rats. Top: time course of fluorescence intensity of a typical spark. The Ca^{2+} spark is defined as an increase in ΔF /Fo of greater than 5% with duration at least 5 frames (79 ms). Labeled points in time course plot correspond to the images below. Each time is represented by two images: at top, pseudo-color image of cell with one spark site indicated by the box. At bottom: surface plots of the same cells show that spark-sites were spatially restricted and independent of each another. When sparks were peaked, the typical spark of VPL rats spread much wider than the typical spark in control cell (panel A2 and B2). During a spark period, 4 spark-sites were observed (panel B4) in this myocyte of a VPL rat, while only 1 spark-site was ever detected in the control myocyte. Insets are the expanded views of spark sites indicated by white boxes. The recording areas were 127 x 24 μm.
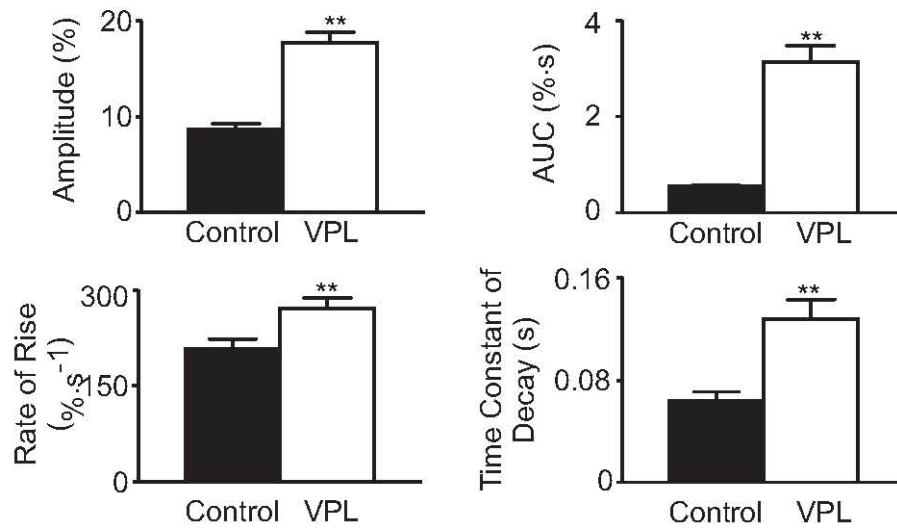
Fig. 2.5 Chronic verapamil treatment alters the kinetics of Ca^{2+} sparks in rat cardiomyocytes. Bar graphs show that Ca^{2+} spark amplitude, the area under the curve (AUC), rate of rise, and time constant of decay were all significantly increased in myocytes from VPL rats. Data presented are means ± SEM for 109 sparks each from 3 control rats and 3 VPL rats. **$P < 0.01$ VPL *vs*. control.
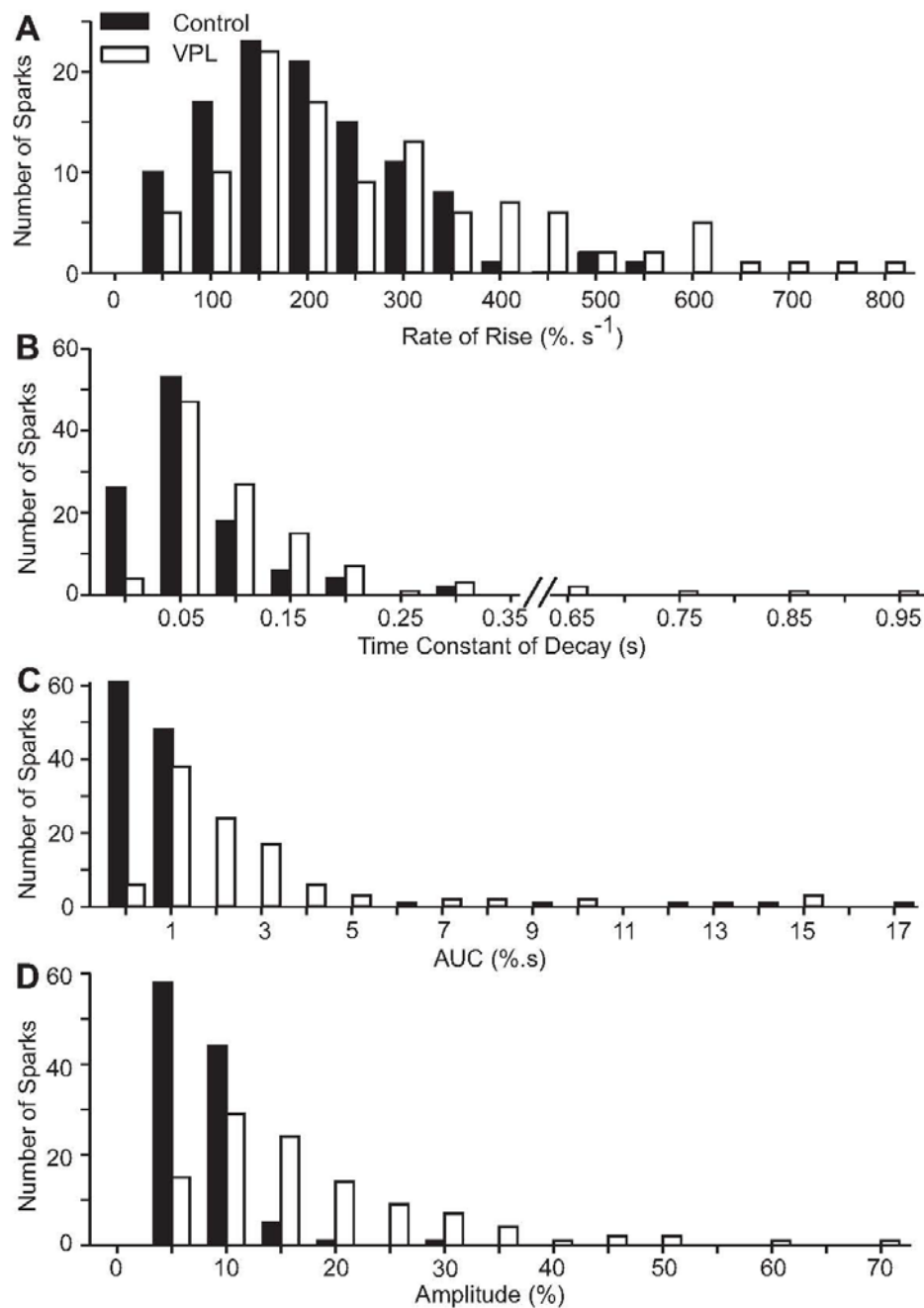
Suppl. Fig. 2.1 Increased heterogeneity of Ca²⁺ sparks kinetics in myocytes from verapamil treated rats. The frequency distribution of spark rising rate (A), time constant of decay (B), area under the curve (AUC, C), and amplitude (D) of Ca^{2+} sparks in myocytes isolated from the control and verapamil-treated (VPL) rats. Numbers of Ca^{2+} sparks were plotted as a function of the various spark parameters. Data are from 109 sparks each from 3 control rats and 3 VPL rats. Sparks monitored in myocytes from VPL rats exhibited a much broader distribution of kinetics compared to myocytes from control animals.

2.4.4 Chronic Verapamil Treatment Increases the Incidence of Ca^{2+} Waves in Resting Cardiomyocytes.

Ca^{2+} waves were apparent during the post-stimulus period in a fraction of the myocytes studied, often propagated along the entire cell (Fig. 2.6A, surface plot). Given that Ca^{2+} sparks underlie the propagation of Ca^{2+} waves [6, 4, 5, 21], we considered that the faster and greater Ca^{2+} release per spark in myocytes from VPL rats, might result in greater Ca^{2+} wave velocity. However, the average velocity of Ca^{2+} waves in the VPL group was not significantly different from that of control (Fig. 2.6B inset). Nevertheless, the incidence of Ca^{2+} waves in myocytes from VPL rats was significantly greater than those in cells from control rats (Fig. 2.6C). We examined whether the increased incidence of waves was associated with a greater frequency of sparks by separating cells from VPL rats into groups with or without waves. Indeed, spark frequency was significantly greater in those myocytes exhibiting Ca^{2+} waves compared to myocytes without waves (Fig. 2.6D), supporting the notion that increased spark frequency contributes to the increased incidence of Ca^{2+} waves.
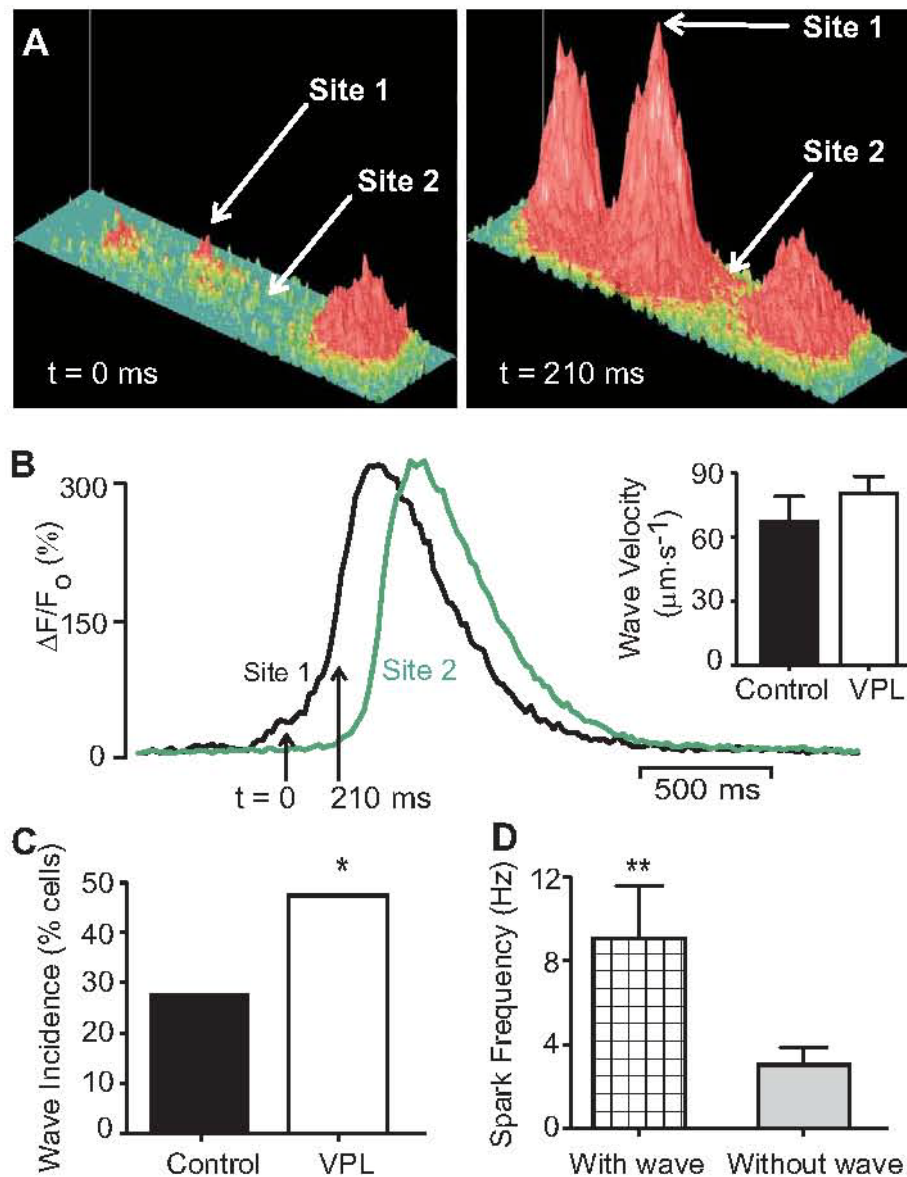
Fig. 2.6 Chronic verapamil treatment increases the incidence of Ca^{2+} waves in cardiomyocytes. A, Surface plots from a myocyte from a VPL rat show the initiation and propagation of Ca^{2+} waves. One wave started at site 1 and propagated to site 2 (a distance of 17.8 μm) over the course of 210 ms. B, Time course of changes of fluorescence intensity for sites 1 and 2 are plotted, clearly displaying the propagation of a Ca^{2+} wave. Inset: Ca^{2+} wave velocity was comparable in myocytes of control and VPL group (data are means ± SEM, n=21 waves from control and n=51 waves from VPL rats). C, However, there was an increased incidence of Ca^{2+} waves in myocytes from VPL rats compared to control (n=40 cells for control n=36 cells for VPL group, * *P*<0.05, χ^2-test). D, Myocytes that exhibited Ca^{2+} waves also had an increased spark frequency. Data presented are means ± SEM. **P*<0.01 myocytes isolated from VPL rats with waves (n=17 cells) *vs*. myocytes isolated from VPL rats without waves (n=19 cells).

2.4.5 Chronic Verapamil Treatment Reduces Speed of Cardiomyocyte Contraction and Relaxation.

To determine whether contractile properties of cardiomyocytes were altered following chronic verapamil treatment, isolated myocytes were stimulated at 0.5 Hz and contraction was monitored using high speed bright field imaging. Edge detection routines were applied to monitor changes of cell length during the contraction-relaxation cycle (Fig. 2.7A, left). A reduction in the instantaneous rate of contraction and relaxation was most apparent in VPL myocytes compared to control (Fig. 2.7A, right). Traces of contraction were normalized and overlapped to reveal slower rates of contraction and relaxation in myocytes from VPL rats (Fig. 2.7B). Normalized and superimposed traces of contraction reveal the slower rates of contraction in myocytes from VPL rats (Fig. 2.7B). When quantified from multiple preparations, the maximum instantaneous velocity ($-dL/dt_{max}$) and the average velocity of contraction were significantly reduced in myocytes from VPL rats (Fig. 2.7C). Although the maximum instantaneous velocity of relaxation ($+dL/dt_{max}$) did not change, the average relaxation velocity of myocytes from VPL rats was significantly reduced by ~20%, compared to control.
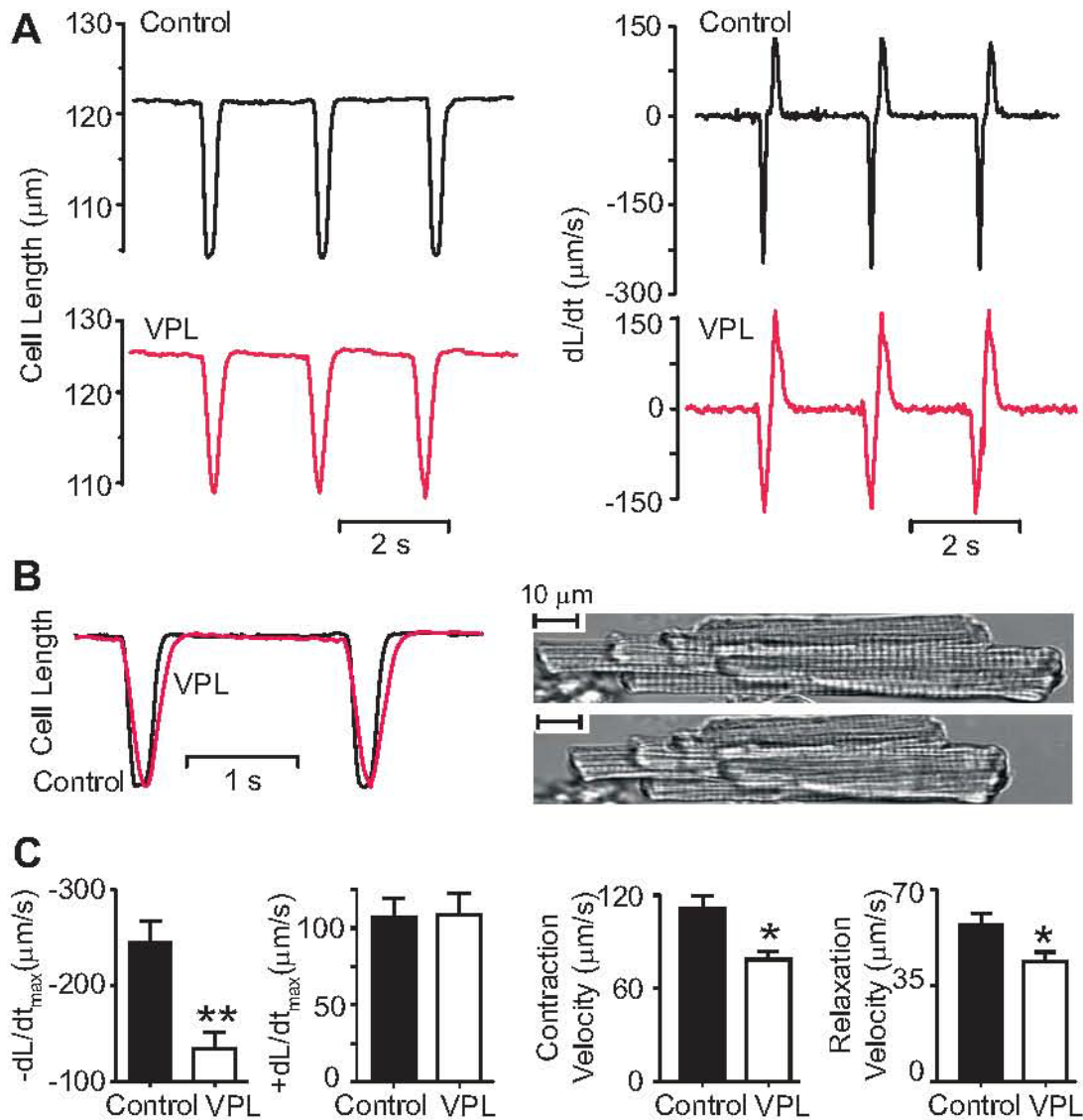
Fig. 2.7 Chronic verapamil treatment reduces the rate of contraction and relaxation of cardiomyocytes. A, Left: representative tracings of cell length (L) from ventricular myocytes of control and VPL rats, with contraction initiated using electrical field stimulation (0.5 Hz). Rate of change of length (dL/dt) is shown at right, representing the instantaneous velocity of the myocyte contracting and relaxing. B, normalized and superimposed traces reveal the slower contraction and relaxation speed in myocytes of VPL rats compared to control. At right, video frames illustrate images of a representative cardiomyocyte during one cycle, showing one typical contraction. C, Bar graphs show maximum instantaneous velocity of contraction (-dL/dt), maximum instantaneous velocity of relaxation (+dL/dt), average velocity of contraction, and average velocity of relaxation of myocytes from control and VPL rats. Each bar represents means ± SEM for 15 cells from 3 control rats, and 17 cells from 3 VPL rats. *$P<0.05$;**$P<0.01$ VPL *vs*. control.

2.4.6 Chronic verapamil treatment enhances susceptibility to ventricular arrhythmias

The findings described thus far have demonstrated the physiological consequences of chronic verapamil treatment at the molecular, subcellular and cellular levels manifested as divergent changes in DHPR/RyR2 protein expression and imbalance in macromolecular stoichiometry, pronounced diastolic SR Ca^{2+} leak and myocyte contractile dysfunction. To determine whether RyR2 remodeling caused functional changes manifested at higher levels, we examined cardiac function in isolated hearts and whole animals. ECG recordings of anaesthetized rats revealed premature ventricular contractions (PVCs) in 2 of 6 VPL rats, during a 10 minute observation period, whereas no PVCs were detected in any of 6 control rats (Fig. 2.8A). To rule out the possibility that circulating verapamil caused the higher incidence of PVC in vivo, we also recorded epicardial electrograms in isolated, perfused hearts. Notably, PVCs were observed in 2 of 6 isolated, spontaneously beating hearts from VPL rats, but none of 6 isolated control hearts (Fig. 2.8B). These observations indicate that chronic verapamil treatment increased the susceptibility to arrhythmia. To further verify this, we induced ventricular arrhythmia by electrical stimulation of isolated hearts. The stimulation threshold to induce arrhythmia in hearts from VPL rats was 36±7 µA, which was 15 times lower than that required for control hearts (553±112 µA; ** $P<0.01$, n=6 hearts per group) (Fig. 2.8C). The Wenckebach cycle length (WCL) was significantly prolonged (Fig. 2.8D), indicating reduced rate of atrioventricular (AV) nodal conduction [17]. This was confirmed by analysis of ECG traces, where P-R interval was found to be significantly increased in

VPL rats, compared to control (Fig. 2.8E). These data from the isolated heart and the whole animal indicate intrinsic electrophysiological remodeling following chronic verapamil treatment.
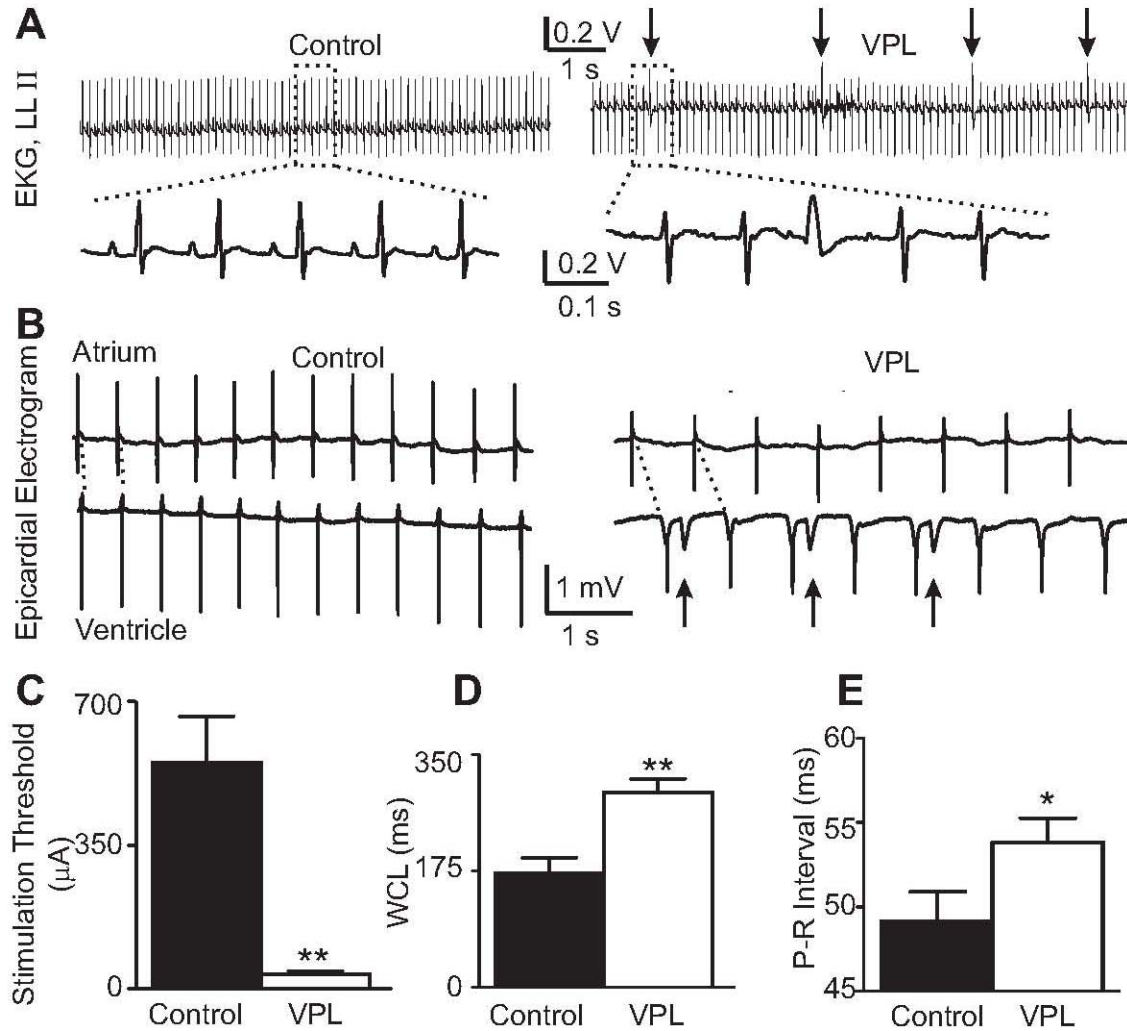
Fig. 2.8 Chronic verapamil treatment increases the susceptibility to ventricular arrhythmias in whole animals and isolated hearts. A, Original tracing of the surface limb lead II electrocardiogram (EKG, LLII) of a control and a VPL rat showing frequent premature ventricular contractions (PVCs, indicated by arrows) only in the VPL rat. Indicated regions are shown on an expanded scale below. Two of six VPL rats had PVCs within the 10 min baseline observation period after anaesthetization, whereas none of six control rats had PVCs using the same protocol. B, Typical recording of epicardial electrogram of isolated hearts from control and VPL rats, with upper sweeps atrial and lower sweeps ventricular cardiograms. Arrows indicate PVCs. C, Bar graph shows the electrical stimulation threshold to induce ventricular arrhythmias of control hearts was significantly reduced in hearts of VPL rats. D, The Wenckebach cycle length (WCL) was ~80% longer in hearts of VPL rats than in control. E, P-R intervals from surface EKG recordings was prolonged significantly in VPL rats compared to that of control. Values are means ± SEM. n=6 rats/group * $P<0.05$, **$P<0.01$ VPL *vs*. control.

2.5   Discussion

The results from the present study provide the first major insights into the impact of long-term verapamil treatment of rats, at a dose comparable to that used clinically in humans, on EC coupling events and heart function at various levels of organization, ranging from molecule to the whole organism. As discussed below, our findings have revealed an integrated framework of mechanistic events which likely underlie the predisposition to arrhythmia and heart failure upon chronic verapamil treatment.

2.5.1   Chronic Verapamil Treatment causes RyR Remodeling and Abnormal Gating Properties, Despite Uncompromised I_{Ca}

Divergent changes in the density of DHPR and RyR in cardiomyocytes, and the striking alterations in the intrinsic functional properties of RyR are the primary physiological consequences observed at the molecular level, ensuing chronic verapamil treatment of rats. The ~50% increase in DHPR density seen in the VPL group likely marks a physiological adaptation to compensate for the partial loss of functional DHPRs due to chronic verapamil blockade, thus ensuring the availability of an adequate number of functional trigger Ca^{2+} entry gates to initiate EC coupling. Indeed, this view is supported by our finding that voltage activation-induced peak I_{Ca} in cardiomyocytes is not compromised significantly due to verapamil treatment. Surprisingly, however, the compensatory up-regulation of DHPR density in cardiomyocytes of the VPL group was accompanied by a nearly similar magnitude (~ 45%) of down-regulation of RyR density. Such divergent changes in density of these two key molecular partners governing EC coupling would result in ~ 3-fold increase in the DHPR/RyR stoichiometry. Assuming

that the 45% increase in DHPR density matches the fraction of DHPRs rendered non-functional by verapamil treatment (an assumption supported by unaltered peak I_{Ca}), an ~ 2-fold increase in the ratio of functional DHPRs:RyRs can be discerned in the VPL group, compared to control. Tight local control of RyRs by DHPRs is central to the stability, fidelity and efficiency of E-C coupling in the heart. Local control is achieved mainly by co-localization of DHPRs and RyRs in a dyadic junction ("couplon") where single DHPR in the sarcolemma controls clusters of RyRs in the abutting SR terminal cisternae [22]. Individual units operate independently by virtue of spatial separation and of sheer Ca^{2+} gradients around channel pores generated upon channel opening [23]. Other factors acting in synergy to promote local control and stability include low intrinsic Ca^{2+} sensitivity of RyRs, high co-operativity of Ca^{2+}-dependent activation and use-dependent RyR inactivation [6, 24, 25]. Clearly, distortion in spatial coupling due to disarray in intermolecular spacing and misalignment of DHPRs and RyRs resulting from their stoichiometric imbalance would have predictable functional consequences, and these were evidenced by altered intrinsic properties of RyR and intermolecular DHPR-RyR signaling.

2.5.2 Evolution of Pathogenic RyRs, Hyperactive Spark Sites and Impaired Local Control

Diastolic Ca^{2+} sparks, although independent of DHPR current, are analogous to the Ca^{2+} sparks elicited by the I_{Ca} trigger [6, 24]. Therefore, the incidence and spatio-temporal characteristics of diastolic Ca^{2+} sparks in cardiomyocytes served as reliable indices in the assessment of alterations in intrinsic properties of RyR upon verapamil

treatment.   Paradoxically, despite a 45% decrease in the number of RyRs, cardiomyocytes from the VPL group exhibited significantly greater number of Ca^{2+} spark sites per cell as well as increased frequency of spark generation per site, when compared with cardiomyocytes from the control group.   In addition, striking differences were evident in the kinetics of Ca^{2+} sparks elicited by cardiomyocytes of the VPL group, compared with control. The sparks in cardiomyocytes of the control group (Fig. 2.4A) consisted of a rapid rising phase reflecting RyR opening, followed by a slow decay phase reflecting channel closure, features which conform to the typical Ca^{2+} spark pattern in normal cardiomyocytes [6, 24]. In contrast, sparks in cardiomyocytes of the VPL group (Fig. 2.4B) had a normal brief opening (rising phase) followed by a sub-conducting opening of longer duration, prolonging the spark decay phase. Also, typical Ca^{2+} sparks in cardiomyocytes of the VPL group had greater amplitudes suggesting recruitment of a relatively larger number of RyRs for each spark generated. In the normal cardiomyocyte, a single DHPR current triggers the opening of only a minor fraction of RyRs in a cluster of RyRs aligned in close proximity to that DHPR. Such local control of RyRs, coupled with the low intrinsic Ca^{2+} sensitivity and Ca^{2+}-dependent activation and use-dependent inactivation of RyRs [6, 24, 25] ensures the spatio-temporal confinement of Ca^{2+} sparks necessary for the efficient and orderly execution of E-C coupling.   Our findings demonstrating the incidence of high-frequency, high amplitude, long-lasting Ca^{2+} sparks, and relative abundance of hyperactive spark sites in cardiomyocytes of the VPL group, point to a pathogenic evolution of RyRs and dramatic weakening of the local control mechanism central to the fidelity, stability and efficiency of the E-C coupling process. Multiple factors may underlie this pathogenic evolution of RyRs.

(i)   Distortion in spatial coupling: The striking ~ 3-fold increase in DHPR/RyR ratio observed in cardiomyocytes of the VPL group clearly implies potential distortion in the spatial alignment and hence, spatial coupling, of these two molecular partners in E-C coupling. On the one hand, increased number of in DHPRs in cardiomyocytes in the VPL group necessitates diminished intermolecular spacing of DHPRs in the sarcolemma and T-tubules. On the other hand, decreased number of RyRs with concurrent paradoxical increase in hyperactive spark sites demands diminution in RyR cluster size coupled with greater intercluster distance and cluster dispersion in the junctional SR. Such disarray in intermolecular spacing and misalignment of DHPRs and RyRs would result in loss of local control leading to impaired E-C coupling, Ca^{2+} instability and heart failure. Indeed, loss of local control and dyssynchronous Ca^{2+} release due to structural abnormalities in the junctional SR Ca^{2+}cycling apparatus have been reported recently in studies using heart failure models. Thus, in the spontaneously hypertensive rat, increased spatial dispersion of T-tubules and orphaned ryanodine receptors were found to lead to a loss of local control and Ca^{2+} instability in heart failure [26]. Also, regional loss of T-tubules has been implicated in impaired Ca^{2+}cycling and cardiac dysfunction in tachycardia-induced heart failure [27]. Simultaneous imaging of T-tubules and Ca^{2+} sparks has also provided evidence supporting the derangement of T-tubule/RyR cluster spatial disposition in heart failure [28]. Furthermore, Ca^{2+} entry via routes other than DHPR, such as reverse mode Na^+/Ca^{2+} exchange [29] and T-type Ca^{2+} current [30], were found to be very inefficient in triggering Ca^{2+} release in cardiomyocytes exemplifying the importance of stringent DHPR-RyR proximity and spatial alignment for effective E-C coupling. It is noteworthy here that our morphological and histological

studies using cardiomyocytes and cardiac tissue sections from control and VPL groups showed no evidence of cardiac hypertrophy or fibrosis due to chronic verapamil treatment (see chapter 4). Therefore, the molecular remodeling of RyRs in the VPL group is not secondary to activation of hypertrophic signaling pathways, and change in myocyte size does not serve to compensate for divergent alterations in the population of DHPRs and RyRs in the VPL group to sustain their normal spatial alignment and functional integrity.

(ii)   Orphaned DHPRs and altered trigger Ca^{2+} intensity: The more dense packing of DHPRs in the sarcolemma and T-tubules, coupled with the greater dispersion of fewer RyR clusters of diminished cluster size in junctional SR, implies that a significant portion of DHPRs in the VPL group lacks spatially coupled RyR clusters, and thus becomes "orphaned". Since the peak trigger Ca^{2+} is not compromised in the VPL group, and given the diminished RyR cluster size, the intensity of DHPR current impacting on RyRs in the DHPR-coupled clusters can be seen to be of greater magnitude; this, in turn, should favor recruitment and activation of more RyRs resulting in the high amplitude Ca^{2+} sparks observed in the VPL group. The trigger Ca^{2+} emanating from orphaned DHPRs may cause untimely activation of RyRs in RyR clusters most proximal to them, and/or serve to prolong the open duration of RyRs by delaying Ca^{2+}-dependent inactivation. These phenomena may underlie the extended life-span of Ca^{2+} sparks and predisposition to arrhythmia observed in the VPL group.

(iii)   RyR phosphorylation status: Cardiac RyRs harbor multiple phosphorylation sites that undergo phosphorylation by PKA and CaMK [3, 20, 31-35]. Enhanced RyR phosphorylation by PKA has been proposed as a major impairment that

contributes to SR Ca^{2+} leak and diminished contractility in heart failure [31, 34, 36], this view, however, remains controversial [32, 37-39]. Growing evidence from several recent studies, on the other hand, implicates increased CaMK activity and hyper-phosphorylation of RyR in the pathogenesis of SR Ca^{2+} store depletion, contractile dysfunction and heart failure [40-43]. In this regard, our studies have revealed that chronic verapamil treatment results in significantly enhanced CaMK protein expression in the heart and this is accompanied by increased level of hyperactive, autophosphorylated CaMK as well as hyper-phosphorylated RyRs in the SR (see chapter 4). RyR phosphorylation by CaMK is known to result in increased RyR open probability augmenting Ca^{2+} leak [43, 44], and the PKA-mediated enhancement in SR Ca^{2+} leak is CaMK-dependent [35, 42, 43, 45]. Therefore, CaMK mediated hyperphosphorylation of RyRs may contribute, in part, to alterations in intrinsic functional properties of RyR reported here.

(iv)   Disruption of intermolecular interactions: In addition to phosphorylation by protein kinases, RyR function is influenced by its association with other proteins such as calmodulin and FKBP 12.6. Calmodulin serves to inhibit RyR Ca^{2+} release [46, 47] and RyR interaction with FKBP 12.6 serves to stabilize the channel in a subconductance state to minimize Ca^{2+} leak during diastole [48-50]. Conceivably, diminished RyR cluster size and increased RyR cluster dispersion (see ii above) as well as the down regulation of FKBP 12.6 (Fig. 2.1C) observed in the VPL group, may also impact adversely on RyR interactions with calmodulin and FKBP 12.6 leading to channel instability and enhanced diastolic Ca^{2+} leak. It is noteworthy that RyR phosphorylation has been shown to cause dissociation of FKBP 12.6 from RyR in some studies [31, 33, 34, 36] but not others [32, 38]. If such effect of phosphorylation is valid, the hyper-phosphorylation of RyR observed in the

VPL group would result in impaired FKBP association with RyR, consequent channel instability and enhanced Ca^{2+} leak. The co-ordinate down regulation of both RyR and FKBP 12.6 seen in the VPL group, however, may help to minimize such adverse impact on channel stability. It should be noted that FKBP interaction with RyRs is also implicated in maintaining normal intermolecular interactions between RyRs within the RyR cluster as well as between adjacent RyR clusters, and such intracluster and intercluster molecular signaling is considered vital to ensuring the stability of tight local control of E-C coupling [2, 24, 51].

2.5.3   Diminished SR Ca^{2+} Content and Increased Spark-Leak Paradox

The persistence of high-frequency, high amplitude diastolic Ca^{2+} sparks in cardiomyocytes of the VPL group can lead to diminished SR Ca^{2+} store, unless Ca^{2+} reuptake by the SR Ca^{2+}pump (SERCA2a) is concurrently enhanced to replenish the store. Results from our studies in this regard, have revealed significantly diminished SERCA2a activity (35%) and SERCA2a protein level (30%), as well as ~ 35% reduction in SR Ca^{2+} content in cardiomyocytes of the VPL group (see chapter 3) [52]. Dynamic decline in local Ca^{2+} in the SR is thought to aid in terminating Ca^{2+} sparks [53, 54] and excessive SR Ca^{2+} is thought to cause increased Ca^{2+} sparks incidence leading to regenerative Ca^{2+} release and arrhythmias [24, 51]. Thus, it appears paradoxical that chronic verapamil treatment results in increased Ca^{2+}sparks-leak incidence concomitant with diminished SR Ca^{2+} content. However, as reviewed and discussed elsewhere [5, 24], the influence of SR Ca^{2+} load on Ca^{2+} sparks-leak incidence and the underlying mechanisms remain controversial and uncertain. While multiple factors outlined in the preceding

discussion can contribute to the increased "spark-leak phenomenon" in cardiomyocytes of the VPL group, the mechanisms which permit the maintenance and operation of hyperactive spark sites in cardiomyocytes on a chronic basis in the phase of diminished SR Ca^{2+} content is perplexing. Increased Ca^{2+} spark frequency with decreased SR Ca^{2+} content in cardiomyocytes has also been observed by Song et al. [55] in severe but compensated canine left ventricular hypertrophy; and spatial heterogeneity in SR Ca^{2+} was suggested as a potential basis for this paradox. An analogous situation may prevail in cardiomyocytes of the VPL rats exhibiting increased "spark-leak phenomenon" concomitant with diminished SR Ca^{2+} content. Conceptually, the evolution of pathogenic RyRs and hyperactive spark sites in cardiomyocytes of VPL rats (noted earlier) can be seen to serve not only in generating a new steady state with diminished global SR Ca^{2+} content but also in the establishment of spatial heterogeneity of Ca^{2+} concentrations within the SR as well as in the on-going chronic operation of the hyperactive spark sites. For example, hyper activity of the pathogenic RyRs in the hyperactive spark sites while promoting excessive Ca^{2+} leak will also serve to set up concurrently an intralumenal Ca^{2+} gradient directed towards the hyperactive spark sites where a transient fall in Ca^{2+} concentration ensues from each burst of Ca^{2+} spark-leak. Thus, the hyperactive spark sites and the spark-leak phenomenon become self-sustaining. Noteworthy in this context is the recently reported experimental evidence showing that SR and nuclear envelope lumen are extensively interconnected in the cardiomyocyte forming a large Ca^{2+} store, and intrastore Ca^{2+} diffusion does occur [56]. Such expanded, interconnected spatial dimension of Ca^{2+} store and intrastore Ca^{2+} diffusion potential may serve to combat, albeit partially, SR Ca^{2+} store depletion and in turn, facilitate the establishment of a new

steady state with less than normal global SR Ca^{2+} content that still permits the occurrence of chronic and self-sustaining spark-leak phenomenon.

2.5.4 Predisposition to Arrhythmia and Heart Failure Ensues From Chronic Verapamil Treatment

Our findings with respect to the impact of chronic verapamil treatment at the organ and organism levels revealed predisposition to heart failure in the VPL group, characterized by greatly enhanced vulnerability to arrhythmias, prolonged PR interval, frequent incidence of PVCs and contractile dysfunction (Fig. 2.8). These manifestations of cardiac pathogenesis can be linked to the molecular remodeling embracing DHPR/RyR and consequent alterations in intermolecular Ca^{2+} signaling discussed earlier. For example, frequent occurrence of high amplitude diastolic Ca^{2+} sparks and consequent rise in cytosolic Ca^{2+} at resting membrane potential in the VPL group can activate inward Na^+/Ca^{2+} exchanger current in exchange for excess Ca^{2+}, which in turn can trigger delayed after depolarization leading to arrhythmias [24, 57]. This view is consistent with the incidence of Ca^{2+} waves and PVCs in cardiomyocytes of the VPL group (Fig. 2.8). Further, the spatial and temporal dyssynchrony of Ca^{2+} release events associated with DHPR/RyR remodeling as well as hyperphosphorylation of RyR likely serve to promote the occurrence of arrhythmia in the VPL group as noted earlier. It is noteworthy here that we have observed approximately 9% mortality of rats in the VPL group, but none in the control group. Fig. 2.9 illustrates the above findings and conceptual framework.
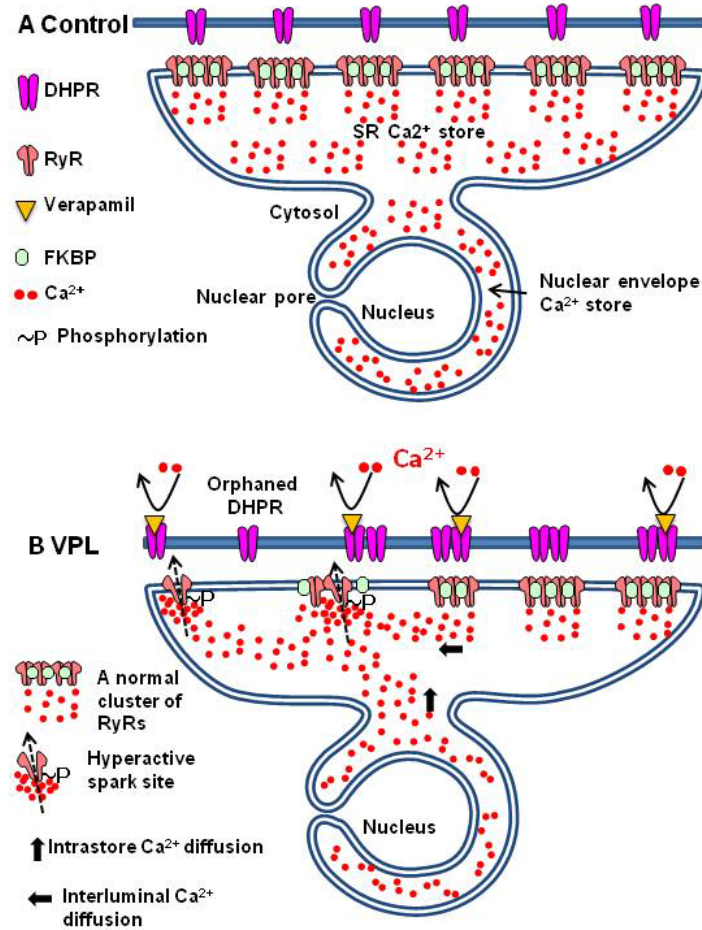
Fig 2.9 Conceptual framework of ryanodine receptor remodeling and spark-leak paradox in verapamil-treated rats. A, illustrates the normal condition where 1) the spatial alignment/coupling of DHPR-RyR ensures the fidelity and efficiency of intermolecular Ca^{2+} signalling and E-C coupling , 2) the SR and nuclear envelope lumen are extensively interconnected forming a large Ca^{2+} store to allow intrastore Ca^{2+} diffusion. B, illustrates that chronic verapamil treatment leads to: 1) a striking increase in DHPR/RyR ratio; 2) distorted DHPR-RyR spatial alignment/coupling; 3) emergence of orphaned DHPRs that lack spatially coupled RyR clusters; 4) increased RyR phosphorylation would result in impaired FKBP association with RyR; 5) altered functional properties of RyR (hyperactive spark sites, increased spark frequency and prolonged spark decay phase; and 6) diminished SR Ca^{2+} content and increased spark-leak paradox (Dynamic decreases in local Ca^{2+} in the SR is thought to aid in terminating Ca^{2+} sparks, and excessive SR Ca^{2+} hyper-activity of the pathogenic RyRs in the hyperactive spark sites while promoting excessive Ca^{2+} leak will also serve to set up concurrently an intralumenal Ca^{2+} gradient directed towards the hyperactive spark sites where a transient fall in the Ca^{2+} concentration ensues from each burst of Ca^{2+} spark-leak. Thus, the hyperactive spark sites and the spark-leak phenomenon become self-sustaining. Morever, intrastore Ca^{2+} diffusion from the nuclear envelope to the SR may serve to combat, albeit partially, SR Ca^{2+} store depletion.).

2.5.5   Conclusions and Clinical Implications

The results presented here demonstrate that long-term treatment of rats with the DHPR blocker, verapamil, causes divergent changes in cardiac DHPR/RyR protein expression and remodeling of RyR functional properties leading to impaired DHPR/RyR Ca^{2+} signaling, and high diastolic Ca^{2+} spark frequency and wave incidence in cardiomyocytes, culminating in predisposition to arrhythmias and heart failure. Surprisingly, this pathogenic remodeling of RyRs occurred in the absence of myocyte hypertrophy or fibrosis, and in the face of up-regulated DHPR density, uncompromised depolarization-induced $I_{Ca,}$ and decrements in RyR density as well as SR Ca^{2+} content. Tight local control of RyR function via DHPR-triggered Ca^{2+} signaling is central to the spatio-temporal confinement of RyR Ca^{2+} release events (Ca^{2+} spark incidence) and orderly execution of E-C coupling [2, 4, 5, 24]. Several factors including (a) derangements in DHPR/RyR spatial alignment and functional coupling, (b) adverse impact of RyR cluster dispersion and diminished RyR cluster size on the temporal integrity and efficiency of E-C coupling, (c) RyR hyper-phosphorylation and disruption of intermolecular interactions between RyRs and their regulatory proteins (e.g. FKBP 12.6, calmodulin), and (d) regional inhomogeneity of Ca^{2+} within the SR lumen and occurrence of self-sustaining hyperactive spark sites in the SR, may underlie the impaired local control and cardiac pathogenesis observed following chronic verapamil treatment. These findings have important physiological, patho-physiological and therapeutic implications. In the physiological context, our findings imply that normal DHPR/RyR stoichiometry and precise spatial alignment and juxtapositioning of these macromolecules are stringent

requirements for ensuring tight local control of intermolecular Ca^{2+} signaling, spatio-temporal synchrony of Ca^{2+} release events, and the integrity and fidelity of E-C coupling, and therefore, maintenance of normal heart rhythm. Consequently, deviation from normal DHPR/RyR stoichiometry will lead to disarray in spatial alignment of these macromolecules and impaired local control of intermolecular Ca^{2+} signaling, thus marking the onset of RyR remodeling and cardiac pathogenesis. The pathophysiological consequences of RyR remodeling, and ensuing impairments in DHPR/RyR Ca^{2+} signaling and E-C coupling, are manifested at the organ and organism levels as the enhanced vulnerability to arrhythmias and heart failure observed in the VPL group. Interestingly, evidence from large scale clinical trials has also revealed increased risk of heart failure and incidence of cardiac arrhythmias in patients following long-term treatment with DHPR blockers [10]. Thus, verapamil, a cardiac-selective DHPR blocker, used clinically as an anti-arrhythmic drug [12], turns out to be pro-arrhythmic over the long-term in both humans and animals. The findings reported in the present study provide the first major insights into an integrated frame-work of mechanistic events underlying cardiac pathogenesis due to chronic verapamil treatment. Since the present study examined the effects of chronic verapamil treatment in rats having no cardiovascular disease, it is uncertain whether a pre-existing disease background will alter the effects of verapamil. However, manifestation of same pathological outcome (arrhythmia and heart failure) following verapamil treatment in humans with disease background and in rats without disease background, suggests that underlying pathogenic mechanisms are likely similar. Additional studies using animal models with disease background (e.g. spontaneously hypertensive rat) may help to further corroborate this. However, multiple

etiological factors underlying cardiovascular disease may impact on observations and conclusions in studies using disease models. Moreover, assessment of the effects of verapamil in the absence of disease is essential to understand its influence on normal cardiac physiology and mechanisms of cardiac adaptation to drug intervention. Finally, in addition to urging caution in the conventional clinical use of DHPR blockers, our findings demonstrate that perturbations in DHPR/RyR communications by knock-out, knock-down, over-expression or under-expression of molecular players demand scrutiny in the design and deployment of therapeutic approaches for heart diseases.

2.6   References

1.   Bers DM. Cardiac excitation-contraction coupling. *Nature*. 2002;415:198-205

2.   Stern MD, Song LS, Cheng H, Sham JS, Yang HT, Boheler KR, Rios E. Local control models of cardiac excitation-contraction coupling. A possible role for allosteric interactions between ryanodine receptors. *J Gen Physiol*. 1999;113:469-489

3.   Bers DM. Macromolecular complexes regulating cardiac ryanodine receptor function. *J Mol Cell Cardiol*. 2004;37:417-429

4.   Wier WG, Balke CW. Ca^{2+} release mechanisms, Ca^{2+} sparks, and local control of excitation-contraction coupling in normal heart muscle. *Circ Res*. 1999;85:770-776

5.   Cheng H, Wang SQ. Calcium signaling between sarcolemmal calcium channels and ryanodine receptors in heart cells. *Front Biosci*. 2002;7:d1867-1878

6.   Cheng H, Lederer WJ, Cannell MB. Calcium sparks: elementary events underlying excitation-contraction coupling in heart muscle. *Science*. 1993;262:740-744

7.   Benitah JP, Kerfant BG, Vassort G, Richard S, Gomez AM. Altered communication between L-type calcium channels and ryanodine receptors in heart failure. *Front Biosci*. 2002;7:e263-275

8.   Gomez AM, Valdivia HH, Cheng H, Lederer MR, Santana LF, Cannell MB, McCune SA, Altschuld RA, Lederer WJ. Defective excitation-contraction coupling in experimental cardiac hypertrophy and heart failure. *Science*. 1997;276:800-806

9.   McCall D. Effect of verapamil and of extracellular Ca^{2+} and Na^+ on contraction frequency of cultured heart cells. *J Gen Physiol*. 1976;68:537-549

10.   Eisenberg MJ, Brox A, Bestawros AN. Calcium channel blockers: an update. *Am J Med*. 2004;116:35-43

11.   Peter Libby RB, Douglas Mann, Douglas Zipes, Eugene Braunwald. Braunwald's Heart Disease:A Textbook of Cardiovascular Medicine. 2008

12.   Das MK, Zipes DP. Antiarrhythmic and nonantiarrhythmic drugs for sudden cardiac death prevention. *J Cardiovasc Pharmacol*. 2010;55:438-449

13.   Jiang M, Xu A, Tokmakejian S, Narayanan N. Thyroid hormone-induced overexpression of functional ryanodine receptors in the rabbit heart. *Am J Physiol Heart Circ Physiol*. 2000;278:H1429-1438

14.   Jones DL, Narayanan N. Defibrillation depresses heart sarcoplasmic reticulum calcium pump: a mechanism of postshock dysfunction. *Am J Physiol*. 1998;274:H98-105

15.   Sathish V, Xu A, Karmazyn M, Sims SM, Narayanan N. Mechanistic basis of differences in Ca^{2+}-handling properties of sarcoplasmic reticulum in right and left ventricles of normal rat myocardium. *Am J Physiol Heart Circ Physiol*. 2006;291:H88-96

16.   Williams BA, Sims SM. Calcium sparks activate calcium-dependent Cl^- current in rat corpus cavernosum smooth muscle cells. *Am J Physiol Cell Physiol*. 2007;293:C1239-1251

17.   Rodenbaugh DW, Collins HL, Nowacek DG, DiCarlo SE. Increased susceptibility to ventricular arrhythmias is associated with changes in Ca^{2+} regulatory proteins in paraplegic rats. *Am J Physiol Heart Circ Physiol*. 2003;285:H2605-2613

18.   Schroder E, Magyar J, Burgess D, Andres D, Satin J. Chronic verapamil treatment remodels ICa,L in mouse ventricle. *Am J Physiol Heart Circ Physiol*. 2007;292:H1906-1916

19.   Coronado R, Morrissette J, Sukhareva M, Vaughan DM. Structure and function of ryanodine receptors. *Am J Physiol*. 1994;266:C1485-1504

20.   Meissner G. Ryanodine receptor/Ca^{2+} release channels and their regulation by endogenous effectors. *Annu Rev Physiol*. 1994;56:485-508

21.   Cheng H, Lederer MR, Lederer WJ, Cannell MB. Calcium sparks and $[Ca^{2+}]_i$ waves in cardiac myocytes. *Am J Physiol*. 1996;270:C148-159

22.   Franzini-Armstrong C, Protasi F, Ramesh V. Shape, size, and distribution of Ca^{2+} release units and couplons in skeletal and cardiac muscles. *Biophys J*. 1999;77:1528-1539

23.   Stern MD. Buffering of calcium in the vicinity of a channel pore. *Cell Calcium*. 1992;13:183-192

24.   Cheng H, Lederer WJ. Calcium sparks. *Physiol Rev*. 2008;88:1491-1545

25.   Sham JS, Song LS, Chen Y, Deng LH, Stern MD, Lakatta EG, Cheng H. Termination of Ca^{2+} release by a local inactivation of ryanodine receptors in cardiac myocytes. *Proc Natl Acad Sci U S A*. 1998;95:15096-15101

26.   Song LS, Sobie EA, McCulle S, Lederer WJ, Balke CW, Cheng H. Orphaned ryanodine receptors in the failing heart. *Proc Natl Acad Sci U S A*. 2006;103:4305-4310

27.   Balijepalli RC, Lokuta AJ, Maertz NA, Buck JM, Haworth RA, Valdivia HH, Kamp TJ. Depletion of T-tubules and specific subcellular changes in sarcolemmal proteins in tachycardia-induced heart failure. *Cardiovasc Res*. 2003;59:67-77

28.   Meethal SV, Potter KT, Redon D, Munoz-del-Rio A, Kamp TJ, Valdivia HH, Haworth RA. Structure-function relationships of Ca spark activity in normal and failing cardiac myocytes as revealed by flash photography. *Cell Calcium*. 2007;41:123-134

29.   Sham JS, Cleemann L, Morad M. Functional coupling of Ca^{2+} channels and ryanodine receptors in cardiac myocytes. *Proc Natl Acad Sci U S A*. 1995;92:121-125

30.   Sipido KR, Carmeliet E, Van de Werf F. T-type Ca^{2+} current as a trigger for Ca^{2+} release from the sarcoplasmic reticulum in guinea-pig ventricular myocytes. *J Physiol*. 1998;508 (Pt 2):439-451

31.   Marx SO, Reiken S, Hisamatsu Y, Jayaraman T, Burkhoff D, Rosemblit N, Marks AR. PKA phosphorylation dissociates FKBP12.6 from the calcium release channel (ryanodine receptor): defective regulation in failing hearts. *Cell*. 2000;101:365-376

32.   Xiao B, Jiang MT, Zhao M, Yang D, Sutherland C, Lai FA, Walsh MP, Warltier DC, Cheng H, Chen SR. Characterization of a novel PKA phosphorylation site, serine-2030, reveals no PKA hyperphosphorylation of the cardiac ryanodine receptor in canine heart failure. *Circ Res*. 2005;96:847-855

33.   Wehrens XH, Lehnart SE, Reiken SR, Marks AR. Ca^{2+}/calmodulin-dependent protein kinase II phosphorylation regulates the cardiac ryanodine receptor. *Circ Res*. 2004;94:e61-70

34.   Lehnart S, Marks AR. Regulation of ryanodine receptors in the heart. *Circ Res*. 2007;101:746-749

35.   Guo T, Zhang T, Mestril R, Bers DM. Ca^{2+}/Calmodulin-dependent protein kinase II phosphorylation of ryanodine receptor does affect calcium sparks in mouse ventricular myocytes. *Circ Res*. 2006;99:398-406

36.   Wehrens XH, Lehnart SE, Reiken S, Vest JA, Wronska A, Marks AR. Ryanodine receptor/calcium release channel PKA phosphorylation: a critical mediator of heart failure progression. *Proc Natl Acad Sci U S A*. 2006;103:511-518

37.   Xiao B, Sutherland C, Walsh MP, Chen SR. Protein kinase A phosphorylation at serine-2808 of the cardiac Ca^{2+}-release channel (ryanodine receptor) does not dissociate 12.6-kDa FK506-binding protein (FKBP12.6). *Circ Res*. 2004;94:487-495

38.   Jiang MT, Lokuta AJ, Farrell EF, Wolff MR, Haworth RA, Valdivia HH. Abnormal Ca^{2+} release, but normal ryanodine receptors, in canine and human heart failure. *Circ Res*. 2002;91:1015-1022

39.   Yang D, Zhu WZ, Xiao B, Brochet DX, Chen SR, Lakatta EG, Xiao RP, Cheng H. Ca^{2+}/calmodulin kinase II-dependent phosphorylation of ryanodine receptors suppresses Ca^{2+} sparks and Ca^{2+} waves in cardiac myocytes. *Circ Res*. 2007;100:399-407

40.   Currie S. Cardiac ryanodine receptor phosphorylation by CaM Kinase II: keeping the balance right. *Front Biosci*. 2009;14:5134-5156

41.   Ai X, Curran JW, Shannon TR, Bers DM, Pogwizd SM. Ca^{2+}/calmodulin-dependent protein kinase modulates cardiac ryanodine receptor phosphorylation and sarcoplasmic reticulum Ca^{2+} leak in heart failure. *Circ Res*. 2005;97:1314-1322

42.   Curran J, Hinton MJ, Rios E, Bers DM, Shannon TR. Beta-adrenergic enhancement of sarcoplasmic reticulum calcium leak in cardiac myocytes is mediated by calcium/calmodulin-dependent protein kinase. *Circ Res*. 2007;100:391-398

43.   Neef S, Dybkova N, Sossalla S, Ort KR, Fluschnik N, Neumann K, Seipelt R, Schondube FA, Hasenfuss G, Maier LS. CaMKII-dependent diastolic SR Ca^{2+} leak and elevated diastolic Ca^{2+} levels in right atrial myocardium of patients with atrial fibrillation. *Circ Res*. 2010;106:1134-1144

44.   Hain J, Onoue H, Mayrleitner M, Fleischer S, Schindler H. Phosphorylation modulates the function of the calcium release channel of sarcoplasmic reticulum from cardiac muscle. *J Biol Chem*. 1995;270:2074-2081

45.   Kockskamper J, Pieske B. Phosphorylation of the cardiac ryanodine receptor by Ca^{2+}/calmodulin-dependent protein kinase II: the dominating twin of protein kinase A? *Circ Res*. 2006;99:333-335

46.   Balshaw DM, Xu L, Yamaguchi N, Pasek DA, Meissner G. Calmodulin binding and inhibition of cardiac muscle calcium release channel (ryanodine receptor). *J Biol Chem*. 2001;276:20144-20153

47.   Yamaguchi N, Xu L, Pasek DA, Evans KE, Meissner G. Molecular basis of calmodulin binding to cardiac muscle Ca^{2+} release channel (ryanodine receptor). *J Biol Chem*. 2003;278:23480-23486

48.   Wehrens XH, Lehnart SE, Reiken SR, Deng SX, Vest JA, Cervantes D, Coromilas J, Landry DW, Marks AR. Protection from cardiac arrhythmia through ryanodine receptor-stabilizing protein calstabin2. *Science*. 2004;304:292-296

49.   Yano M, Kobayashi S, Kohno M, Doi M, Tokuhisa T, Okuda S, Suetsugu M, Hisaoka T, Obayashi M, Ohkusa T, Kohno M, Matsuzaki M. FKBP12.6-mediated

stabilization of calcium-release channel (ryanodine receptor) as a novel therapeutic strategy against heart failure. *Circulation*. 2003;107:477-484

50. Wehrens XH, Lehnart SE, Marks AR. Intracellular calcium release and cardiac disease. *Annu Rev Physiol*. 2005;67:69-98

51. Sobie EA, Guatimosim S, Gomez-Viquez L, Song LS, Hartmann H, Saleet Jafri M, Lederer WJ. The Ca^{2+} leak paradox and rogue ryanodine receptors: SR Ca^{2+} efflux theory and practice. *Prog Biophys Mol Biol*. 2006;90:172-185

52. Zhou J, Xu A, Chakrabarti S, Jones DL, Sims SM, Narayanan N. Remodelling of cardiac sarcoplasmic reticulum calcium pump and diastolic dysfunction ensue chronic L-type calcium channel blockade in the rat. *Circ Heart Fail*. 2010

53. Sobie EA, Dilly KW, dos Santos Cruz J, Lederer WJ, Jafri MS. Termination of cardiac Ca^{2+} sparks: an investigative mathematical model of calcium-induced calcium release. *Biophys J*. 2002;83:59-78

54. Terentyev D, Viatchenko-Karpinski S, Valdivia HH, Escobar AL, Gyorke S. Luminal Ca^{2+} controls termination and refractory behavior of Ca^{2+}-induced Ca^{2+} release in cardiac myocytes. *Circ Res*. 2002;91:414-420

55. Song LS, Pi Y, Kim SJ, Yatani A, Guatimosim S, Kudej RK, Zhang Q, Cheng H, Hittinger L, Ghaleh B, Vatner DE, Lederer WJ, Vatner SF. Paradoxical cellular Ca^{2+} signaling in severe but compensated canine left ventricular hypertrophy. *Circ Res*. 2005;97:457-464

56. Wu X, Bers DM. Sarcoplasmic reticulum and nuclear envelope are one highly interconnected Ca^{2+} store throughout cardiac myocyte. *Circ Res*. 2006;99:283-291

57. Bers DM. Altered cardiac myocyte ca regulation in heart failure. *Physiology (Bethesda)*. 2006;21:380-387

CHAPTER THREE

REMODELING OF CARDIAC SARCOPLASMIC RETICULUM CALCIUM PUMP AND DIASTOLIC DYSFUNCTION ENSUED FROM CHRONIC L-TYPE CALCIUM CHANNEL BLOCKADE WITH VERAPAMIL IN THE RAT

3.1   Chapter Summary

Depolarization-induced Ca^{2+} influx into cardiomyocytes via L-type Ca^{2+} channels (dihydropyridine receptor, DHPR) results in Ca^{2+}-induced Ca^{2+} release from sarcoplasmic reticulum (SR) via ryanodine receptors (RyRs) and promotes muscle contraction. Chronic DHPR blockade by verapamil is clinically beneficial to treat hypertension. Recent clinical trials, however, revealed increased risk of heart failure in patients undergoing chronic treatment with DHPR blockers. Our studies in a rat model showed RyR remodeling and systolic dysfunction as part of the underlining mechanism. Here we investigated whether chronic DHPR blockade impacts on diastolic function by influencing cardiac SR Ca^{2+}-ATPase (SERCA2) function responsible for Ca^{2+} sequestration and muscle relaxation. Adult rats received verapamil (625 µg/h/kg) or vehicle for 4 weeks *via* implanted osmotic mini-pumps. Western immunoblotting analysis showed diminished (~30%) SERCA2 level and increased (~25%) level of SERCA2 inhibitor, phospholamban in verapamil-treated (VPL) rats, compared with control. The rates of Ca^{2+} sequestration by SERCA2 also diminished significantly (~35%) in VPL rats without altering $K_{0.5}$ for Ca^{2+}. Intracellular Ca^{2+} imaging revealed several alterations in myocyte Ca^{2+} cycling in VPL rats compared to control: (a) prolonged twitch $[Ca^{2+}]_i$ decay; (b) elevated diastolic $[Ca^{2+}]_i$ at > 0.5 Hz stimulation frequency; (c) increased time to restore steady-state SR Ca^{2+} upon store depletion; (d) decreased SR Ca^{2+} content. Left ventricular function examined in isolated hearts and *in vivo* was compromised, with developed pressure reduced by ~30% and peak dP/dt reduced by 40-50% in VPL rats compared to control. In conclusion, SERCA remodelling and diastolic dysfunction ensue from chronic DHPR blockade.

3.2   Introduction

In cardiac excitation-contraction coupling (E-C coupling), the voltage-gated L-type Ca^{2+} channel (dihydropyridine receptor, DHPR) in the sarcolemma initiates the cardiac contraction-relaxation cycle by conversion of electrical signals into Ca^{2+} signals. The opening of DHPRs by depolarization of cardiomyocyte permits the influx of a small amount of Ca^{2+} into the cell to activate the ryanodine receptors (RyRs), resulting in a large amount of Ca^{2+} release from the sarcoplasmic reticulum (SR) by a process termed "Ca^{2+}-induced Ca^{2+} release" (CICR) [1]. The resulting Ca^{2+} transient activates the myofilaments and generates contraction. The subsequent return of cytosolic Ca^{2+} concentration to basal levels signals the beginning of diastole. Ca^{2+} sequestration back to the SR by sarco/endoplasmic reticulum Ca^{2+} ATPase (SERCA) accounts for 70 to 92% of cytosolic Ca^{2+} removal for relaxation and refills the SR for next contraction [1-3]. Therefore, the activity of SERCA is a major determinant for both cardiac diastolic and systolic function.

The DHPR Ca^{2+} signals are finely controlled to ensure intracellular Ca^{2+} homeostasis and proper cell contraction. Long-term enhancement of DHPR Ca^{2+} signaling by over-expressing DHPR in transgenic mice triggers Ca^{2+} imbalances and induces cardiac hypertrophy and dilatory remodeling [4]. However, the impact of chronic inhibition of DHPR Ca^{2+} signals on the heart is not clear. Long-term DHPR blocker treatment in patients represents a model of chronic inhibition of DHPR Ca^{2+} signals in the clinical setting. Recent large scale clinical trials have suggested long-term use of DHPR blockers increases the risk of heart failure and incidence of cardiac arrhythmias [5]. However, the mechanisms underlying this pathogenic phenomenon are not fully

explored. Therefore, it is imperative to investigate the impact of chronic inhibition of

DHPR Ca^{2+} signals on cardiac E-C coupling to fill the important gaps of knowledge in

physiology and clinical practice.

As DHPR Ca^{2+} signals orchestrate the RyR and the SERCA performance in E-C

coupling, we speculate that perturbations of DHPR Ca^{2+} signals will cause functional

adaptation of RyRs and SERCAs. Indeed, we have found that chronic inhibition of

DHPRs by cardiac selective DHPR blocker, verapamil, leads to molecular and functional

remodeling of RyRs and predisposes to arrhythmia. The present study investigated the

impact of chronic, yet partial DHPR blockade using verapamil on SERCA-related cardiac

E-C coupling events in rats. We demonstrate for the first time that remodeling of

SERCA and depression of heart function ensue from chronic, yet partial blockade of

DHPRs.

3.3   Methods

An expanded methods section is available at appendix B.

3.3.1   Animals.

Male Wistar rats weighing 190 to 210 g were randomly assigned to control and verapamil-treated (VPL) groups.   Verapamil was dissolved in distilled water and administrated at a rate of 625 µg/h/kg for 4 weeks via subcutaneously implanted osmotic mini pumps (Model 2ML4; ALZET, Cupertino, CA).   Control rats received vehicle solution in similar manner. All procedures were approved by the Animal Use and Care Committee of The University of Western Ontario and followed the Guidelines of the Canadian Council on Animal Care.

3.3.2   Western Immunoblotting And Ca^{2+} Uptake By SR Vesicles.

The protein levels of SERCA and its accessory protein PLN as well as calsequestrin (SR Ca^{2+} storage protein) were determined by western immunoblotting of isolated cardiac SR vesicles utilizing antibodies as described previously [6], [7].   ATP-dependent, oxalate-faciliated Ca^{2+} uptake by isolated cardiac SR vesicles was determined using Millipore filtration technique as described previously [8].

3.3.3   Cytosolic free Ca^{2+} Concentration ($[Ca^{2+}]_i$).

Myocytes were isolated from myocardium of control and VPL rats, and single cell twitch $[Ca^{2+}]_i$ transients were monitored at room temperature (25°C) during field stimulation of fura-2-loaded myocytes according to procedures described previously [8]. For some experiments, 10 mM caffeine was applied by pressure ejection from a micropipette to monitor SR Ca^{2+} fluxes.

3.3.4 Hemodynamic Studies in Langendorff Perfused Hearts and *in vivo*.

The procedures were followed essentially as described previously [9, 10]. Isolated hearts from control and VPL rats were perfused with normal Tyrodes solution at 10 ml min^{-1} at 35±1°C. A water-filled latex balloon, connected to a pressure transducer (COBE, Lakewood, CO, USA), was inserted into the left ventricle to continuously monitor isovolumic contractions. A pair of electrodes from a Grass S88 stimulator (Grass Instrument Inc., Quincy, MA, USA) was placed on the right atrial appendage to deliver trains of pulses for atrial pacing.

For *in vivo* assessment, a pressure-volume catheter (Scisense Inc., London, ON, Canada) was introduced into the left ventricles through the right carotid artery to record the hemodynamic parameters in anesthetized rats (Ketamine 70 mg/kg and Xylazine 5 mg/kg) from control and VPL groups. The catheter was connected to a pressure-volume control unit (Scisense Inc., London, ON, Canada) then to a strain-gauge amplifier (EMKA Technologies, France). Data were processed and analyzed by IOX Data Acquisition software (EMKA Technologies, France).

3.3.5 Statistical Analysis.

Results are presented as means ± SEM. Statistical significance was evaluated by the Student's t-test with $P < 0.05$ indicating a significant difference.

3.4   Results

3.4.1   Chronic verapamil treatment down-regulates SERCA expression.

We started from the molecular level to examine whether chronic DHPR blockade affects the protein level of SERCA. Western blotting experiments using isolated cardiac SR vesicles revealed that SERCA2, the cardiac isoform, was significantly reduced by ~30% in VPL rats compared to control (Fig. 3.1A). We also probed for PLN, which in its unphosphorylated state inhibits SERCA function [11]. In contrast to the change of the SERCA, the level of PLN was significantly increased by ~25% in VPL rats compared to control (Fig. 3.1B). Taken together, the protein ratio of SERCA2: PLN in VPL rats was reduced by ~ 40% compared to control (Fig.3.1C).
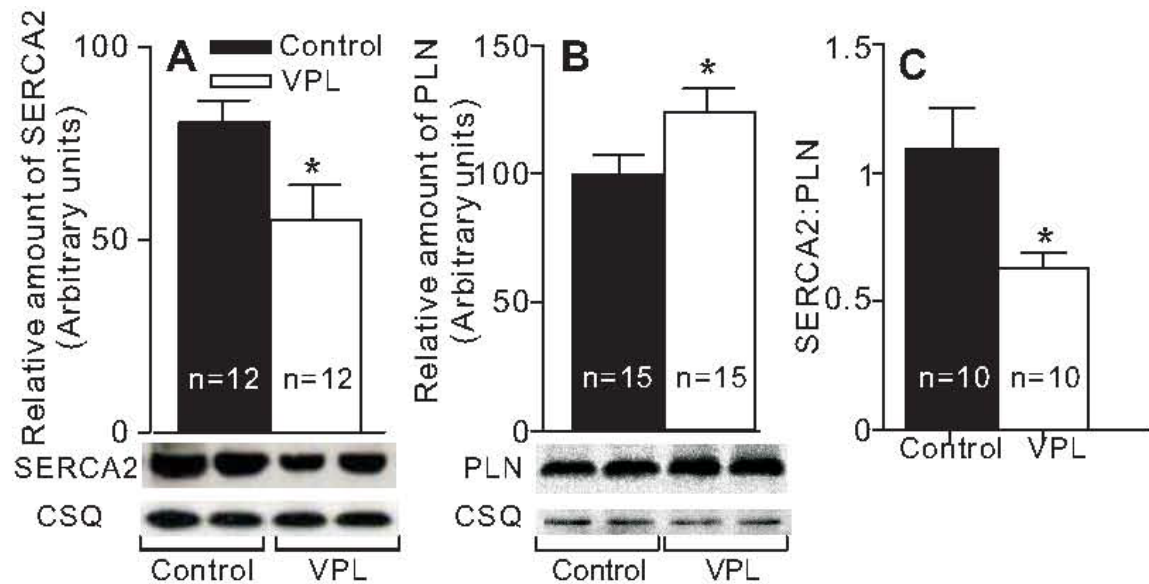
Fig. 3.1 Chronic verapamil treatment alters levels of cardiac SERCA2 and PLN. Cardiac SR vesicles were purified by density gradient centrifugation were obtained from control and verapamil-treated (VPL) rats then subjected to Western immunoblotting analysis. Bar graphs depict the relative amount of immunoreactive protein as determined by densitometry of Western blots, with n indicating the number of independent preparations. Representative immunoblots from four separate preparations are shown at the bottom of panels. Identical amounts of SR (25 µg protein) were applied in each lane. A, B, Immunoblotting for SERCA2 and PLN revealed that verapamil treatment caused significant decrease in SERCA2 and increase in PLN. To demonstrate equivalent loading conditions, membranes were stripped and reprobed for the SR protein calsequestrin (CSQ). C, Normalization of PLN immunoreactive protein level to SERCA2 immunoreactive protein level (SERCA2:PLN). Data represent means ± SEM. * *P* <0.05 VPL *vs.* control.

Note: CSQ was used as an internal protein-loading control as the relative amount of CSQ did not differ in control and VPL rats[12].

3.4.2 Chronic verapamil treatment reduces the rate of ATP-dependent Ca^{2+} uptake by cardiac SR vesicles.

We next examined SERCA function at the subcellular level by studying ATP-dependent Ca^{2+} uptake by cardiac SR vesicles. Compared to control, we observed reduced SR Ca^{2+} uptake from a saturating 8.2 μM free Ca^{2+} medium in VPL group (Fig. 3.2A). This depression of SR Ca^{2+} uptake activity was further reflected as reduced SR Ca^{2+} uptake rate over a wide range of Ca^{2+} concentrations (0.01 – 8.2 μM) (Fig. 3.2B). Quantification of the kinetic parameters from the data in Fig. 3.2B revealed that the maximum velocity of SR Ca^{2+} pumping (V_{max}) was significantly diminished by ~35% in the VPL rats compared to control, indicating reduced SR Ca^{2+} pump function (Fig. 3.2, Table 3.1). We did not observe significant changes in the apparent affinity of the Ca^{2+} pump for Ca^{2+} ($K_{0.5}$) between control and VPL rats.
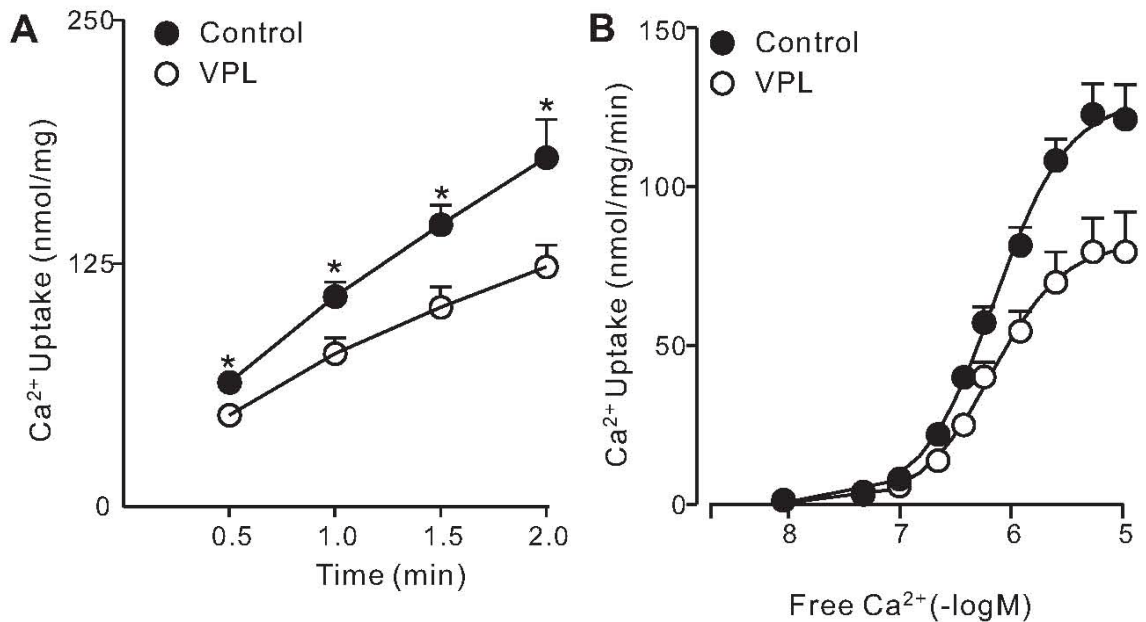
Fig. 3.2 Chronic verapamil treatment reduces the rate of ATP-dependent Ca^{2+} uptake by cardiac SR vesicles. A, Time course of ATP-dependent Ca^{2+} uptake by cardiac SR vesicles from control and VPL rats. Ca^{2+} uptake rates were examined at a saturating free Ca^{2+} concentration of 8.2 µM. Values represents mean ± SEM, n=10/group. *$P < 0.05$ *vs.* control. B, Effects of varying Ca^{2+} concentration of the incubation medium on ATP-dependent Ca^{2+} uptake by cardiac SR vesicles from control and VPL rats. The data represent means ± SEM, n=13/group. Kinetic parameters of Ca^{2+} transport derived from these data (B) are summarized in Table 3.1.

Table 3.1 Kinetic parameters of Ca^{2+} transport by cardiac SR from control and verapamil-treated rats.

	Control	Verapamil
Vmax (nmol Ca^{2+}/mg protein/min)	129 ± 10	84 ± 11 *
K$_{0.5}$ (µM) Control	1.3 ± 0.2	1.4 ± 0.3
n_H	1.4 ± 0.1	1.5 ± 0.3

Values are means ± SEM.; n=13/group. Vmax, maximum velocity of Ca^{2+} uptake; K$_{0.5}$, Ca^{2+} concentration giving one-half of Vmax ; n_H, Hill coefficient. *$P < 0.05$ *vs.* control.

3.4.3 Chronic verapamil treatment reduces the decay rate of twitch [Ca^{2+}]$_i$ transients in cardiomyocytes

In rat cardiomyocytes, it is estimated that SERCA accounts for 92% of the removal of cytosolic Ca^{2+}, contributing to the decline of twitch [Ca^{2+}]$_i$ transients [2]. Therefore, we examined the decay kinetics of twitch [Ca^{2+}]$_i$ transients, by stimulating isolated myocytes at 0.5 Hz (Fig. 3.3A). When transients were normalized to same height and superimposed, slower decline of twitch [Ca^{2+}]$_i$ transients was evident in myocytes isolated from VPL rats (VPL myocytes) compared to control (Fig. 3.3B). To quantify this, we fitted the decline of twitch [Ca^{2+}]$_i$ transients with a single exponential decay equation. Quantification of 45 cells each from 8 control and 8 VPL rats revealed that the time constant (τ) of decay in the VPL group was significantly longer than that of control (Fig. 3.3C).
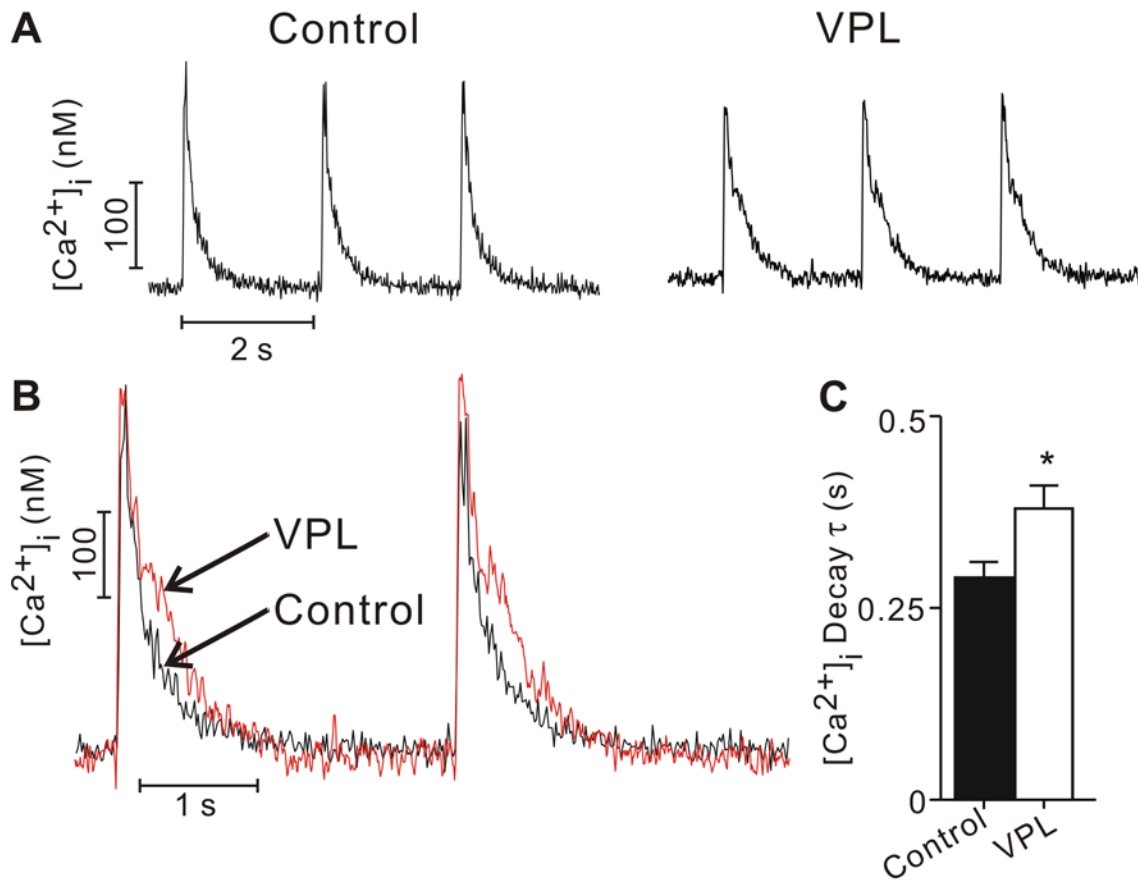
Fig. 3.3 Chronic verapamil treatment slows twitch $[Ca^{2+}]_i$ transient decline in cardiomyocytes.

Cytosolic free Ca^{2+} concentration ($[Ca^{2+}]_i$) was monitored by microspectrofluorimetry of fura-2-loaded cardiomyocytes. A, Representative steady-state twitch $[Ca^{2+}]_i$ transients of myocytes from VPL rats (VPL myocytes) and control rats (control myocytes) under field-stimulation of 0.5 Hz. B, Normalized and superimposed twitch $[Ca^{2+}]_i$ transients from A reveal apparent slower decay in VPL group. C, The decay of twitch $[Ca^{2+}]_i$ transient was well fit into a single exponential decline equation. The time constant of decay (τ) was significantly prolonged in VPL myocytes compared to control. Data represent means ± SEM for 45 cells each from 8 control and 8 VPL rats.

3.4.4   Chronic verapamil treatment elevates diastolic $[Ca^{2+}]_i$ and reduces twitch $[Ca^{2+}]_i$ transients.

Prolongation of twitch $[Ca^{2+}]_i$ transients reflects altered Ca^{2+} handling. We also noted that the amplitude of transients ($\Delta[Ca^{2+}]_i$, the difference between the systolic and diastolic $[Ca^{2+}]_i$) was changed. To further characterize this change, we examined twitch $[Ca^{2+}]_i$ transients in myocytes under a range of stimulation frequencies (Fig. 3.4A). $\Delta[Ca^{2+}]_i$ of VPL myocytes was generally smaller than that in control myocytes (Fig. 3.4B, left panel). During stimulation, the diastolic $[Ca^{2+}]_i$ in control rats effectively recovered to resting levels, reflecting efficient SERCA function. In contrast, during stimulation of VPL myocytes, the diastolic levels remained above resting levels at all frequencies (Fig. 3.4A). Diastolic levels of VPL myocytes were significantly greater than those of control myocytes at 0.5 Hz and higher frequencies (Fig. 3.4B, middle panel). When steady-state systolic $[Ca^{2+}]_i$ was measured, the levels were reduced in VPL myocytes at 0.25 Hz, unchanged at 0.5, 0.75, 1 Hz, but significantly higher at 2 Hz compared to those of control myocytes (Fig. 3.4B, right panel).
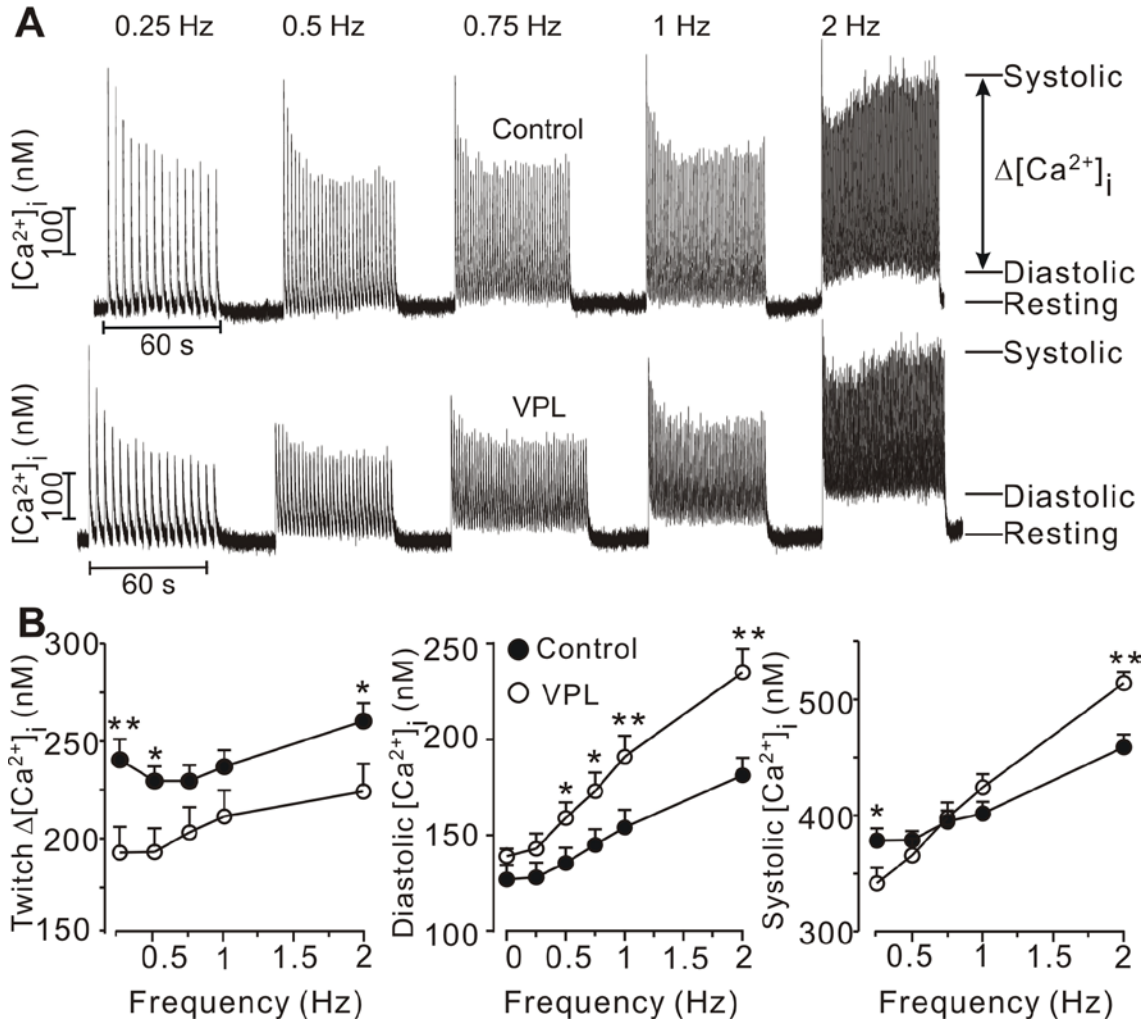
Fig. 3.4 Chronic verapamil treatment alters frequency-dependent changes of twitch $[Ca^{2+}]_i$ transients in cardiomyocytes. A, Typical recordings of twitch $[Ca^{2+}]_i$ transients from control and VPL myocytes show the experimental protocol for studying frequency-dependent alterations of twitch $[Ca^{2+}]_i$ transients. Myocytes were field-stimulated at frequencies from 0.25 Hz to 2 Hz. Stimulation lasted for ~ 60 s at one frequency then stopped for 30 s before being resumed at the next higher frequency. B, Quantification of diastolic, systolic $[Ca^{2+}]_i$ and the size of twitch $[Ca^{2+}]_i$ transient ($\Delta[Ca^{2+}]_i$). Data represent means ± SEM. n=18 cells from 4 control rats and 17 cells from 4 VPL rats. * $P < 0.05$, ** $P < 0.01$ *vs.* control.

3.4.5 Time-course of recovery from caffeine-induced SR Ca^{2+} depletion in cardiomyocytes.

The time to restore steady-state twitch $[Ca^{2+}]_i$ transients following caffeine-induced depletion of SR Ca^{2+} stores was used to evaluate the orchestration of SR Ca^{2+} cycling proteins to recover SR Ca^{2+} content. With continuous field stimulation to elicit twitch $[Ca^{2+}]_i$ transients, myocytes were treated with caffeine (10 mM) to empty the SR Ca^{2+} stores. VPL myocytes took strikingly longer time to restore steady-state twitch $[Ca^{2+}]_i$ transients than control cells (Fig. 3.5A). When quantified in 48 cells from 9 control and 60 cells from 9 VPL rats, the time to recover was ~50% longer in VPL compared to control myocytes (Fig. 3.5B).
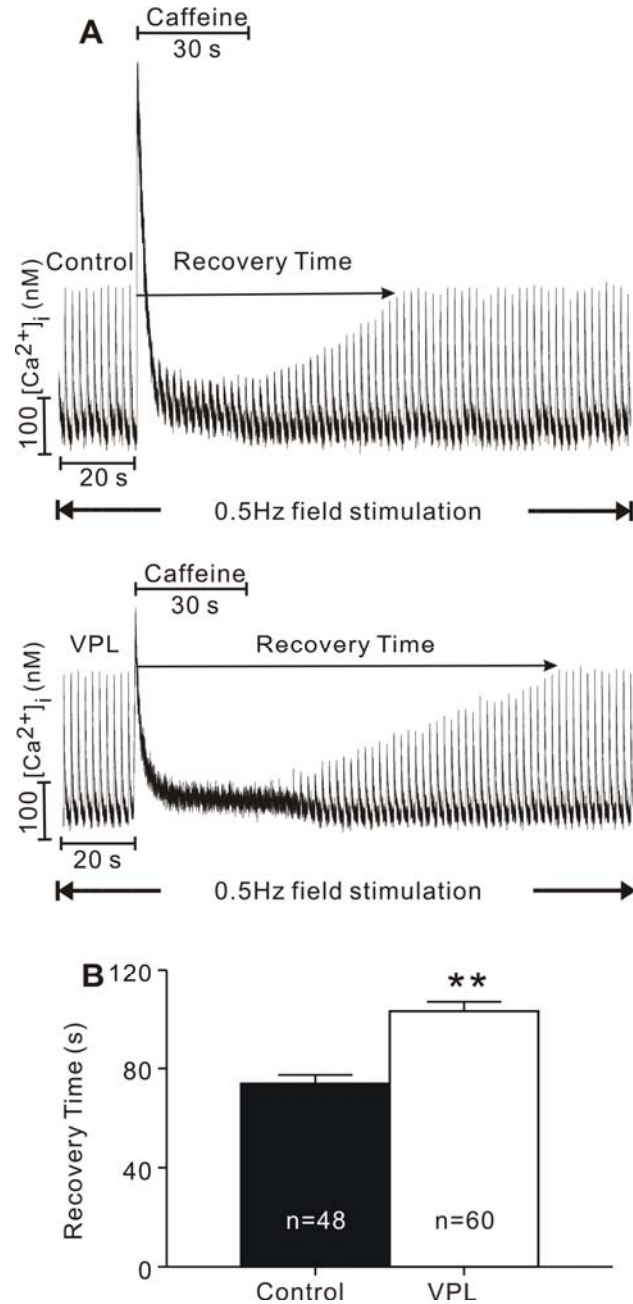
Fig.3.5 Chronic verapamil treatment slows recovery of twitch [Ca^{2+}]$_i$ transients following caffeine-induced depletion of Ca^{2+} store in cardiomyocytes. A, Typical recordings of twitch [Ca^{2+}]$_i$ transients from control and VPL myocytes illustrate the experimental protocol used to investigate the time to restore the steady state of twitch [Ca^{2+}]$_i$ transients after SR Ca^{2+} store depletion by caffeine (recovery time). Myocytes were field-stimulated at 0.5 Hz. When twitch [Ca^{2+}]$_i$ transients reached a steady state, caffeine (10 mM) was applied for 30 s to deplete SR Ca^{2+} store as indicated. B, Bar graphs show significantly prolonged recovery time in VPL group compared to control. Data represent means ± SEM for 48 cells from 9 control rats and 60 cells from 9 VPL rats. ** $P < 0.01$ *vs.* control.

3.4.6   Chronic verapamil treatment reduces SR Ca^{2+} content and increases the fractional SR Ca^{2+} release.

Caffeine releases all the SR Ca^{2+} and is often used to assess SR Ca^{2+} content and transport [13]. Myocytes were field stimulated to elicit twitches, and after reaching a steady state, 10 mM caffeine was applied to empty the SR Ca^{2+} store (Fig. 3.6A). Caffeine-induced $[Ca^{2+}]_i$ transients were consistently smaller in VPL myocytes compared to control (Fig. 3.6A). The amplitude of caffeine-induced transients was significantly reduced in VPL myocytes compared to control (Fig. 3.6B). When we took the time-course into account, the area under the curve (AUC) of the caffeine-induced Ca^{2+} transient was also significantly reduced in VPL myocytes (Fig. 3.6C). These characteristics indicate diminished SR Ca^{2+} content. The ratio of twitch/caffeine-induced $[Ca^{2+}]_i$ is an index of SR fractional Ca^{2+} release reflecting Ca^{2+} released during a twitch compared to total Ca^{2+} stored in the SR [14]. This ratio was significantly increased by 29% in VPL group versus control (Fig. 3.6D). Thus, whereas SR Ca^{2+} content is reduced, the fraction of SR Ca^{2+} released during a twitch is greater in VPL myocytes, reflecting reduced SR functional reserve.

When tracings of caffeine-induced $[Ca^{2+}]_i$ transients were normalized and superimposed, VPL myocytes showed slower rising and decline of caffeine-induced $[Ca^{2+}]_i$ transients compared to control (Supplemental Fig. 3.1A,B). When quantified in 20 myocytes from 5 control rats and 38 myocytes from VPL rats, caffeine-induced $[Ca^{2+}]_i$ transient rising rate was reduced by 48% in VPL myocytes compared to control (Supplemental Fig. 3.1C), consistent with the down-regulation of RyRs we have previously shown in VPL rats (see chapter 2) [12]. The decline of the caffeine-induced

$[Ca^{2+}]_i$ transient was prolonged, with the time constant of decay ~24% greater in VPL myocytes compared to control (Supplemental Fig. 3.1D), further reflecting reduced SERCA2 Ca^{2+} uptake function.
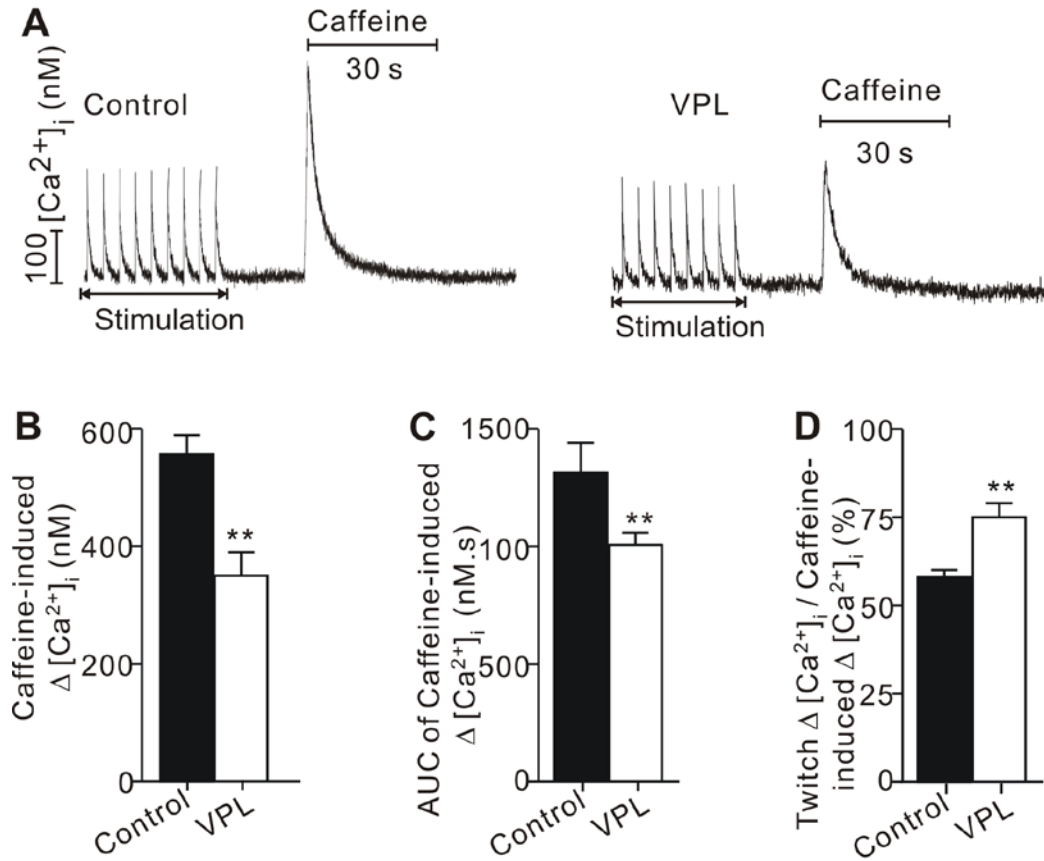
Fig.3.6 Chronic verapamil treatment reduces caffeine-induced $[Ca^{2+}]_i$ transient in cardiomyocytes. A, Representative time course recording shows the experimental protocol to study caffeine-induced $[Ca^{2+}]_i$ transient in control and VPL cardiomyocytes. Myocytes were field stimulated at 0.25 Hz. When a steady state of twitch $[Ca^{2+}]_i$ transient was reached, stimulation was stop and 20 s later caffeine 10 mM was applied for 30 s. B, C, Bar graphs revealed significant decrease in amplitude ($\Delta[Ca^{2+}]_i$) and area under the curve (AUC) of caffeine-induced $[Ca^{2+}]_i$ transient in VPL myocytes. D, Bar graphs revealed the amplitude ratio of twitch $[Ca^{2+}]_i$ transients to caffeine-induced $[Ca^{2+}]_i$ transient (Twitch $\Delta [Ca^{2+}]_i$ / Caffeine-induced $\Delta [Ca^{2+}]_i$) was significantly higher in VPL group. Data represent means $\pm$ SEM for 20 cells from 4 control rats and 24 cells from 4 VPL rats. ** $P < 0.01$ *vs.* control.
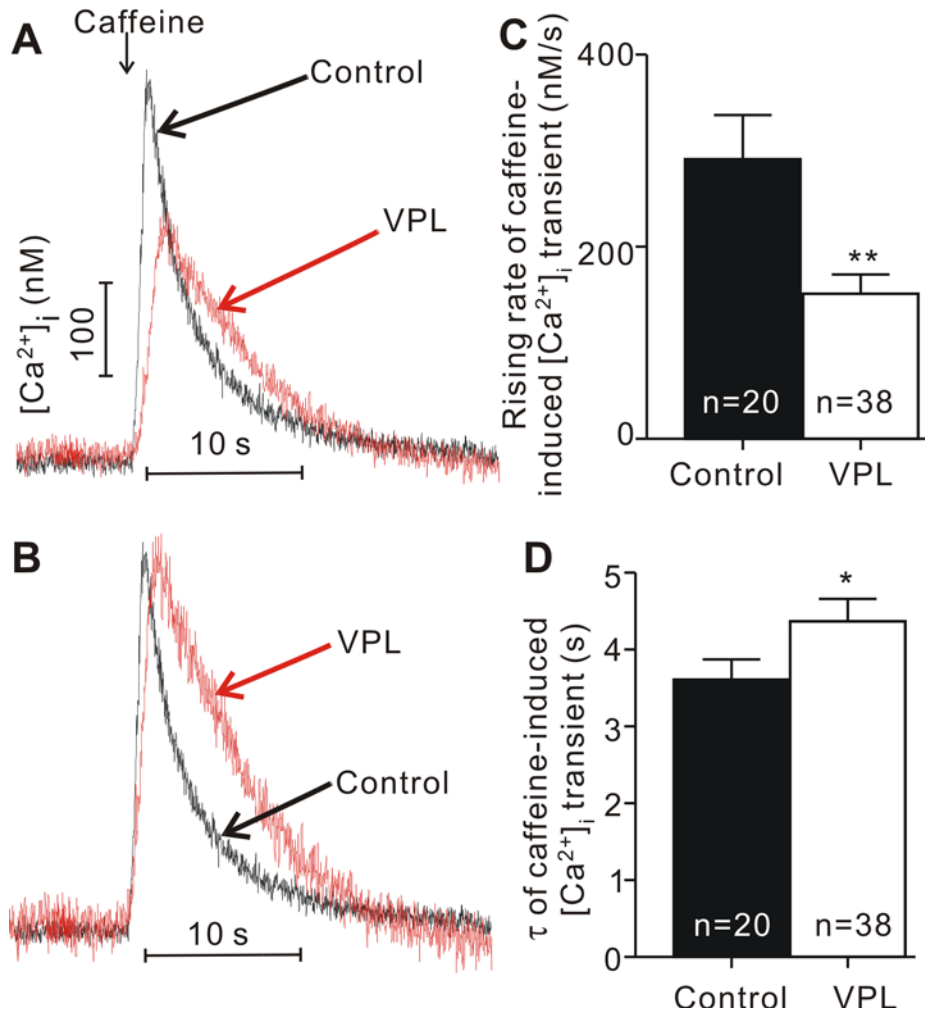
Supplemental Fig. 3.1 Chronic verapamil treatment slows caffeine-induced [Ca^{2+}]$_i$ transients of cardiomyocytes. A, Superimposed representative caffeine-induced [Ca^{2+}]$_i$ transient traces of a control and a VPL myocyte reveal slower rising rate of the caffeine-induced [Ca^{2+}]$_i$ transient in VPL myocyte compared to control. B, Normalized and superimposed same traces in A reveal slower decline of caffeine-induced [Ca^{2+}]$_i$ transient in the VPL myocyte than the control myocyte. C, D, Quantification of 20 myocytes from 5 control rats and 38 myocytes from 5 VPL rats reveals significant decrease in rising rate and increase in time constant of decline (τ) of caffeine-induced [Ca^{2+}]$_i$ transients in VPL group. Data represent means $\pm$ SEM. * $P < 0.05$, ** $P < 0.01$ *vs.* control.

3.4.7   Chronic verapamil treatment depresses left ventricular function in isolated hearts and in whole animals.

Up to now we have demonstrated that chronic verapamil treatment depresses SERCA function at the molecular, subcellular and cellular levels. We next considered the impact of reduced SERCA function on contractile function *in vivo* and in isolated hearts. Catheters were inserted into the left ventricle of anaesthetized rats to monitor pressure without any cardiac pacing. VPL rats showed markedly reduced developed pressure accompanied by slower heart rate compared to control rats (Fig. 3.7A, top panel). We also noted that the end diastolic pressure was greater in VPL rats compared to control (arrows, Fig. 3.7A, top panel).   When these parameters were quantified, developed pressure and heart rate were significantly reduced in VPL rats compared to those of control (Fig. 3.7B,C), whereas end diastolic pressure was increased ~8 fold (Fig. 3.7D). The instantaneous rate of change of pressure reflects the speed of the contraction-relaxation cycle, and showed marked changes between the two groups (Fig. 3.7A, lower panels). The maximum rates of change, both positive and negative peak values (dP/dt_{Max}, $-dP/dt_{Min}$), were reduced in VPL rats (Fig. 3.7E,F).   The time constant tau of relaxation was also significantly longer in VPL rats, demonstrating slower recovery *in vivo* (Fig. 3.7G).

To exclude the effects of circulating verapamil and varying heart rate on diastolic and systolic function, we further examined cardiac contractile function in isolated, perfused hearts using atrial pacing at 3Hz. Compared to control, the isolated hearts from VPL rats consistently showed reduced developed pressure and rate of change (Fig. 3.8A). When representative traces were normalized and overlapped, the slower contraction and

relaxation was apparent in VPL hearts (Fig. 3.8B). When these functional parameters were quantified, VPL hearts exhibited significantly reduced developed pressure and peak +/- dP/dt (Fig. 3.8C), reflecting intrinsically depressed heart function.
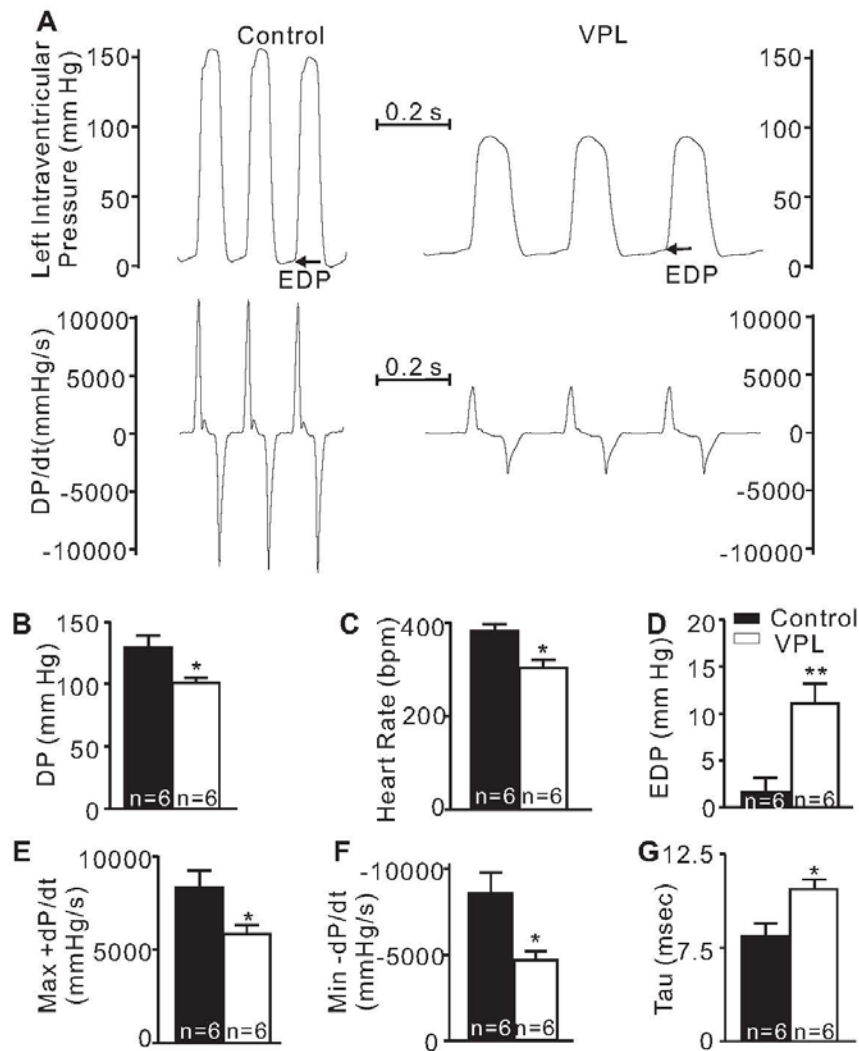
Fig. 3.7 Chronic verapamil treatment leads to reduced cardiac contractile function in rats.
Pressure-volume catheter was inserted into left ventricles of anaesthetized control and VPL rats to monitor cardiac functions. A, Representative recordings of left intraventricular pressure reveal higher end diastolic pressure (EDP) and slower heart rate in a VPL rat than those of a control rat. Arrows indicate EDP, the pressure at the end diastolic point. A bottom, instantaneous rate of intraventricular pressure change (dP/dt) derived from above data show the VPL rat had smaller peak dP/dt values than those of the control rat. B, Quantification of 6 control and 6 VPL rats reveal significant changes in EDP, developed pressure (DP), maximum rate of pressure rise during contraction (Max +dP/dt), maximum rate of pressure decrease during relaxation (Min -dP/dt), heart rate, and time constant of relaxation (tau). Tau was calculated from the peak of systolic pressure to the beginning of diastolic pressure. Data represent means $\pm$ SEM, $* P < 0.05$, $** P < 0.01$ $vs.$ control.
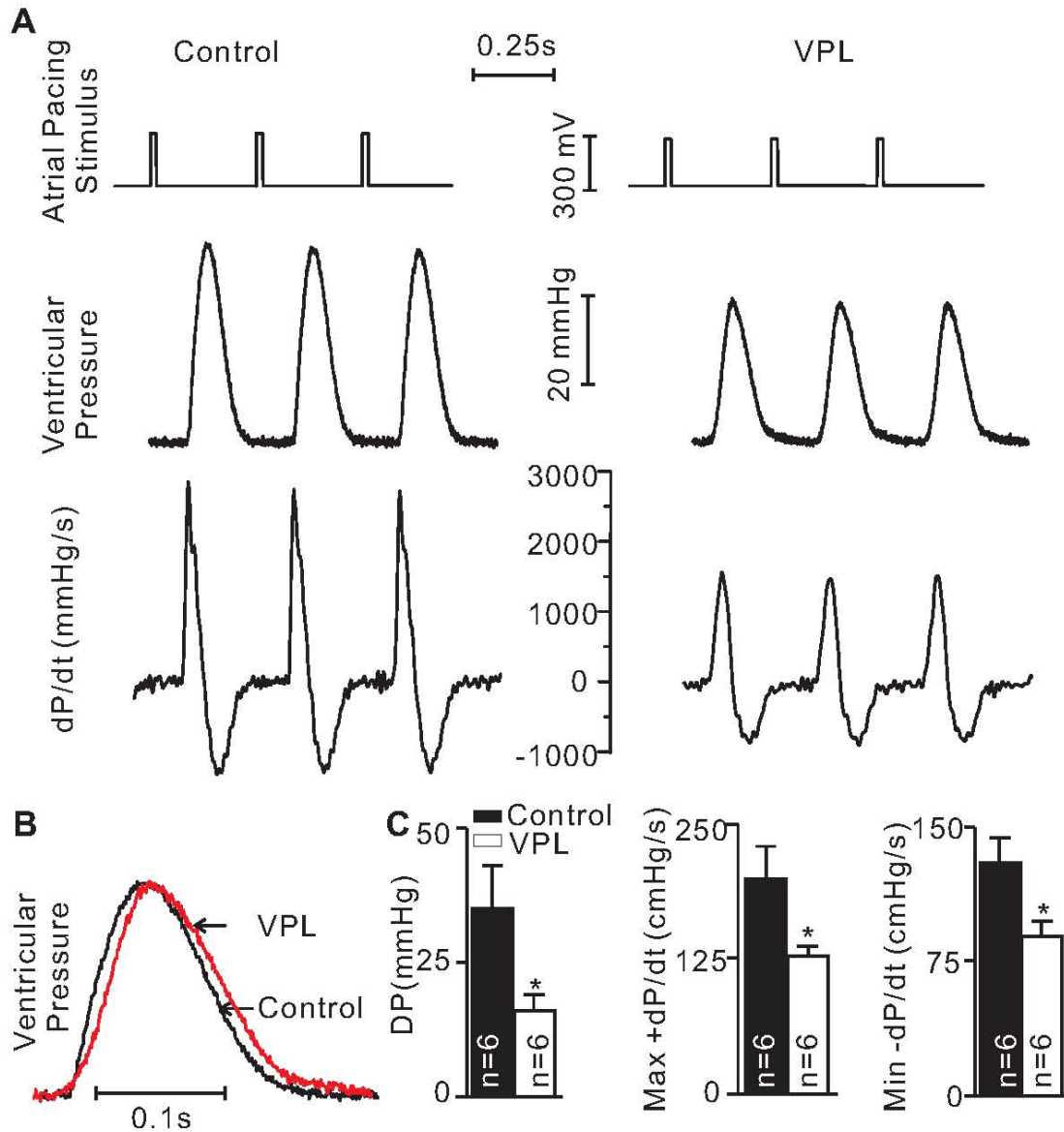
Fig.3.8 Chronic verapamil treatment leads to reduced left ventricular function in isolated hearts. A, representative contraction recordings of atrial-paced, perfused hearts from a control and a VPL rat show the time courses of the atrial pacing stimulus voltage (top), left ventricular pressure (middle), and rate of change of left ventricular pressure (dP/dt, bottom). Note the clear reduction in developed pressure (DP) and peak dP/dt (Max +dP/dt, Min –dP/dt) in the VPL group. B, Normalized and superimposed traces from left ventricular pressure in middle panel of A reveal a slower contraction and relaxation speed in VPL hearts compared to control. C, Bar graphs show that DP, Max +dP/dt, and Min –dP/dt were significantly reduced in VPL group compared to control. Each bar represents means ± SEM with "n" indicating the number of independent preparations. * $P < 0.05$, *vs.* control.

3.5   Discussion

In this study, we made the following key observations in long-term verapamil-treated rats: 1) reduced SERCA and increased PLN protein levels; 2) reduced rate of ATP-dependent Ca^{2+} uptake by cardiac SR vesicles; 3) altered myocyte $[Ca^{2+}]_i$ handling with slower and smaller Ca^{2+} transients, increased diastolic $[Ca^{2+}]_i$, and decreased SR Ca^{2+} content, and 4) reduced cardiac contractility *in vivo* and in isolated, perfused hearts. Revealed at molecular, subcellular, cellular, organ and whole animal levels, these abnormalities demonstrate depressed heart function incurred from chronic DHPR inhibition, providing a novel explanation for increased risk of heart failure in patients receiving long-term treatment with DHPR blockers.

3.5.1   Chronic DHPR Inhibition Alters the Levels of SR Ca^{2+} Cycling Proteins.

Our research revealed for the first time that inhibition of DHPR Ca^{2+} signals by chronic, partial DHPR blockade down-regulates SERCA and up-regulates PLN in the heart.   In line with our previous finding of down-regulation of the RyR and the FKBP12.6 resulted from DHPR inhibition [12], these observations suggest that DHPR Ca^{2+} signals influence the levels of SR Ca^{2+} cycling proteins. Ca^{2+} is a critical regulator of gene transcription and expression [15].   Through various classes of Ca^{2+}-regulated enzymes, long-term (hours/days) alterations of Ca^{2+} signaling can activate gene expression to modulate cardiac function in a process named as excitation–transcription (E-T) coupling [15, 16].   Chronically reduced DHPR Ca^{2+} signals resulted from DHPR blockade may regulate the SR Ca^{2+} cycling protein level though E-T coupling mechanism.

SERCA protein levels have been found to be regulated in a number of conditions. SERCA is down-regulated in aging, heart failure, and hypothyroid condition [17-19]. Our studies have shown that pharmacologic intervention can also result in depression of SERCA expression and function, which is associated with depressed heart function.

Interestingly, under conditions where heart function is enhanced, such as during ontogenic development, exercise training, or in hyperthyroid conditions, SERCA expression is up-regulated [17-19]. Thus, it appears that basal heart contractility is closely linked to SERCA protein levels and Ca^{2+} transport function. Adrenergic stimulation of the heart up-regulates SERCA2 through the calcineurin/NFAT (nuclear factor of activated T cells) pathway [20]. While sustained increases in cytosolic free Ca^{2+} concentrations are usually associated with activation of NFAT and subsequent regulation of gene expression, it is now recognized that beat-to-beat elevation of Ca^{2+} in cardiomyocytes influences this transcription factor [21]. Our studies now reveal that chronic inhibition of DHPR Ca^{2+} signaling down-regulates SERCA protein levels, indicating that DHPR Ca^{2+} signals carry information both for contraction and gene transcription of SR Ca^{2+} cycling proteins.

3.5.2   Chronic DHPR Inhibition Attenuates SERCA Ca^{2+} Transport Activity.

Consistent with down-regulation of SERCA and up-regulation of PLN, we also found chronic DHPR blockade causes a depression of SERCA Ca^{2+} uptake function. Depressed Ca^{2+} sequestration rate of isolated SR from VPL rats was evident over a wide range of Ca^{2+} concentrations compared to control (Fig. 3.1). This depressed SERCA Ca^{2+} function was also evident at the cellular level. Compared to control, marked

slowing of the decay phase of contractile $[Ca^{2+}]_i$ transients in VPL myocytes was evident at a wider range of stimulation frequency (Fig. 3.4). It is estimated that SERCA transports 92% of Ca^{2+} for the contractile $[Ca^{2+}]_i$ transient decline in rat cardiomyocytes [2]. Therefore, this prolonged Ca^{2+} transient decline corroborates the attenuation of SERCA Ca^{2+} transport activities on a cell beat-to-beat basis.

SERCA expression and functional changes seem to be, at least initially, a homeostatic mechanism to prevent SR Ca^{2+} overload. By the mechanism of CICR, the inhibition of DHPR Ca^{2+} signals by DHPR blockade reduces the steady-state contractile $[Ca^{2+}]_i$ transients and the amount of SR Ca^{2+} cycling on a beat to beat basis. As a result, basal SERCA activity before the DHPR blockade becomes relatively enhanced and can cause SR Ca^{2+} overload if not proportionally reduce to a new lower SR Ca^{2+} cycling workload as reset by DHPR blockade. Since the SR Ca^{2+} overload causes cardiomyoctye apoptosis and can be lethal and [22], the down-regulation of SERCA and up-regulation of PLN to restrain basal SERCA activity seem to be an adaptive response to the reduced basal DHPR Ca^{2+} current. Therefore, at least initially, this stoichiometry change between SERCA and PLN prevents SR Ca^{2+} overload and intracellular Ca^{2+} imbalance.

3.5.3   Chronic DHPR Inhibition Causes Abnormal Myocyte Ca^{2+} Handling.

Is cardiac adaptation to chronic DHPR inhibition physiologically benign, or pathologically lethal? In order to investigate this question, we further examined Ca^{2+} handling at the cellular level and found chronic DHPR blockade attenuated myocyte Ca^{2+} handling.

The attenuated myocyte Ca^{2+} handling was first revealed at increased diastolic $[Ca^{2+}]_i$ levels at high myocyte beating rates. Compared to control, VPL myocytes displayed markedly higher diastolic $[Ca^{2+}]_i$ levels at high stimulation frequencies (0.5 Hz and above) but no difference at low stimulation frequencies (0, 0.25 Hz) (Fig. 3.4). Moreover, the faster the stimulation frequency, the higher the diastolic $[Ca^{2+}]_i$ levels of VPL myocytes than those of control cells (Fig. 3.4). As SERCA is the dominant Ca^{2+} transporter for keeping diastolic $[Ca^{2+}]_i$ low and stable, the elevation of diastolic $[Ca^{2+}]_i$ at high stimulation frequencies indicates the inability of the SERCA to maintain intracellular Ca^{2+} homeostasis at high beating rates. In response to stress and exercise, heart rate increases and so does the speed of SR Ca^{2+} sequestration. When the SERCA no longer efficiently counterbalances increasing $[Ca^{2+}]_i$, the resulting $[Ca^{2+}]_i$ overload can introduce arrhythmia and heart failure. Thus, the elevation of diastolic $[Ca^{2+}]_i$ at high stimulation frequencies reveals a predisposition to diastolic dysfunction at high heart rate, though the heart may work normally at the basal heart rate with chronic DHPR blockade.

The observation of reduced myocyte ability to reach a steady state of $[Ca^{2+}]_i$ transients solidifies the finding that Ca^{2+} handling of VPL myocytes is attenuated. As shown in Fig. 3.5, VPL myocytes took a much longer time to restore a steady state of contractile $[Ca^{2+}]_i$ transients upon depletion of SR Ca^{2+} stores by caffeine compared to control. The steady state of contractile $[Ca^{2+}]_i$ transients reflects a steady state of SR Ca^{2+} content where a dynamic balance has been established between SR Ca^{2+} release and SR Ca^{2+} uptake. When Ca^{2+} in the SR is depleted by caffeine, the SERCA is the only source to refill the SR Ca^{2+} and recover contractile $[Ca^{2+}]_i$ transients. Thus the markedly prolonged time to restore the steady state $[Ca^{2+}]_i$ transients further reflect an attenuation

of SERCA Ca^{2+} uptake function at the cellular level. In addition, we have reported previously that chronic DHPR blockade promotes RyR Ca^{2+} leak [12], which can contribute to the prolongation to reach steady state as well. This prolongation reveals an attenuated orchestration and efficiency of SR Ca^{2+} cycling proteins in keeping Ca^{2+} homeostasis, a harbinger of heart dysfunction when the heart rate and contractility need to change frequently.

Reduced SR Ca^{2+} content and increased SR fractional release in VPL myocytes further substantiates the finding of the attenuated VPL myocyte Ca^{2+} cycling in maintaining Ca^{2+} homeostasis (Fig. 3.6). SR Ca^{2+} content reflects two transmembrane Ca^{2+} cycling balances: 1) the balance across the SR membrane between Ca^{2+} release via RyRs and Ca^{2+} uptake via SERCA, and 2) transsarcolemmal balance between Ca^{2+} ingress via DHPR and Ca^{2+} extrusion via Na^+-Ca^{2+} exchanger [23]. Thus, there may be 3 known factors contributing to reduce SR Ca^{2+} content with chronic DHPR blockade: 1) reduced SERCA function, 2) increased diastolic SR Ca^{2+} leak (see chapter 2) [12], and 3) reduced I_{Ca} by DHPR blockade. Depression of SR Ca^{2+} content can reduce SR Ca^{2+} release and contractility [23], explaining the reduced twitch $[Ca^{2+}]_i$ transient amplitude of VPL myocytes at certain stimulation frequencies (0.25 Hz, 0.5 Hz, and 2 Hz) (Fig. 3.4B).

Intriguingly, fractional SR Ca^{2+} release in each beat of a VPL myocyte was increased in the face of reduced SR Ca^{2+} content (Fig.3.6D). This paradoxical result is in contrast to a previous report that reduced SR Ca^{2+} content reduces fractional SR Ca^{2+} release [24]. The likely explanation for this paradox is the up-regulation of DHPR induced by chronic DHPR blockade (see chapter 2) [12]. Since the fractional SR Ca^{2+} release was measured in perfused, isolated myocytes where verapamil is absent, up-regulated DHPRs

increases trigger Ca^{2+} and recruits additional Ca^{2+} sparks via CICR and offsets the

reduced systolic SR Ca^{2+} release resulting from reduced SR Ca^{2+} load. This increased

trigger DHPR Ca^{2+} ingress explains the observation that the $[Ca^{2+}]_i$ transient amplitude of

VPL myocytes was significantly reduced under low frequency stimulation at 0.25Hz and

0.5 Hz (incompletely offsets by increased DHPRs) but became no difference at higher

frequencies of 0.75Hz and 1 Hz (completely offsets) (Fig. 3.4B). The $[Ca^{2+}]_i$ transient

amplitude of VPL myocytes became significantly reduced again at 2Hz (Fig. 3.4B). This

can be explained by significantly increased diastolic $[Ca^{2+}]_i$ at 2 Hz, which further

reduces the Ca^{2+} gradient across the SR membrane and reduces systolic SR Ca^{2+} release

(Fig. 3.4B). Reduced SR Ca^{2+} content along with the increased SR fractional release

indicates a reduced reserve for SR Ca^{2+} release, a predisposition to cardiac dysfunction

when the demand on the heart increases.

Altered intracellular Ca^{2+} handling plays an important role in the pathogenesis of

heart diseases with changes in Ca^{2+} cycling preceding cardiac dysfunction. Compelling

evidence has demonstrated that altered function of SERCA [11, 19, 25-30] and the RyR [31-37] contributes to intracellular Ca^{2+} mishandling and cardiac dysfunction in heart failure

and arrhythmias. The above abnormalities of myocyte Ca^{2+} handling indicate that the

heart becomes pathologically adapted to chronic DHPR Ca^{2+} inhibition and is subject to

deteriorating function.

3.5.4   Cardiac Contractile Function Becomes Intrinsically Reduced with Chronic DHPR Inhibition.

SERCA removes about 92% of cytosolic Ca^{2+} in rats [1, 38]. Thereby, the Ca^{2+} uptake activity of SERCA determines the rate of relaxation of the heart, and influences cardiac contractility by determining the size of SR Ca^{2+} load that is available for release for the next beat [1]. Thus we studied whether the depressed SERCA function incurred from the chronic DHPR blockade would affect cardiac contractile function at the organ and whole animal levels.

When isolated, perfused hearts were paced at the same frequency to eliminate the inherent heart rate effects on cardiac contraction, we observed significantly reduced developed pressure and peak dP/dt of left ventricle in VPL group compared to control. When examined in *vivo*, these hemodynamic parameters were reduced as well. These observations both at organ and whole animal levels suggest that chronic DHPR blockade reduces cardiac contractile function. These observations are consistent with the observations at molecular, subcellular, and cellular levels. Specifically, the depressed SERCA expression and function, reduced SR Ca^{2+} content, decreased the amplitude of twitch $[Ca^{2+}]_i$ transients can be responsible for reduced heart basal contraction and developed pressure. It could argue that reduced contraction may be a direct effect of verapamil as verapamil acutely modulates the E-C coupling and reduces the contraction by inhibiting CICR. However, verapamil was absent in the perfused, isolated cells and hearts. Thus this supports an intrinsic reduction of contractile ability of heart occurred from the chronic DHPR blockade, which was independent of the direct pharmacological effects of verapamil on inhibition of CICR.

3.5.5   Clinical Relevance

DHPR blockers are frequently prescribed for long-term treatment of cardiovascular diseases such as hypertension and angina pectoris [5, 39]. Given complete DHPR blockade is accompanied by immediate cessation of the heat beat [40], the DHPR Ca^{2+} current is only partially blocked by DHPR blockers in clinically used doses, which cause an acute decrease in cardiac contractility by reducing the amount of CICR and contractile Ca^{2+} transient. Although several large clinical trials have reported an increased risk of heart failure among patients with long-term treatment of DHPR blockers, systematic studies to examine the underlying mechanisms and cardiac functional changes from animals following chronic DHPR blockade are lacking [5]. The present study is the first to provide evidence from molecular to whole animal levels of depressed SERCA function and predisposition to heart dysfunctions ensued from chronic DHPR blockade in rats. Thus this study provides insights into the mechanisms for the increased risk of heart failure encountered following long-term verapamil treatment.

3.5.6   Conclusions

Both DHPR and SERCA play central roles in the orchestration of Ca^{2+} cycling during E-C coupling to ensure the Ca^{2+} homeostasis and proper contraction. In agreement with our previous results in Chapter 2, the results presented here demonstrate that DHPR Ca^{2+} signaling is physiologically important both in regulation of cardiac contraction and Ca^{2+} cycling protein levels in E-C coupling. Here we provide novel evidence that artificial depression of DHPR Ca^{2+} signaling by DHPR blockade leads to expression and functional depression of SERCA, impaired myocyte Ca^{2+} handling, and

intrinsically reduced cardiac contractility. These findings suggest cardiac adaptation to chronic inhibition of DHPR is potentially pathological and harbingers cardiac dysfunction, which may underlie the increased risk of heart failure encountered following long-term verapamil treatment.

3.6   References

1.   Bers DM. Cardiac excitation-contraction coupling. *Nature*. 2002;415:198-205

2.   Bassani JW, Bassani RA, Bers DM. Relaxation in rabbit and rat cardiac cells: species-dependent differences in cellular mechanisms. *J Physiol*. 1994;476:279-293

3.   Periasamy M, Bhupathy P, Babu GJ. Regulation of sarcoplasmic reticulum Ca^{2+} ATPase pump expression and its relevance to cardiac muscle physiology and pathology. *Cardiovasc Res*. 2008;77:265-273

4.   Muth JN, Bodi I, Lewis W, Varadi G, Schwartz A. A Ca^{2+}-dependent transgenic model of cardiac hypertrophy: A role for protein kinase Calpha. *Circulation*. 2001;103:140-147

5.   Eisenberg MJ, Brox A, Bestawros AN. Calcium channel blockers: an update. *Am J Med*. 2004;116:35-43

6.   Jiang M, Xu A, Tokmakejian S, Narayanan N. Thyroid hormone-induced overexpression of functional ryanodine receptors in the rabbit heart. *Am J Physiol Heart Circ Physiol*. 2000;278:H1429-1438

7.   Jones DL, Narayanan N. Defibrillation depresses heart sarcoplasmic reticulum calcium pump: a mechanism of postshock dysfunction. *Am J Physiol*. 1998;274:H98-105

8.   Sathish V, Xu A, Karmazyn M, Sims SM, Narayanan N. Mechanistic basis of differences in Ca^{2+}-handling properties of sarcoplasmic reticulum in right and left ventricles of normal rat myocardium. *Am J Physiol Heart Circ Physiol*. 2006;291:H88-96

9.   Cerra MC, De Iuri L, Angelone T, Corti A, Tota B. Recombinant N-terminal fragments of chromogranin-A modulate cardiac function of the Langendorff-perfused rat heart. *Basic Res Cardiol*. 2006;101:43-52

10.   Zhao X, Wu N, Deng M, Yin Y, Zhou J, Fang Y, Huang L. An improved method of left ventricular catheterization in rats. *Physiol Meas*. 2006;27:N27-33

11.   MacLennan DH, Kranias EG. Phospholamban: a crucial regulator of cardiac contractility. *Nat Rev Mol Cell Biol*. 2003;4:566-577

12.   Zhou J, Xu A, Jiang M, Jones DL, Sims SM, Narayanan N. Chronic L-type calcium channel blockade with verapamil causes cardiac ryanodine receptor remodeling and predisposition to heart failure in the rat. *Circ Heart Fail*. 2010

13.   Bassani JW, Bassani RA, Bers DM. Twitch-dependent SR Ca accumulation and release in rabbit ventricular myocytes. *Am J Physiol*. 1993;265:C533-540

14.   Maier LS, Zhang T, Chen L, DeSantiago J, Brown JH, Bers DM. Transgenic CaMKIIdeltaC overexpression uniquely alters cardiac myocyte Ca^{2+} handling: reduced SR Ca^{2+} load and activated SR Ca^{2+} release. *Circ Res*. 2003;92:904-911

15.   Bers DM, Guo T. Calcium signaling in cardiac ventricular myocytes. *Ann N Y Acad Sci*. 2005;1047:86-98

16.   Zhang T, Brown JH. Role of Ca^{2+}/calmodulin-dependent protein kinase II in cardiac hypertrophy and heart failure. *Cardiovasc Res*. 2004;63:476-486

17.   Cain BS, Meldrum DR, Joo KS, Wang JF, Meng X, Cleveland JC, Jr., Banerjee A, Harken AH. Human SERCA2a levels correlate inversely with age in senescent human myocardium. *J Am Coll Cardiol*. 1998;32:458-467

18. Lompre AM, Lambert F, Lakatta EG, Schwartz K. Expression of sarcoplasmic reticulum Ca^{2+}-ATPase and calsequestrin genes in rat heart during ontogenic development and aging. *Circ Res*. 1991;69:1380-1388

19. Periasamy M, Huke S. SERCA pump level is a critical determinant of Ca^{2+} homeostasis and cardiac contractility. *J Mol Cell Cardiol*. 2001;33:1053-1063

20. Anwar A, Schluter KD, Heger J, Piper HM, Euler G. Enhanced SERCA2A expression improves contractile performance of ventricular cardiomyocytes of rat under adrenergic stimulation. *Pflugers Arch*. 2008;457:485-491

21. Houser SR, Molkentin JD. Does contractile Ca^{2+} control calcineurin-NFAT signaling and pathological hypertrophy in cardiac myocytes? *Sci Signal*. 2008;1:pe31

22. Chen X, Zhang X, Kubo H, Harris DM, Mills GD, Moyer J, Berretta R, Potts ST, Marsh JD, Houser SR. Ca^{2+} influx-induced sarcoplasmic reticulum Ca^{2+} overload causes mitochondrial-dependent apoptosis in ventricular myocytes. *Circ Res*. 2005;97:1009-1017

23. Bers DM, Eisner DA, Valdivia HH. Sarcoplasmic reticulum Ca^{2+} and heart failure: roles of diastolic leak and Ca^{2+} transport. *Circ Res*. 2003;93:487-490

24. Bassani JW, Yuan W, Bers DM. Fractional SR Ca release is regulated by trigger Ca and SR Ca content in cardiac myocytes. *Am J Physiol*. 1995;268:C1313-1319

25. Haghighi K, Kolokathis F, Pater L, Lynch RA, Asahi M, Gramolini AO, Fan GC, Tsiapras D, Hahn HS, Adamopoulos S, Liggett SB, Dorn GW, 2nd, MacLennan DH, Kremastinos DT, Kranias EG. Human phospholamban null results in lethal dilated cardiomyopathy revealing a critical difference between mouse and human. *J Clin Invest*. 2003;111:869-876

26.   Netticadan T, Temsah RM, Kawabata K, Dhalla NS. Sarcoplasmic reticulum Ca^{2+}/Calmodulin-dependent protein kinase is altered in heart failure. *Circ Res*. 2000;86:596-605

27.   Minamisawa S, Hoshijima M, Chu G, Ward CA, Frank K, Gu Y, Martone ME, Wang Y, Ross J, Jr., Kranias EG, Giles WR, Chien KR. Chronic phospholamban-sarcoplasmic reticulum calcium ATPase interaction is the critical calcium cycling defect in dilated cardiomyopathy. *Cell*. 1999;99:313-322

28.   Beuckelmann DJ, Nabauer M, Kruger C, Erdmann E. Altered diastolic $[Ca^{2+}]_i$ handling in human ventricular myocytes from patients with terminal heart failure. *Am Heart J*. 1995;129:684-689

29.   Vafiadaki E, Papalouka V, Arvanitis DA, Kranias EG, Sanoudou D. The role of SERCA2a/PLN complex, Ca^{2+} homeostasis, and anti-apoptotic proteins in determining cell fate. *Pflugers Arch*. 2009;457:687-700

30.   Hovnanian A. SERCA pumps and human diseases. *Subcell Biochem*. 2007;45:337-363

31.   Gomez AM, Rueda A, Sainte-Marie Y, Pereira L, Zissimopoulos S, Zhu X, Schaub R, Perrier E, Perrier R, Latouche C, Richard S, Picot MC, Jaisser F, Lai FA, Valdivia HH, Benitah JP. Mineralocorticoid modulation of cardiac ryanodine receptor activity is associated with downregulation of FK506-binding proteins. *Circulation*. 2009;119:2179-2187

32.   Blayney LM, Lai FA. Ryanodine receptor-mediated arrhythmias and sudden cardiac death. *Pharmacol Ther*. 2009;123:151-177

33.   Gyorke S, Terentyev D. Modulation of ryanodine receptor by luminal calcium and accessory proteins in health and cardiac disease. *Cardiovasc Res*. 2008;77:245-255

34.   Sipido KR. CaM or cAMP: linking beta-adrenergic stimulation to 'leaky' RyRs. *Circ Res*. 2007;100:296-298

35.   Wehrens XH, Lehnart SE, Reiken S, Vest JA, Wronska A, Marks AR. Ryanodine receptor/calcium release channel PKA phosphorylation: a critical mediator of heart failure progression. *Proc Natl Acad Sci U S A*. 2006;103:511-518

36.   Song LS, Sobie EA, McCulle S, Lederer WJ, Balke CW, Cheng H. Orphaned ryanodine receptors in the failing heart. *Proc Natl Acad Sci U S A*. 2006;103:4305-4310

37.   Sobie EA, Guatimosim S, Gomez-Viquez L, Song LS, Hartmann H, Saleet Jafri M, Lederer WJ. The Ca^{2+} leak paradox and rogue ryanodine receptors: SR Ca^{2+} efflux theory and practice. *Prog Biophys Mol Biol*. 2006;90:172-185

38.   Maier LS, Bers DM. Calcium, calmodulin, and calcium-calmodulin kinase II: heartbeat to heartbeat and beyond. *J Mol Cell Cardiol*. 2002;34:919-939

39.   Peter Libby RB, Douglas Mann, Douglas Zipes, Eugene Braunwald. Braunwald's Heart Disease:A Textbook of Cardiovascular Medicine. 2008

40.   McCall D. Effect of verapamil and of extracellular Ca^{2+} and Na^+ on contraction frequency of cultured heart cells. *J Gen Physiol*. 1976;68:537-549

CHAPTER FOUR

IMPACT OF CHRONIC L-TYPE CALCIUM CHANNEL BLOCKADE ON PHOSPHORYLATION-DEPENDENT REGULATION OF CARDIAC SARCOPLASMIC RETICULUM FUNCTION IN THE RAT

4.1   Chapter Summary

The voltage-gated, L-type Ca^{2+} channel (dihydropyridine receptor, DHPR) in the sarcolemma is the main portal for Ca^{2+} entry into cardiomyocytes and thus crucial to excitation-contraction coupling. Chronic DHPR blockade causes functional remodeling of cardiac sarcoplasmic reticulum (SR). We report here the impact of chronic verapamil treatment on protein phosphorylation-dependent regulation of SR function and cardiac contractile reserve by CaM kinase II (CaMKII) and cAMP-dependent protein kinase (PKA) in rats. Adult rats received verapamil (625 µg/h/kg) or vehicle for 4 weeks through subcutaneously implanted osmotic mini-pumps.   Western immunoblotting analysis revealed up-regulated CaMKII expression, and hyper-phosphorylated cardiac ryanodine receptor (RyR), phospholamban, and CaMKII in verapamil-treated (VPL) rats compared to control. CaMKII in isolated SR vesicles of VPL rats displayed increased ability to phosphorylate sarco/endoplasmic reticulum Ca^{2+} ATPase (SERCA) by ~ 60%, compared to control. Cardiac SR vesicles from VPL rats exhibited diminished maximum rates of ATP-energized Ca^{2+} uptake under CaMKII− and PKA−stimulation compared to control. Cardiomyocytes isolated from VPL rats displayed preserved the frequency dependent acceleration of relaxation but prolonged decline of Ca^{2+} transients. *In vivo*, VPL rats exhibited depressed inotropic response to isoproterenol stimulation compared to control. Macroscopic and microscopic morphological studies revealed that pathogenic abnormalities described above occurred in the absence of ventricular hypertrophy. The above findings, ranging from molecules to the organism, demonstrate that chronic DHPR blockade attenuates cardiac contractile reserve with up-regulation of CaMKII− and PKA− dependent phosphorylation.

4.2   Introduction

In the heart, the voltage-gated, L-type Ca^{2+} channel (dihydropyridine receptor, DHPR) in the sarcolemma is the molecule that converts the electrical stimulus into the Ca^{2+} signal to initiate excitation-contraction coupling (E-C coupling).   When a cardiomyocyte is depolarized by an action potential, DHPRs open to let a small amount of Ca^{2+} enter the cell.   This DHPR Ca^{2+} influx triggers a large amount of Ca^{2+} release from the sarcoplasmic reticulum (SR) via ryanodine receptors (RyRs), a process termed as "Ca^{2+} induced Ca^{2+} release" (CICR) [1].   The resulting rise in cytosolic free Ca^{2+} concentration ($[Ca^{2+}]_i$) activates the myofilaments and generates contraction.   The subsequent return of $[Ca^{2+}]_i$ to basal levels signals the beginning of diastole.   The majority of cytosolic Ca^{2+} is removed by the sarco/endoplasmic reticulum Ca^{2+} ATPase (SERCA), which is negatively regulated by phospholamban (PLN).

Studies described in preceding chapters have provided novel insights into the impact of chronic DHPR blockade on the expression and function of molecular partners governing E-C coupling events. Given the close communication among DHPRs and SR Ca^{2+} cycling proteins (namely, RyR, SERCA, and PLN) in cardiac E-C coupling, it is not surprising that chronic inhibition of DHPRs causes functional remodeling of SR (see chapter 2 and 3). We have shown that chronic inhibition of DHPRs by verapamil causes imbalanced stoichiometry of the DHPR and RyR, altered functional properties of cardiac RyRs, and increased diastolic Ca^{2+} leak from the SR in the rat (see chapter 2). Furthermore, chronic verapamil treatment depresses the intrinsic ability of SR to uptake Ca^{2+}, contributing to altered myocyte $[Ca^{2+}]_i$ handling, prolonged Ca^{2+} transients, and

decreased SR Ca^{2+} content (see chapter 3). This functional remodeling of the SR is accompanied by depressed basal contractility and increased susceptibility to arrhythmia in isolated hearts and *in vivo* (see chapter 2 and 3) [2-5]. This finding of functional remodeling of SR provides major insights into the molecular mechanisms for the increased risk of heart failure in patients with chronic DHPR blocker treatment [2, 5-7].

Considering the pathophysiological impact of functional remodeling of SR, it is logical to explore how chronic inhibition of DHPRs affects the physiological mechanisms that regulate SR function. The physiological regulation of SR function is achieved mainly through phosphorylation of SR Ca^{2+} cycling proteins [8]. Phosphorylation of RyRs is generally regarded as an important regulatory mechanism, though the exact effects on channel function remain controversial as both stimulatory and inhibitory effects have been reported [9, 10 11 12, 13]. Phosphorylation of PLN is thought to relieve PLN inhibition on SERCA and restore SERCA affinity for Ca^{2+} [1, 8, 14]. A direct phosphorylation of SERCA at serine 38 is associated with activation of SR Ca^{2+} transport [15]. In addition, the interactions among molecular partners (e.g. SERCA-PLN, SERCA-Calmodulin, RyR-FKBP12.6) are phosphorylation status dependent and likely govern the conformation and function of the RyR and SERCA [16, 17].

Ca^{2+}/calmodulin-dependent protein kinase II (CaMKII) and cAMP-dependent protein kinase (PKA) are two major protein kinases that regulate the phosphorylation status of SR proteins in the heart. Present in the SR and cytosol, CaMKII plays a central role in controlling the SR function by its ability to phosphorylate the RyR, SERCA and PLN [10, 18, 19]. On the other hand, PKA regulates SR function by its ability to phosphorylate the RyR and PLN (but not the SERCA) [20].

To decipher the mechanism(s) underlying functional remodeling of cardiac SR by chronic inhibition of DHPRs, the present study investigated the impact of chronic verapamil-treatment on proteinphosphorylation-dependent regulation of SR function by CaMKII and PKA in the rat.

4.3   Methods

An expanded methods section is provided in appendix B.

4.3.1   Animals.

Male Wistar rats weighing 190 to 210 g were randomly assigned to control and verapamil-treated (VPL) groups. Verapamil was dissolved in distilled water and administrated at a rate of 625 µg/h/kg for 4 weeks via subcutaneously implanted osmotic mini pumps (Model 2ML4; ALZET, Cupertino, CA). Control rats received vehicle solution in similar manner. All procedures were approved by the Animal Use and Care Committee of The University of Western Ontario and followed the Guidelines of the Canadian Council on Animal Care.

4.3.2   Western Immunoblotting and Ca^{2+} Uptake by SR Vesicles.

Protein levels of CaMKII and calsequestrin (Ca^{2+} storage protein) in isolated cardiac SR vesicles were determined by Western immunoblotting analysis; phosphorylation site-specific antibodies were used for the detection and estimation of pre-existing phosphorylation level of CaMKII, RyR and PLN [21, 22]. ATP-dependent, oxalate-faciliated Ca^{2+} uptake by isolated cardiac SR vesicles was determined using Millipore filtration technique as described previously [23]. To evaluate the effect of endogenous CaMKII on Ca^{2+} uptake, assays were performed in the absence of exogenous calmodulin (CaM) and in the presence of 3 µM exogenous CaM. The Ca^{2+} uptake

reaction was initiated by either the addition of SR or ATP to the rest of the assay components pre-incubated for 3 min at 37°C.

4.3.3   Measurement of SR Protein Phosphorylation by PKA.

Phosphorylation of SR proteins by PKA was determined as described previously [24, 25]. PKA catalytic subunit was purchased from Sigma. Aliquots containing 250 units of the lyophilized protein were dissolved in 10 mM DTT and stored on ice until used, usually within 2 h. Cardiac SR vesicles were resuspended in a solution of 50 mM Tris-HCl (pH 6.8), and 10 mM $MgCl_2$. In each phosphorylation assay, 25 units of the catalytic subunit of PKA were used per 100 µg of SR protein. The salt from the lyophilized powder was carried over so that the PKA phosphorylation reaction mixture, in a total volume of 100 µl, contained 50 mM Tris-HCl (pH 6.8), 10 mM $MgCl_2$, 1mM ATP, and the components from lyophilized PKA: 1 mM DTT, 1.2 mM 2-mercaptoethanol, 16.5 mM potassium phosphate, 0.8 µM EDTA, and 35 mM sucrose. Following pre-incubation of the assay components for 2 min at 37 °C, the reaction was initiated by the addition of SR and was allowed to proceed for 3 min. The reactions were terminated by addition of 15 µl of SDS sample buffer and the samples were subjected to SDS-polyacrylamide gradient gel (4-18%) electrophoresis and autoradiography. The phosphorylation of substrate proteins was quantified using standard procedures as reported previously [24].

4.3.4   Measurement of SR Protein Phosphorylation by Endogenous CaMKII

Phosphorylation of SR proteins by endogenous CaMKII was determined as described previously [26]. The phosphorylation assay medium (total volume 50 μl) contained 50 mM HEPES (pH = 7.4), 10 mM $MgCl_2$, 0.1 mM $CaCl_2$, 0.1 mM EGTA, 1 μM CaM, 0.8 mM [γ-^{32}P] ATP (specific activity 200-300 cpm/pmol), and SR (25 μg of protein). The phosphorylation reaction was carried out for 2 min at 37°C. The samples were subjected to SDS-polyacrylamide gradient gel (4-18%) electrophoresis and autoradiography and phosphorylation of substrate proteins was quantified using standard procedures as reported previously [26, 27].

4.3.5   Cytosolic Free Ca^{2+} Concentration

Myocytes were isolated from myocardium of control and VPL rats, and single cell twitch $[Ca^{2+}]_i$ transients were monitored at room temperature (22-25°C) during field stimulation of fura-2-loaded myocytes according to procedures described previously [23]. To examine the frequency-dependent acceleration of relaxation (FDAR), myocytes were stimulated at frequencies from 0.25 Hz to 2 Hz. Cells were stimulated at each frequency for 60 s and then were given 30 s resting interval before stimulation resumed at the next higher frequency.

4.3.6   Histology

Chambers of the heart were slit open, any excess blood was removed using paper towels, and then the heart was weighed. The atria and large blood vessels were then removed. The ventricular myocardium was separated into the right ventricular (RV) free

wall and left ventricular (LV) free wall including the septum, and weighed separately. Then myocardial tissues were fixed in 10% buffered formalin, paraffin-embedded and sectioned. Five-micrometer sections stained with hematoxylin and eosin as well as Mason's trichrome stains were used for light microscopic examination and assessment of histology. Cell volume was determined in myocytes isolated from RV and LV using the formula $v = (\pi lwd)/4$, where l and w are the measured cell length and width, respectively [28]. The cell depth (d) was calculated by assuming the cell to be an elliptical cylinder with a minor-to-major axis ratio of 1:3 [28].

4.3.7   Statistical Analysis

The data on Ca^{2+} concentration-dependent Ca^{2+} uptake were analyzed by nonlinear regression (SigmaPlot) as described earlier [23]. The time constant of $[Ca^{2+}]_i$ decline (τ) was determined by a single exponential decay equation. Results are means $\pm$ SEM with significance ($P<0.05$) determined using Student's t test or one-way ANOVA.

4.4   Results

4.4.1   Enhanced CaMKII Protein Expression and Autophosphorylation in Cardiac SR of VPL Rats.

CaMKII is known to play an important role in regulating the Ca^{2+} uptake function of cardiac SR through phosphorylation of PLN [14, 29] and SERCA [26, 27, 30-34]. We first carried out immunoblotting analysis to assess the potential impact of chronic DHPR blockade on protein expression of CaMKII and its autophosphorylation status in isolated cardiac SR vesicles. We found a significant increase by ~ 35% in protein levels of CaMKII in cardiac SR vesicles isolated from VPL rats, compared to control (Fig. 4.1A). Since the autophosphorylation level at threonine 286 influences the CaMKII activity [35], we further probed phospho-threonine 286 of CaMKII (PT^{286}-CaMKII) using phosphorylation site-specific antibodies. Western blotting revealed that PT^{286}-CaMKII in VPL rats was increased by ~ 100% compared to control (Fig. 4.1B), indicating enhancement of CaMKII activity. However, the ratio of PT^{286}-CaMKII: CaMKII immunoreactive protein level was not significantly different between control and VPL rats (Fig. 4.1C).
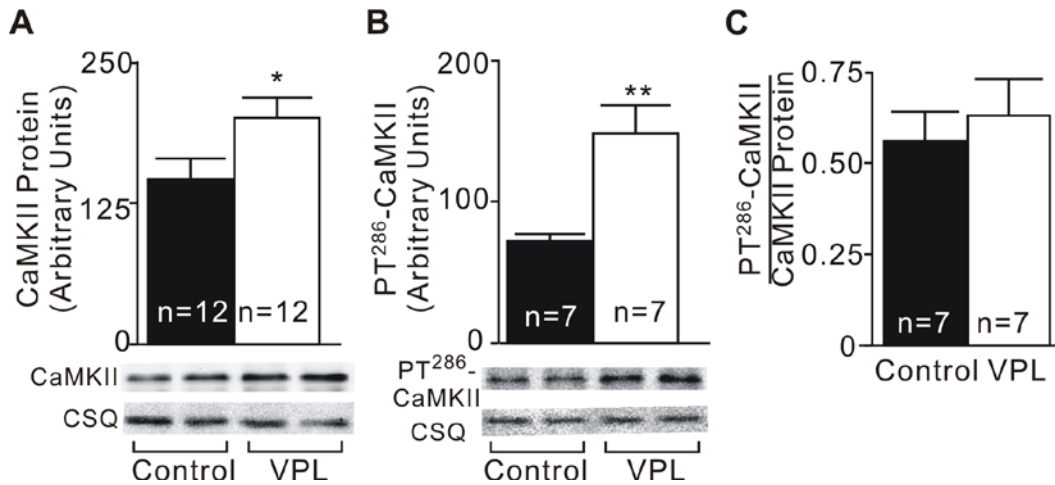
Fig. 4.1 The protein and autophosphorylation levels of CaMKII are up-regulated in VPL rats. CaMKII and the phospho-Threonine 286 (PT286) in CaMKII were detected using the CaMKII specific and phosphorylation site-specific antibodies. Identical amounts of SR (25 μg protein) from control and verapamil-treated (VPL) rats were subjected to Western immunoblotting analysis of CaMKII (A, n=12/group) and PT286-CaMKII (B, n=7/group). Representative immunoblots obtained using 2 separate SR preparations each from control and VPL rats are shown at the bottom. Also shown are immunoblots of calsequestrin (CSQ) generated by stripping and re-probing of the same blots; the CSQ blots served as an internal protein loading control as CSQ protein level did not differ between control and VPL rats. The amount of PT286-CaMKII was further normalized to immunoreactive protein content of CaMKII and expressed as the ratio of PT286-CaMKII to CaMKII (C, n=7/group). Values are means ± SEM. * $P<0.05$, **$P<0.01$ VPL *vs*. control.

4.4.2   RyR and PLN Become Hyper-phosphorylated in Cardiac SR of VPL Rats.

Both CaMKII and PKA regulate SR Ca^{2+} cycling by virtue of their ability to phosphorylate RyR [1, 36, 37 20, 38] and PLN [1, 39, 40 20]. We utilized phosphorylation site-specific antibodies to evaluate pre-existing phosphorylation levels of RyR and PLN in cardiac SR vesicles isolated from control and VPL rats. Compared to control, phospho-serine^{2809} of RyR (PS^{2809}-RyR) was significantly increased by ~70% in VPL rats (Fig. 4.2A). Since RyR-PS^{2809} is a substrate both for CaMKII and PKA [11], the hyper-phosphorylation of RyR-PS^{2809} indicates an increase of activity of either or both of CaMKII and PKA. Assessment of the phosphorylation status of PLN revealed strikingly increased levels of phospho-threonine^{17} (PT^{17}-PLN) by 300% and phospho-serine^{16} (PS^{16}-PLN) by 200% in VPL rats (Fig. 4.2B,C). Since PT^{17}-PLN is specific for CaMKII [41] and PS^{16}-PLN is specific for PKA [41], the hyper-phosphorylation of PT^{17}-PLN and PS^{16}-PLN further indicate that the activity of both CaMKII and PKA were enhanced. Considering the amount of protein levels can influence the pre-existing phosphorylation levels, we normalized phosphorylation to the unit amount of each substrate as previously reported [2, 5]. Even with this normalization, we found consistently higher ratios of phosphorylation of each substrate in VPL rats compared to control (Suppl. Fig. 4.1). This suggests increased endogenous CaMKII and PKA activity most likely contributes to the hyper-phosphorylation of substrates *in vivo*.
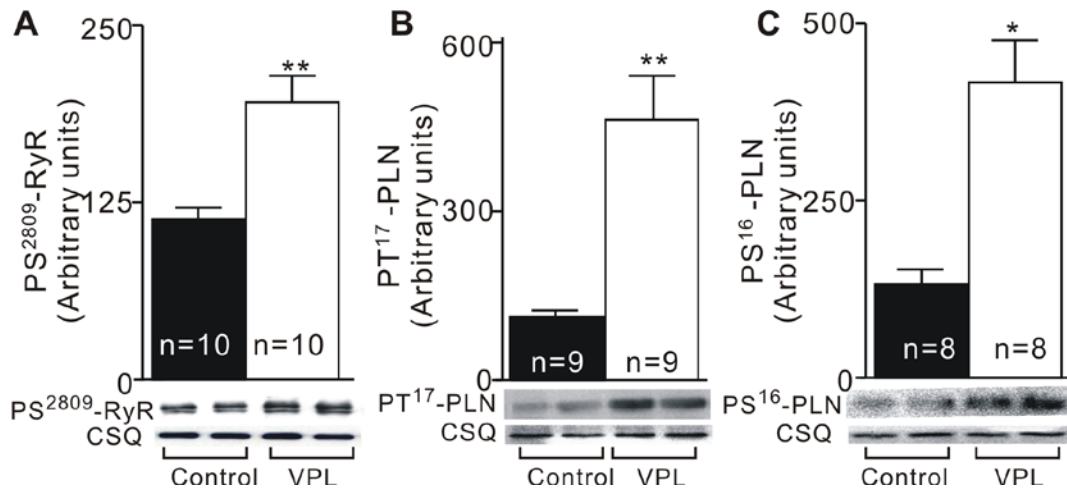
Fig. 4.2 RyR and PLN become hyper-phosphorylated in VPL rats. The phospho-serine^{2809} (PS2809) in RyR, phospho-threonine^{17} (PT17), and phosphor-serine^{16} (PS16) in PLN were detected using the phosphorylation site-specific antibodies. Identical amounts of SR (25 µg protein) from control and verapamil-treated (VPL) rats were subjected to Western immunoblotting analysis of PS2809-RyR (A, n=10/group), PT17-PLN (B, n=9/group), PS16-PLN (C,n=8/group). Representative immunoblots obtained using 2 separated SR preparations each from control and VPL rats are shown at the bottom. Also shown are Western blots of calsequestrin (CSQ) used as protein loading control. Values are means ± SEM. * $P<0.05$, **$P<0.01$ VPL *vs*. control.
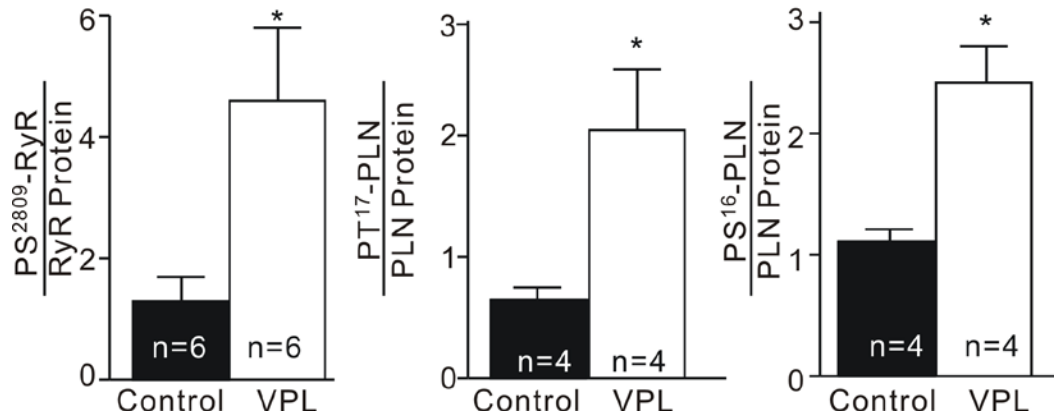
Suppl. Fig. 4.1 *In vivo* **phosphorylation status of RyR and PLN normalized to immunoreactive substrate proteins.** The relative amounts of PS2809-RyR, PT17-PLN and PS16-PLN were quantified by computer-assisted scanning densitometry of Western blots. The amount of PS2809-RyR, PT17-PLN and PS16-PLN were further normalized to immunoreactive protein content of RyR and PLN respectively. The relative amount of RyR and PLN were determined by scanning densitometry of Western immunoblots. The normalized amount of PS2809-RyR, PT17-PLN and PS16-PLN were expressed as the ratio of PS2809-RyR:RyR (n=6/group), PT17-PLN:PLN(n=4/group) and PS16-PLN:PLN (n=4/group). Values are means ± SEM. * *P*<0.05 *vs*. control.

4.4.3   The Activity of SR-associated CaMKII is Enhanced in VPL Rats.

Endogenous CaMKII is associated with the SR and present in the cytosol [23, 42].

Given the hyper-phosphorylation of SR substrates *in vivo* in VPL rats, we next examined

the activity of SR-associated CaMKII by using SR vesicles isolated from control and

VPL rats.   The results are presented in Fig. 4.3.   This study utilized $[\gamma\text{-}^{32}P]ATP$ for

CaMKII reaction and equal amount of SR (25 µg of protein) from control and VPL rats.

The SDS-PAGE protein profiles from control and VPL rats were similar (Fig. 4.3A, left

panel), indicating the relative purity of SR vesicles did not differ between the

experimental groups.   The corresponding autoradiogram of the gel reveals selective

phosphorylation of RyR, SERCA and PLN only in the presence of Ca^{2+} and CaM, (Fig.

4.3A, right panel), providing direct evidence of activation of endogenous, SR-associated

CaMKII.   A striking increase in phosphorylation of SERCA was apparent, whereas

phosphorylation of PLN was decreased in VPL rats.

To quantify ^{32}P incorporation, we excised bands from the gel for scintillation

counting.   No significant differences in RyR or PLN phosphorylation were apparent

when comparing equivalent amounts of SR protein (Fig. 4.3B).   However, there was

significantly greater phosphorylation of SERCA in the VPL group compared to control

(Fig. 4.3B).   This could be due to altered levels of proteins.   Accordingly, we normalized

phosphorylation to the unit amount of each substrate protein (Fig. 4.3C).   Such analysis

consistently showed that the phosphorylation of RyR (Fig. 4.3C, top) and SERCA (Fig.

4.3C, middle) was increased in the VPL group compared to control, confirming the

increased activity of SR-associated CaMKII.   However, phosphorylation of PLN was

lower in VPL group compared to control (Fig. 4.3C, bottom). This is likely due to the

pre-existing hyper-phosphorylation of PLN in VPL rats (Fig. 4.2), which reduces the

availability of PLN for CaMKII-mediated phosphorylation.
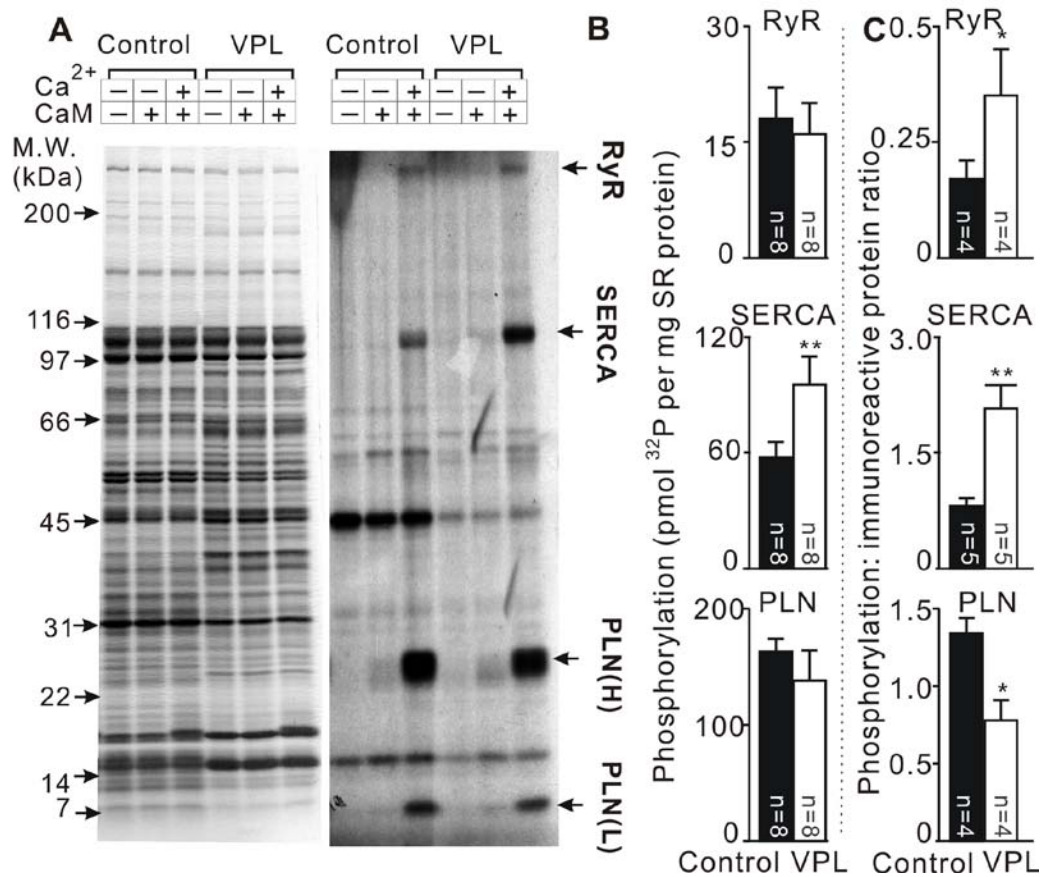
Fig. 4.3. The activity of SR-associated CaMKII is enhanced in VPL rats. The phosphorylation reaction was conducted for 2 min in the absence (−) and presence (+) of Ca^{2+}/calmodulin (CaM) as indicated. A, coomassie blue-stained gel showing protein profiles (left panel) of SR from control and VPL rats and autoradiogram of the same gel depicting protein phosphorylation (right panel). PLN(H) and PLN(L) denote high and low molecular weight forms of PLN. B, phosphorylation of individual substrates quantified and expressed as per unit amount of total SR protein. C, phosphorylation of individual substrates quantified and normalized as per unit amount of immunoreactive protein. The relative amount of each immunoreactive substrate was determined by scanning densitometry of Western immunoblots. Values are means ± SEM. * $P<0.05$, **$P<0.01$ VPL vs. control.

4.4.4   Exogenous PKA-catalyzed Phosphorylation of PLN in Control and VPL Rats.

PKA-mediated phosphorylation of PLN is a major mechanism for the heart to mobilize its contractile reserve in response to stress and exercise [40, 43]. The previous results showed that VPL rats had hyper-phosphorylation of PLN at the PKA phosphorylation site serine[16] *in vivo* (Fig. 4.2 C). Unlike CaMKII that is present both in the cytosol and in the SR, PKA is present in the cytosol but not in the SR. Therefore, we utilized exogenous PKA (catalytic subunit) to test further phosphorylation of PLN *in vitro* in cardiac SR vesicles derived from control and VPL rats. The phosphorylation reaction was carried out in the presence of $[\gamma\text{-}^{32}P]ATP$ as substrate for 2 minutes under the standard assay conditions. The results are presented in Fig. 4.4. The autoradiogram showed diminished phosphorylation of PLN by PKA in the VPL compared to control SR vesicles (Fig. 4.4 A, right panel). To quantify phosphorylation, bands were excised from the gel for scintillation counting. A decrease in PLN phosphorylation was apparent, but non-significant when comparing equivalent amounts of SR protein (Fig. 4.4B). When the data were normalized to unit amount of immunoreactive PLN protein, there were significantly lower levels of phosphorylation in VPL rats compared to control (Fig. 4.4C). A similar finding was noted earlier when the PLN phosphorylation *in vitro* by CAMKII was lower in VPL compared to control SR vesicles (Fig. 4.3 C). Thus, the reduced PLN phosphorylation *in vitro* in VPL group is likely due to the pre-existing hyper-phosphorylation of PLN by both PKA and CaMKII *in vivo*. Together, these data suggest that the preexisting hyper-phosphorylation of PLN reduces further PKA− and CaMKII−mediated PLN phosphorylation, which may cause depletion of cardiac contractile reserve in VPL rats.
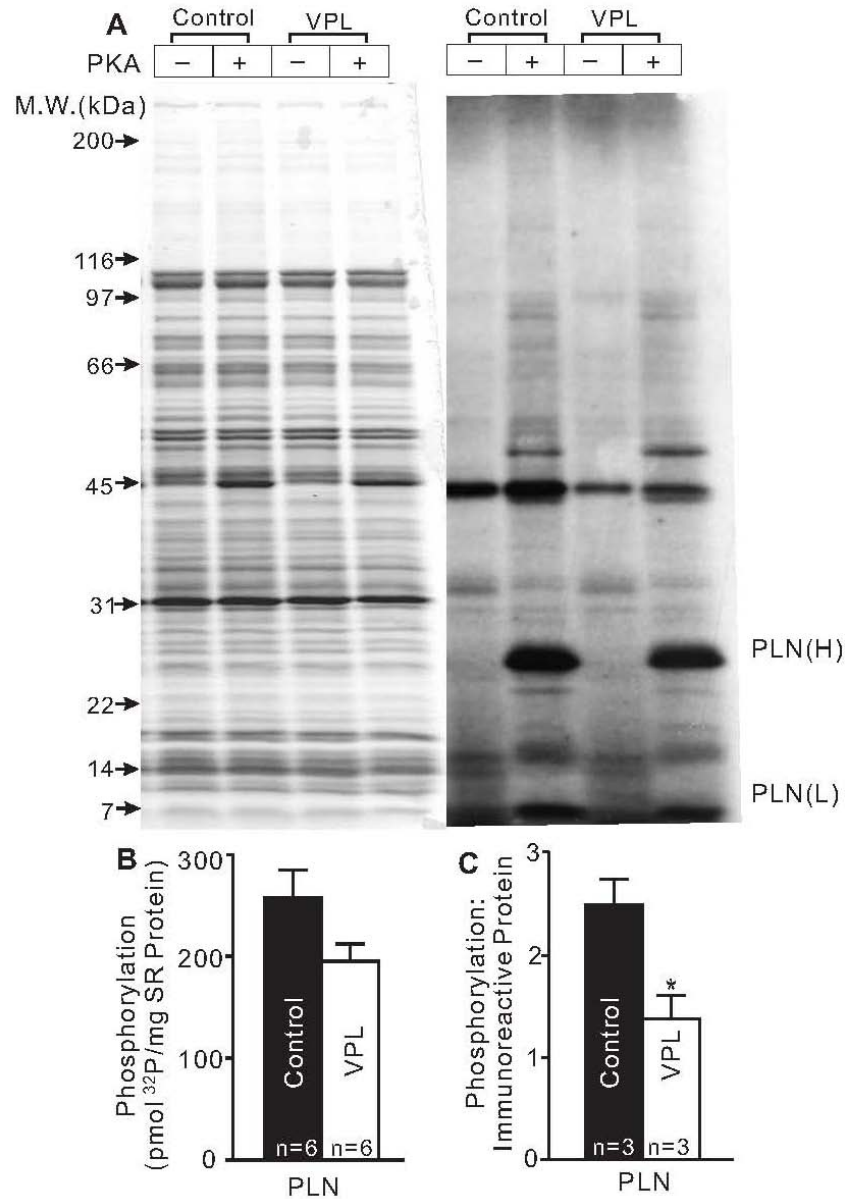
Fig. 4.4 Exogenous PKA−catalyzed phosphorylation of PLN in control and VPL rats. The phosphorylation reaction was conducted for 2 min in the absence (−) and presence (+) of catalytic subunit of PKA as indicated. A, coomassie blue-stained gel showing protein profiles (left panel) of SR from control and VPL rats and autoradiogram of the same gel depicting protein phosphorylation (right panel). PLN(H) and PLN(L) denote high and low molecular weight forms of PLN. B, phosphorylation of PLN quantified and expressed as per unit amount of total SR protein. C, phosphorylation of PLN is normalized and expressed as per unit amount of PLN immunoreactive protein content. The relative amount of each immunoreactive substrate was determined by scanning densitometry of Western immunoblots. Values are means ± SEM. * $P<0.05$, *vs*. control.

4.4.5 CaMKII−mediated Regulation of SR Calcium Pump Activity.

We next examined the functional consequence of CaMKII-mediated phosphorylation of SR calcium pumps. For this, ATP−dependent, oxalate−facilitated Ca^{2+} uptake by SR vesicle was measured in the absence or presence of CaM (3 µM). The latter condition promotes CaMKII activation and substrate phosphorylation. In the absence CaM, the Ca^{2+} uptake rate by SR vesicles both from control and VPL rats was increased at a wide range of free Ca^{2+} concentrations (0.01−8.2 µM) (Fig. 4.5A), confirming the widely known functional regulation of SERCA activity by CaMKII−mediated phosphorylation. Quantification of the kinetic parameters from the data in Fig. 4.5A revealed significantly increased maximum velocity of SR Ca^{2+} pumping (V_{max}) by addition of CaM in both groups (Fig. 4.5B, Table 4.1). The maximum stimulatory effect by CaM was significantly reduced by ~30% in VPL rats, indicating impairment in the CaM-dependent process for SERCA activation (Fig. 4.5B, Table 4.1). The relative stimulation of V_{max} by CaM was comparable in both groups (Fig. 4.5C). Considering SERCA protein levels are decreased in VPL rats [5], we normalized CaM-stimulating effect to SERCA protein levels. We found that the percentage of CaM-induced increase in V_{max} in VPL rats was significantly increased compared to control (Fig. 4.5D). Consistent with our previous findings, this suggests that SR-associated, endogenous CaMKII activity was enhanced in VPL rats.

In another parallel series of experiments, we performed the Ca^{2+} uptake assay by initiating the reaction by the addition of SR vesicles (instead of ATP as described above) following pre-incubation of the rest of the assay components. The observed Ca^{2+} uptake profiles as a function of Ca^{2+} concentrations were similar to those seen previously when

reaction was initiated by ATP (Fig. 4.5A *vs.* Suppl. Fig. 4.2A). However, the stimulatory

effect of exogenous CaM was less pronounced (Fig. 4.5B *vs.* Suppl. Fig. 4.2B). In those

experiments where exogenous CaM was absent, the V_{max} of SR Ca^{2+} uptake was

significantly greater when the reaction was initiated by SR than that when the reaction

was initiated by ATP (Fig. 4.5 B and Suppl. Fig. 4.2 B). Previous studies have

documented that Ca^{2+} uptake activity of cardiac SR was enhanced when the Ca^{2+}

transport cycle is initiated by the addition of SR, instead of ATP [44]. Such differences in

Ca^{2+} transport activity apparently result from qualitatively different conformations of

SERCA2 due to differences in the order in which SERCA2 encounters Ca^{2+} and ATP [44].

Table 4.1. Kinetic parameters of Ca^{2+} transport by cardiac SR from control and verapamil-treated rats in the absence or presence of calmodulin (CaM).

	V_{max} (nmol Ca^{2+}/mg protein/min)	$K_{0.5}$ (µM)	n_H
Control – CaM	159 ± 10	1.8 ± 0.1	1.3 ± 0.1
Control + CaM	256 ± 14**	1.9 ± 0.2	1.2 ± 0.1
VPL – CaM	103 ± 21**	1.9 ± 0.2	1.2 ± 0.1
VPL + CaM	174 ± 29##;!	2.0 ± 0.3	1.3 ±0.1

Ca^{2+} uptake reaction was started with ATP . Values are means ± SEM; n=7/group. V_{max}, maximum velocity of Ca^{2+} uptake; $K_{0.5}$, Ca^{2+} concentration giving one-half of V_{max} ; n_H, Hill coefficient. ** $P<0.01$ *vs.* control – CaM; ## $P<0.01$ *vs.* VPL – CaM; ! $P<0.05$ *vs.* Control + CaM.
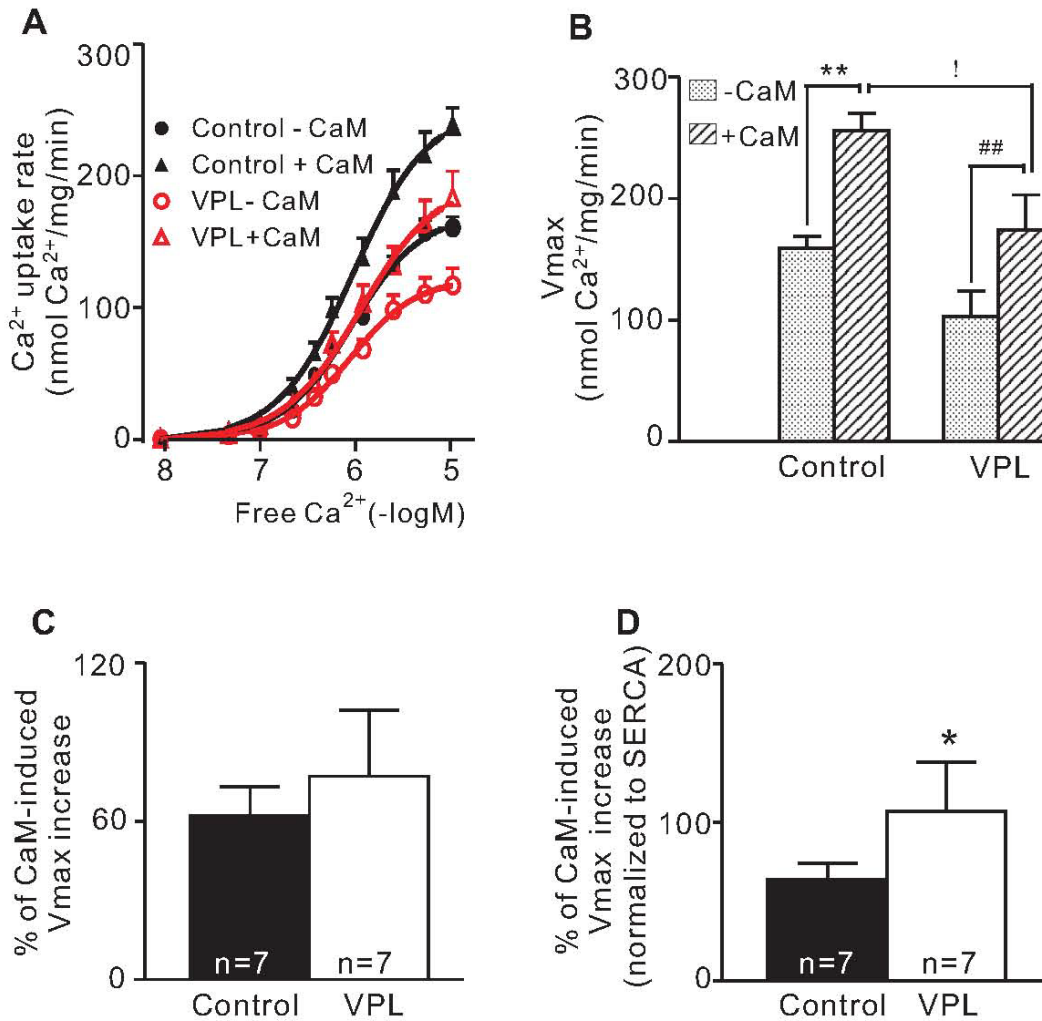
Fig. 4.5 CaMKII−mediated regulation of SR calcium pump activity. Calmodulin (CaM, 3 μmol/L) stimulation of SR Ca^{2+} uptake was examined by starting the Ca^{2+} uptake reaction with ATP. A, the Ca^{2+} uptake reaction was conducted for 1 min in the standard assay medium with varying free Ca^{2+} concentrations as indicated. B, Bar graphs represent the maximum velocity of SR Ca^{2+} uptake (V_{max}) derived from the data shown in panel A. C, Bar graphs represent the percentage of CaM-induced V_{max} increase. D, the percentage of CaM-induced V_{max} was normalized and expressed as per unit amount of immunoreactive SERCA protein content. The relative amount of SERCA in SR was determined by scanning densitometry of western blots. n=7 preparations/group. Values are means ± SEM. ** $P<0.01$; ## $P<0.01$; ! $P<0.05$.
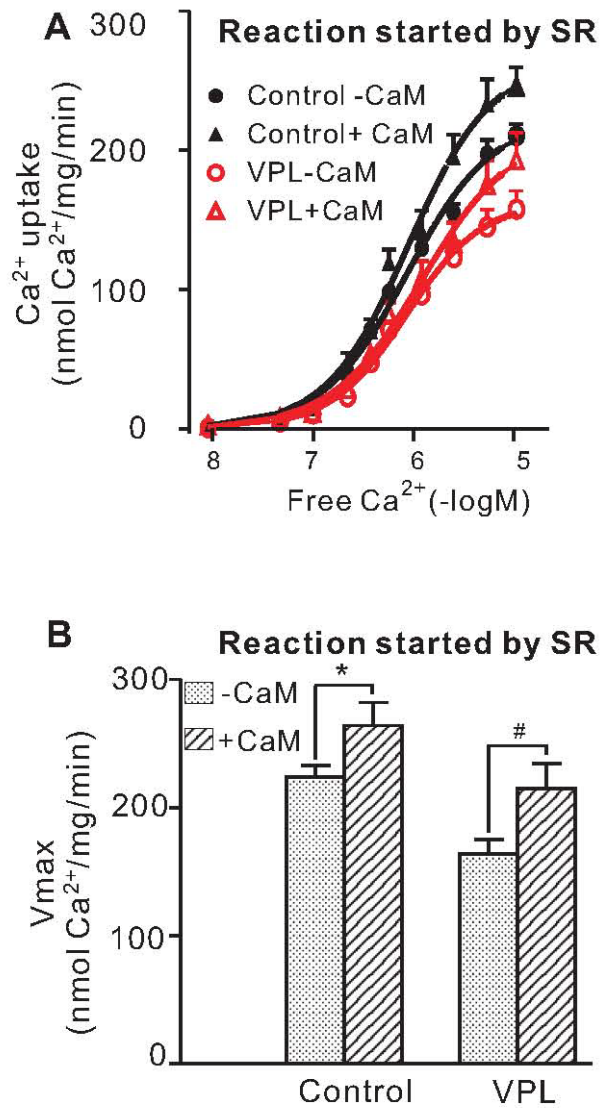
Suppl. Fig. 4.2 Endogenous CaMKII–mediated stimulation of SR Ca^{2+} sequestration when reaction is started by SR vesicles.   A, CaM (3 μmol/L) stimulation of SR Ca^{2+} uptake at varying Ca^{2+} concentrations was repeated by starting Ca^{2+} sequestration with SR vesicles. B, bar graphs represent the maximum velocity of SR Ca^{2+} uptake (V_{max}) derived from A. n=4 preparations/ group. Values are means ± SEM. * $P<0.05$ *vs.* control – CaM; # $P<0.05$ *vs.* VPL – CaM.

4.4.6   Effects of exogenous PKA on SR Calcium Pump Activity.

Since SR membrane lacks PKA, the influence of PKA on SR Ca^{2+} pump function was examined using exogenous catalytic subunits of PKA. For this, Ca^{2+} uptake assays were performed at saturating and sub-saturating free Ca^{2+} assay medium in the absence or presence of PKA (catalytic subunits). At sub-saturating Ca^{2+} (1 μM free Ca^{2+}), PKA significantly increased the rate of Ca^{2+} uptake in both control and VPL groups (Fig. 4.6, left panel), showing the expected stimulatory effect of PKA on SR Ca^{2+} transport. However, PKA-mediated V_{max} for SR Ca^{2+} transport at saturating Ca^{2+} (11 μM free Ca^{2+}) was significantly increased in control, but not in the VPL group (Fig. 4.6, right panel). Moreover, the Ca^{2+} uptake rate was reduced in VPL rats compared to control. These findings reveal reduced responsiveness of SR calcium pump to PKA in VPL rats. The diminished responsiveness may be explained in part by the pre-existing hyper-phosphorylation (Figs. 4.2 and 4.4).
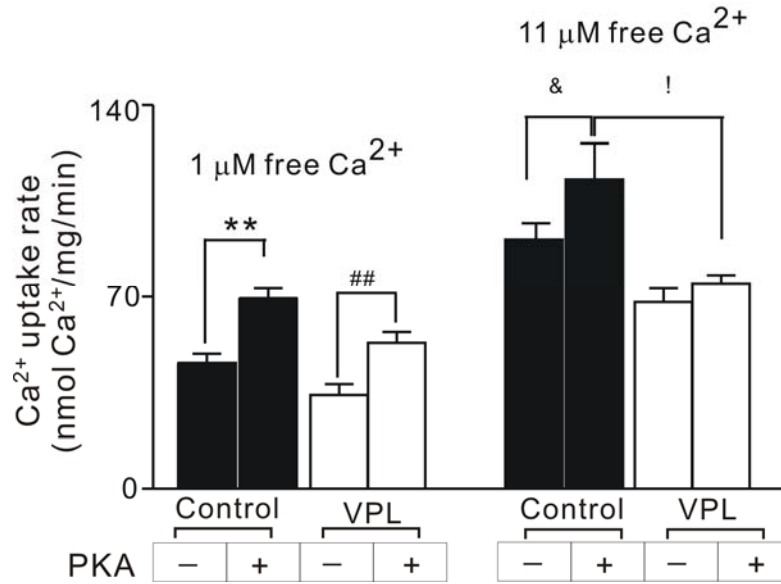
Fig. 4.6 Effects of exogenous PKA on cardiac SR Ca^{2+} pump function in control and VPL rats. The Ca^{2+} uptake was measured in the absence or presence of catalytic subunit of PKA in the standard assay medium with 1 μmol/L free Ca^{2+} and 11 μmol/L free Ca^{2+}. Our previous experiments demonstrated that 1 μmol/L free Ca^{2+} gives rise to half of maximum velocity (V_{max}) of Ca^{2+} uptake and 11 μmol/L free Ca^{2+} gives rise to V_{max} of Ca^{2+} uptake. n=5 preparations/ group. Values are means ± SEM. $^{\&}$ $P<0.05$, $^{!}P<0.05$, $^{**}P<0.01$, $^{\#\#}P<0.01$.

4.4.7 Frequency-dependent Acceleration of Relaxation (FDAR).

So far we demonstrated that chronic DHPR blockade leads to alterations in phosphorylation of key calcium cycling proteins, involving CaMKII and PKA, at the molecular and subcellular levels. We extended these studies to examine SR Ca^{2+} pump function at the cellular level. Since CaMKII is implicated to mediate FDAR [45-47], we investigated the characteristics of FDAR in myocytes isolated from control and VPL rats. Freshly isolated ventricular myocytes were loaded with the Ca^{2+} indicator dye fura-2, field-stimulated over a range of frequencies, and $[Ca^{2+}]_i$ transients were monitored. When $[Ca^{2+}]_i$ transients were normalized to same height and superimposed, we noticed that increased frequency of stimulation gave rise to faster recovery times of the calcium transients in control and VPL myocytes (Fig. 4.7A and B). Thus the FDAR phenomenon [37, 48] was apparent in both control and VPL myocytes. However, the rate of recovery of calcium was slower at all frequencies in VPL myocytes compared to control (compare Fig. 4.7A and B), consistent with previous findings [5]. To quantify this, we fitted the decline of twitch $[Ca^{2+}]_i$ transients with a single exponential decay. The τ of $[Ca^{2+}]_i$ decline was longer in VPL myocytes compared to control (Fig. 4.7C), reflecting depressed SR Ca^{2+} transport activity, possibly accounted for by diminished SR pump quantity in VPL myocytes [5]. Analysis of the ratio of τ at 2 Hz / 0.25 Hz (Fig. 4.7D) showed no significant difference between the two groups, indicating that FDAR is preserved in VPL rats.
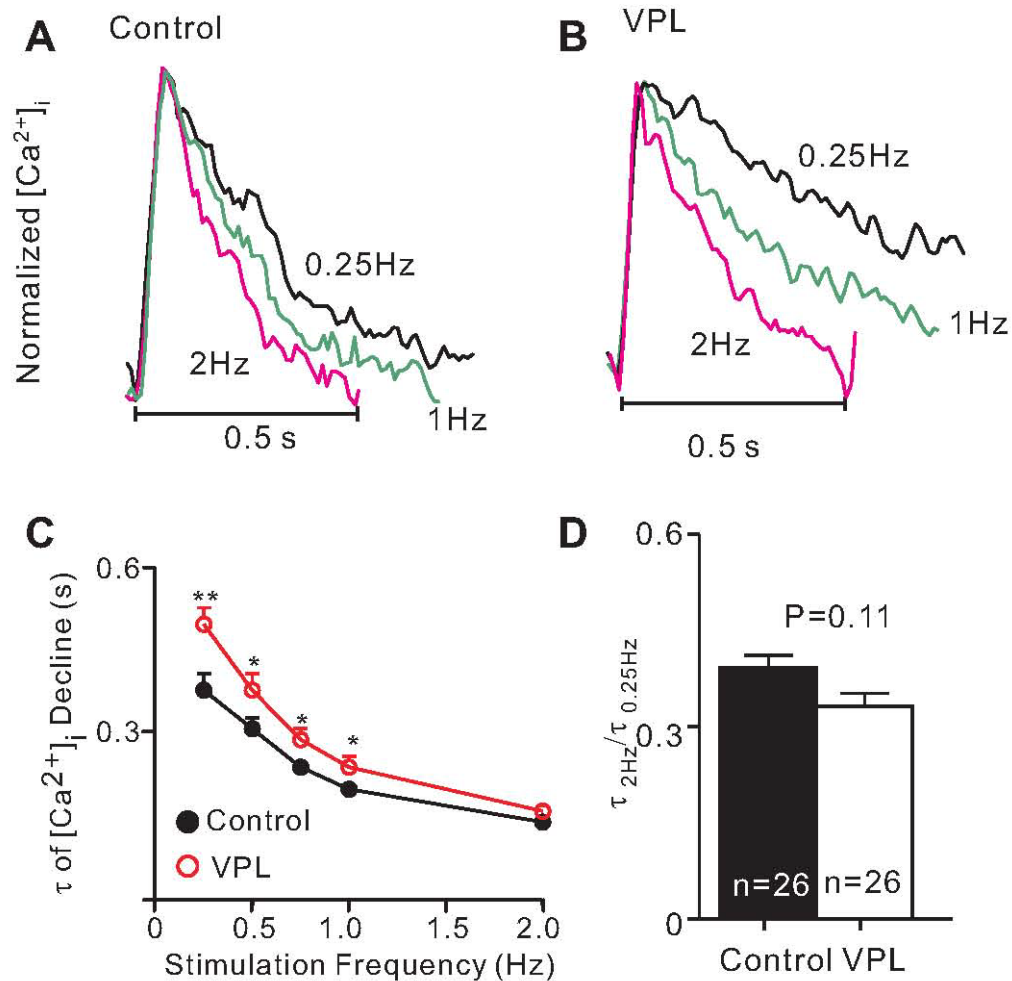
Fig. 4.7 Frequency-dependent acceleration of relaxation (FDAR). A, B $[Ca^{2+}]_i$ transients of a control (A) and VPL myocyte (B) at stimulation frequencies of 0.25, 1, 2 Hz were normalized to same height and superimposed, showing evident FDAR in both control and VPL myocytes. C, the decline of twitch $[Ca^{2+}]_i$ transients were fitted with a single exponential decay equation and τ of $[Ca^{2+}]_i$ decline at different frequencies was plotted to show FDAR in both control and VPL myocytes (Fig.4.7C). τ of $[Ca^{2+}]_i$ decline of VPL myocytes was apparently longer than that of control myocytes at all stimulation frequencies, indicating depressed SR Ca^{2+} transport function in VPL rats. D, Bar graphs represent the extent of FDAR at the extremes of the frequencies tested as ratio of τ 2Hz versus 0.25 Hz(τ 2Hz/τ0.25 Hz). n=26 cells / group. Values are means $\pm$ SEM. * $P<0.05$, **$P<0.01$ VPL *vs*. control.

4.4.8   Cardiac Response to the β-adrenergic Stimulation is Compromised in VPL Rats.

The present studies have demonstrated that chronic verapamil treatment leads to altered phosphorylation status of Ca^{2+} cycling proteins, with functional changes apparent in isolated SR vesicles and intact cardiomyocytes. To establish whether these adaptive changes are manifested at the whole animal level, we examined cardiac contractile response to β-adrenergic stimulation *in vivo*. Catheters were inserted into the left ventricle of anaesthetized rats to monitor intraventricular pressure, and isoproterenol (Iso, 0.3 to 3 μg/kg body weight) was administered intravenously. In control rats, Iso elicited marked, dose-dependent stimulation of developed pressure, reflecting activation of PKA signaling pathways (Fig. 4.8A, left panel). Developed pressure was markedly reduced and end-diastolic pressure was elevated at all doses of Iso in VPL compared to control rats. In contrast to control rats, Iso did not elicit any change in developed pressure in VPL rats (Fig. 4.8A, right panel). To quantify this functional response, we analysed developed pressure, heart rate and peak rates of pressure change (+dP/dt Max and -dP/dt Min). All of these functional indices were depressed over the range of concentrations of Iso in VPL rats compared to control (Fig. 4.8B), consistent with the depressed heart function reported previously [5]. We note that the chronotropic response of Iso was preserved, whereas the inotropic response to Iso was impaired.

We found that VPL rats exhibit significantly reduced +dP/dt Max and -dP/dt Min and percentage increase at peak Iso dose compared to control (Suppl. Fig.4.3), further suggesting reduced contractile reserve and attenuated reserve recruitment by β-adrenergic stimulation.
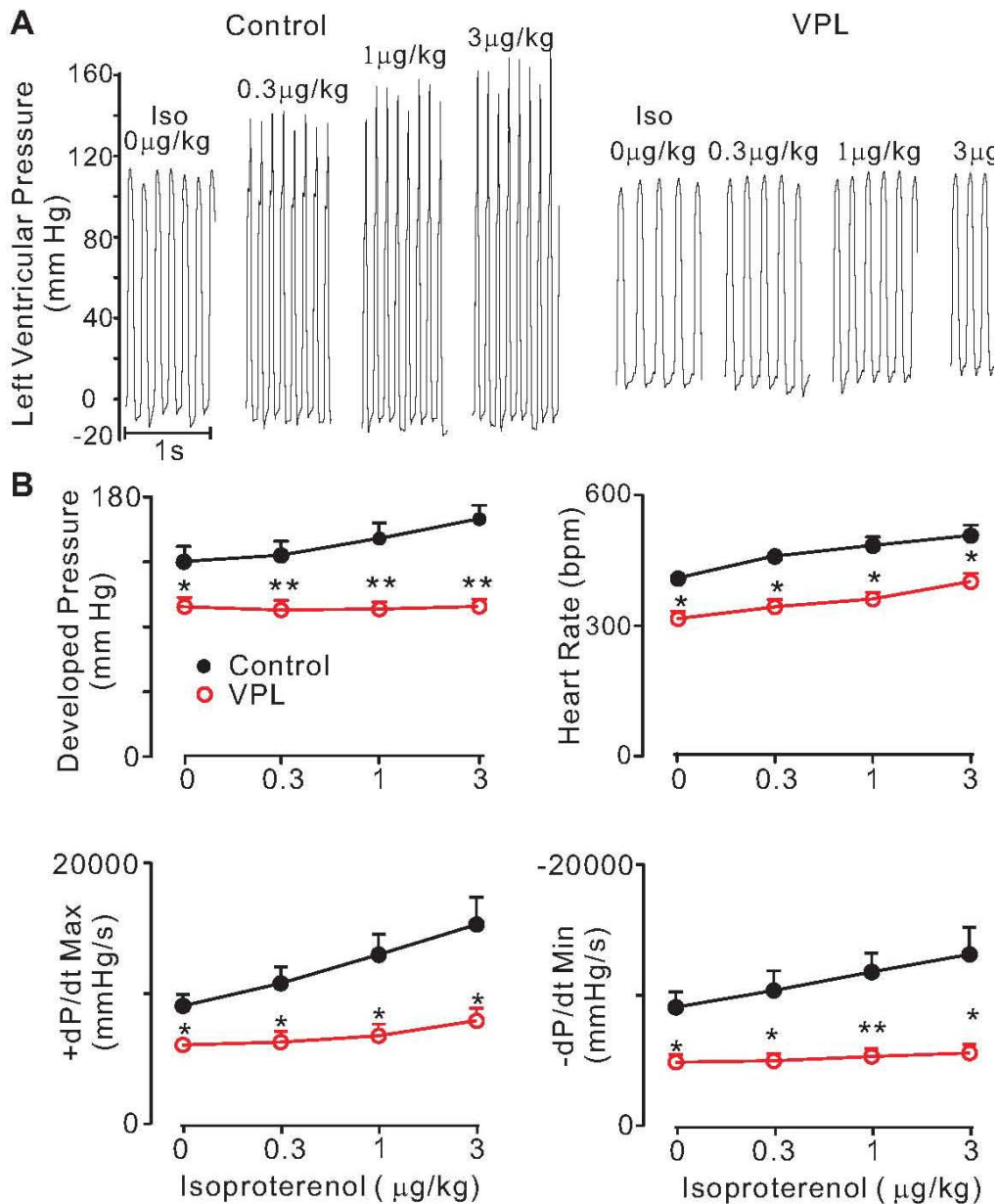
Fig. 4.8 Cardiac response to the β-adrenergic stimulation is compromised in VPL rats. Catheters were inserted into the left ventricle of anaesthetized rats to monitor pressure and 0.3 to 3 μg/kg isoproterenol (Iso) was given intravenously. A, Representative recordings of left intraventricular pressure reveal markedly reduced developed pressure, heart rate and blunted dose-dependent Iso stimulatory effect on developed pressure in VPL rats compared to control. B, Quantification of developed pressure, heart rate, and the maximum rates of intraventricular pressure change (dP/dt Max, -dP/dt Min). n=5 rats/ group. Values are means ± SEM. * P<0.05, **P<0.01 VPL vs. control.
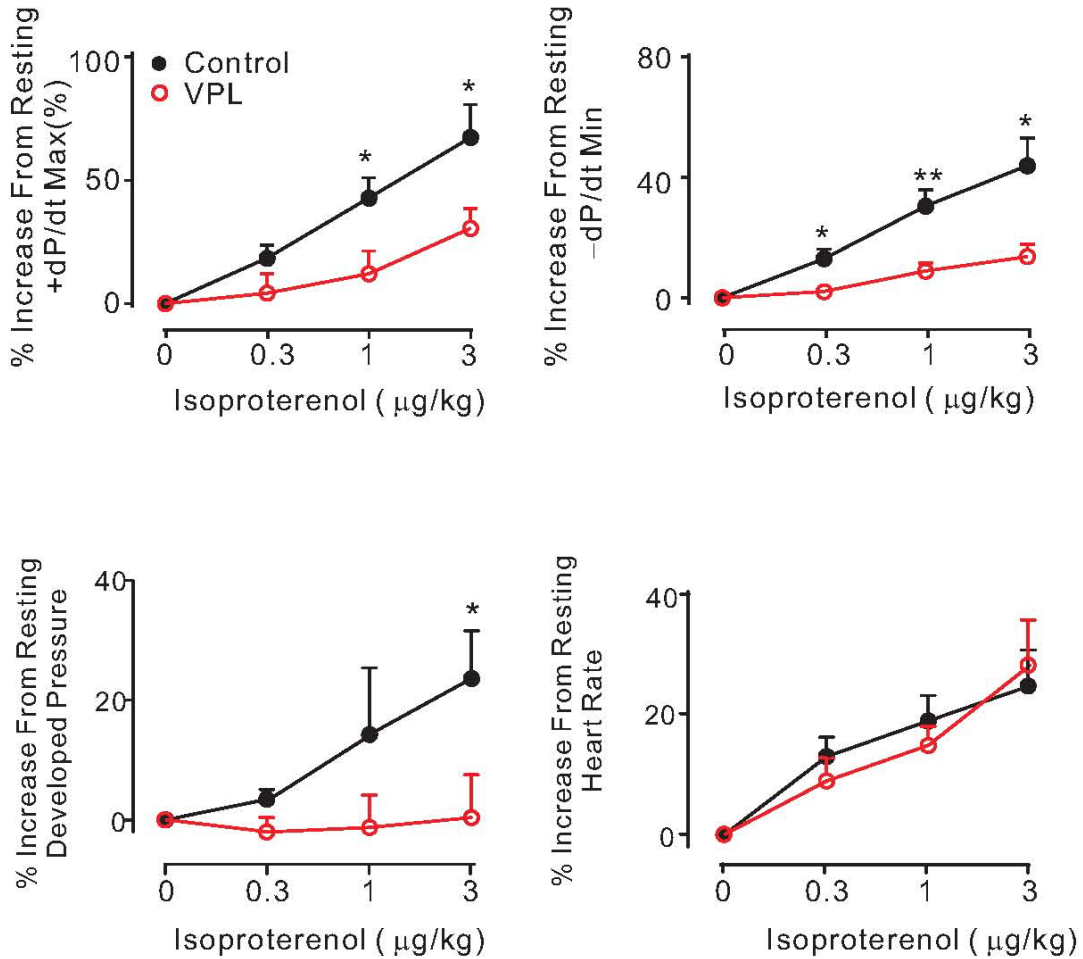
Suppl. Fig. 4.3 Isoproterenol-mediated stimulation of cardiac contraction *in vivo*. Supplemental to figure 4.8, the maximum rates of intraventricular pressure change (+dP/dt Max, -dP/dt Min), the developed pressure and the heart rate under isoproterenol stimulation were quantified as percentage change from the resting state. n=5 rats/ group. Values are means ± SEM. * *P<0.05*, ***P<0.01* VPL *vs*. control.

4.4.9   Chronic Verapamil Treatment Does Not Lead to Ventricular Hypertrophy.

Cardiac hypertrophy is the natural response of the myocardium to various stressors, including neurohormonal stimuli, hemodynamic overload, and injury [49]. Depression of the myocardium's intrinsic contractility is an important mechanism underlying the transition from hypertrophy to heart failure [50]. We have observed that myocardium's intrinsic contractile properties are compromised in response to chronic, yet partial blockade of DHPRs. Thus it is imperative to explore whether cardiac adaptation to the chronic stressor of DHPR blockade is associated with hypertrophy. To address this we examined a number of different hypertrophic indices. Measurement of cell dimensions of isolated ventricular myocytes enabled us to calculate cell volume, which was not different between the two groups of rats (Fig. 4.9A). Histological analysis of whole heart tissue stained with Masson's trichrome showed no apparent change of cell size (Fig. 4.9B) or ventricular wall thickness (Fig. 4.9C). Quantification of these parameters revealed no significant difference between VPL and control rats (Fig. 4.9D). We took the analysis even further by comparing heart and lung weights, normalized to whole body weight. We found no significant difference in the ratio of left ventricle (LV) to body weight, the right ventricle (RV) to body weight, suggesting there was no cardiac hypertrophy in VPL rats (Fig. 4.9E). Moreover, the ratio of lung to body weight in VPL rats did not differ from control (Fig. 4.9E), showing no evidence for pulmonary edema.
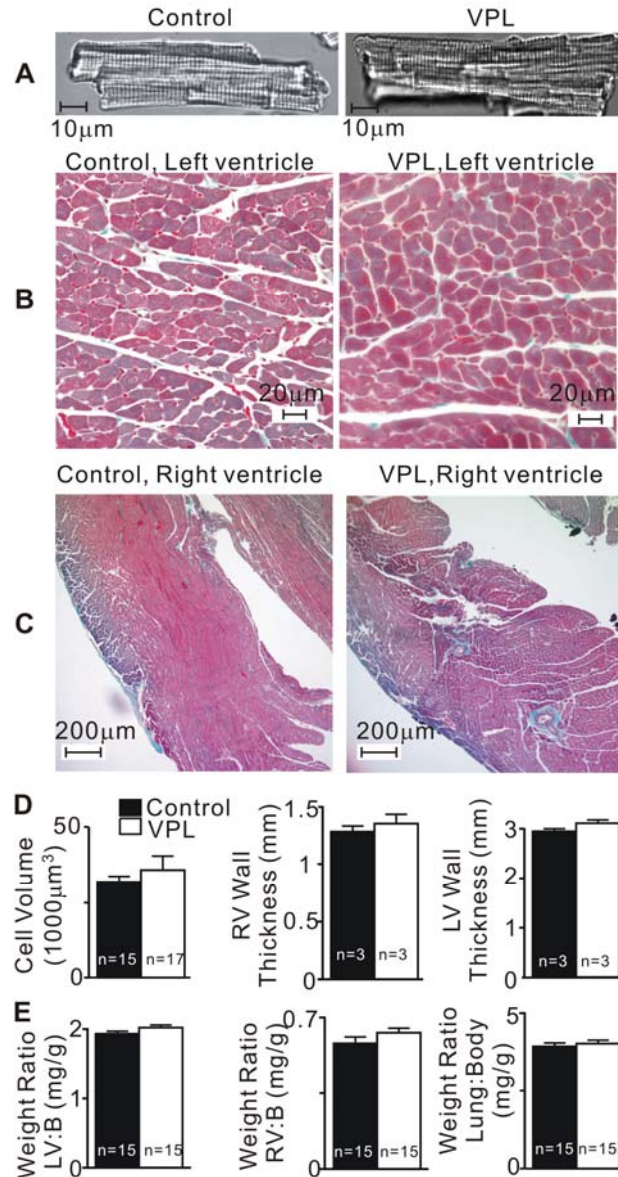
Fig. 4.9 Chronic verapamil treatment does not lead to ventricular hypertrophy. Macroscopic and microscopic morphological parameters indicate no cardiac hypertrophy in the verapamil-treated (VPL) rats compared to control. A, typical ventricular cardiomyocytes isolated from control and VPL rats. B, Typical Masson's trichrome-stained histological sections show the cell size of left ventricles (LV) from control and VPL rats (Magnification, 60X). C, Typical Masson's trichrome-stained histological sections show wall thickness of right ventricles (RV) from control and VPL rats (Magnification, 10X). D, Bar graphs represent cell volume (n=15 cells for control and 17 cells for VPL from 3 preparations of each group), thickness of RV free wall (n=3 rats / group), thickness of LV free wall (n = 3 rats /group). E, Bar graphs represent weight ratio of LV :body weight (n =15 rats /group), weight ratio of RV :body weight (n =15 rats /group), and lung to body weight (n = 15 rats /group).

4.5   Discussion

In this study, we made the following key observations in long-term verapamil-treated rats: 1) hyper-phosphorylation of SR Ca^{2+} cycling proteins, 2) up-regulation of CaMKII and PKA activities, 3) reduced substrate reserve in the SR for CaMKII− and PKA−medicated protein phosphorylation, and 4) decreased cardiac contractile reserve. These observations, ranging from molecular, subcellular, cellular, organ to whole animal level, provide mechanisms for the functional remodeling of SR and a predisposition to heart dysfunction incurred from chronic DHPR blockade.

4.5.1   Hyper-phosphorylation of SR Ca^{2+} Cycling Proteins Remodels RyR Function and Predisposes Heart to Contractile Dysfunction and Arrhythmias.

Phosphorylation-dependent regulation of SR activity is physiologically and pathologically important, as it underlies the mobilization of cardiac functional reserve during exercise and it is implicated in cardiac diseases such as heart failure and atrial fibrillation [51, 52]. Phosphorylation of RyR is generally regarded as an important mechanism for modulating the channel's gating properties [11] and regulating channel Ca^{2+} release function [12, 13]. RyR can be phosphorylated by CAMKII and PKA [10, 19, 51, 53]. So far, three phosphorylation sites have been identified. In humans and rodents, they are serine (S) 2808 (S2809 in rabbit), S2814 (S2815 in rabbit), and S2030 (S2031 in rabbit) [11]. RyR S2808/S2809 is suggested to be phosphorylated by both PKA and CAMKII [11]; whereas S2814/S2815 is suggested only by CaMKII [20] and S2030/S2031 only by PKA [54]. The exact effects of phosphorylation on channel function remain controversial as both stimulatory and inhibitory effects have been reported [9, 10, 53]. However, recent evidence

supports that RyR phosphorylation leads to increased RyR open probability and SR Ca^{2+} leak [13, 13, 51, 55, 56], which can lead to heart failure [51] and arrhythmias [55]. The PKA-mediated enhancement in SR Ca^{2+} leak is CaMKII-dependent [13]. Hyper-phosphorylation of RyR has been implicated in RyR dysfunction and heart failure [36, 51, 57]. This increased "leakiness" of the SR could underlie the increased propensity for arrhythmia in heart failure and eventually contribute to decreased contractility by reducing SR Ca^{2+} load. However, several studies have questioned RyR hyper-phosphorylation in heart failure [58, 59], and the functional consequence of RyR phosphorylation remains controversial [60]. Considering chronic verapamil treatment leads to abnormal gating properties of cardiac RyRs and hyperactive spark sites (see chapter 2), the current finding of hyper-phosphorylation of RyR supports the notion that phosphorylation of RyRs increases SR Ca^{2+} leak from SR that can lead to arrhythmia and heart failure.

4.5.2   The Paradox of PLN Hyper-phosphorylation and Reduced SERCA Function.

The phosphorylation of PLN is thought to release the inhibition of PLN on SERCA2 and restore SERCA2 affinity for Ca^{2+} [1, 8, 14]. On the other hand, dephosphorylated PLN inhibits V_{max} of Ca^{2+} transport and lowers the affinity of SERCA2 for calcium [8]. Studies have shown that dephosphorylation of PLN acts as a brake on the SERCA2 pump whereas phosphorylation releases the "brake" and substantially increases Ca^{2+} transport activity and relaxation rate [40]. Our study has shown the PLN was hyper-phosphorylated but basal SERCA Ca^{2+} uptake activity was paradoxically reduced after chronic DHPR blockade. Since the PLN can be phosphorylated at threonine 17 by CaMKII [14, 43, 61], the hyper-phosphorylation of PLN can be partially explained by the

observed up-regulation of CaMKII expression and activity in VPL rats. This paradoxical phenomenon of up-regulated CaMKII, hyper-phosphorylated PLN with reduced SERCA function is also observed in many animal models of heart failure [37, 62, 63]. This paradox can be partially explained by the reduced SERCA and increased PLN protein levels in VPL rats (see chapter 3). However, the phosphorylation of PLN at serine 17 was increased by 300% while SERCA protein level is only reduced by ~30% and PLN up-regulated ~20% in VPL rats (see chapter 3). As the phosphorylation change is disproportional to protein level change, the alteration of protein levels cannot fully explain why PLN hyper-phosphorylation fails to increase the basal SERCA activity. Thus this paradox indicates that the phosphorylation alone is not enough to release PLN inhibition on SERCA, and an event down-stream of PLN phosphorylation likely controls SERCA function. Such event could be the CaM-SERCA interaction and consequent PLN-SERCA dissociation to stimulate SR Ca^{2+} transport. As the classic mechanistic concept, phosphorylation of PLN is thought to dissociate the inhibited PLN–SERCA2 complex [8]. However, this long-standing view has been questioned by a study from Dr. MacLennan's group which reported that PLN phosphorylation does not cause dissociation of PLN-SERCA complex, but Ca^{2+} does [64]. However, recent work from our laboratory has shown that the dissociation of PLN-SERCA complex is not an autonomous function of Ca^{2+}; it is a Ca^{2+}-dependent function of calmodulin [33,16]. Thus, it appears that a CaM-dependent process, in addition to or independent of PLN phosphorylation, is required for relief from PLN inhibition of SERCA. It is likely that the reduced SERCA function despite PLN hyper phosphorylation in the VPL rats reflects impairment of a CaM-dependent process that is obligatory for SERCA activation.

4.5.3 Hyper-phosphorylation of SR Ca^{2+} Cycling Proteins Reduces Cardiac Contractile Reserve.

In response to stress and exercise, the reserve of heart contractility is utilized to meet the body's increased demand for blood flow. Cardiac contractile reserve is defined as the difference between the basal and maximum cardiac work [65]. Reduced contractile reserve can be reflected as either reduced maximal performance that the heart can achieve or increased basal activity. Both the magnitude of this reserve and its responsiveness to recruitment are determinants of the risk of heart failure and prognosis in patients with cardiovascular diseases [65] [66]. In theory, how good the heart is as a pump can be best represented by the maximum cardiac work achieved by the heart during maximal stimulation, and this value is termed the cardiac pumping capability [67]. Cardiac contractile reserve assessed by pharmacological stimulation has been shown to correlate with that assessed by physiological stimulation via exercise testing [67, 68]. Thus cardiac reserve as estimated by isoproterenol challenge can be taken to represent the functional capacity of the heart [68]. Administration of isoproterenol revealed that chronic verapamil treatment attenuates cardiac response to the β-adrenergic stimulation *in vivo*. This strongly indicates chronic inhibition of DHPRs reduces cardiac contractile reserve. In response to stress and exercise, the fall in contractile reserve can lead to heart failure and provides an explanation for the increased risk encountered by the patients receiving long-term DHPR blocker treatment [6, 7].

The mobilization of cardiac reserve is mainly achieved by recruiting SR functional reserve (i.e. reserve for faster, stronger SR Ca^{2+} release and reuptake) through phosphorylation of Ca^{2+} cycling proteins in E-C coupling [8] [17]. CaMKII and PKA are the

major protein kinases that mediate phosphorylation of these proteins and thus regulate the SR functional reserve [8, 20]. Unphosphorylated PLN preserves SR function by inhibiting SR Ca^{2+} pump activity [8]. When PLN is phosphorylated at threonine 17 by CaMKII or at serine 16 by PKA, the PLN inhibition of SERCA is relieved and the SR functional reserve is mobilized for faster cardiac relaxation [14]. In addition, CaMKII can mobilize SR functional reserve through direct phosphorylation of SERCA as well [15, 32, 69, 70]. Our laboratory discovered a direct phosphorylation of SERCA2 at serine 38 by CaMKII, and consequent activation of Ca^{2+} transport through an increase in V_{max} [15]. This phenomenon has been confirmed by studies in other laboratories [69, 70]. Finally, as RyR phosphorylation by CaMKII and/or PKA increases the propensity of RyRs to open and accelerates SR Ca^{2+} release [51, 55, 71-74], CaMKII−, PKA−dependent phosphorylation of RyRs potentially could be another intrinsic mechanism to mobilize SR functional reserve for stronger, faster contractions in response to stress and exercise.

In present study, SR functional reserve was apparently reduced in VPL rats because of a) increased preexisting phosphorylation levels of SR Ca^{2+} cycling proteins; b) reduced availability of substrates for PKA− and CaMKII−mediated phosphorylation; and c) reduced stimulatory effects of CaMKII and PKA on SR Ca^{2+} transport. Furthermore, we have reported previously that SR Ca^{2+} content is reduced after chronic verapamil treatment (see chapter 2 and 3), which can further depress SR functional reserve by reducing the availability of Ca^{2+} in the SR lumen to be released for stronger contraction. Therefore, reduced SR functional reserve provides a subcellular mechanism for reduced contractile reserve in VPL rats.

4.5.4   Myocardial Intrinsic Contractile Properties Can Be Compromised Without Passing Through a Compensated Stage of Hypertrophy.

Following a pathological stress, the heart can adapt by cardiac hypertrophy, which improves contractile force to meet the new body demands [49, 75]. Cardiac hypertrophy may be considered as a mechanism for compensation as in "physiologic" cardiac hypertrophy in response to exercise, pregnancy, etc. When the stimulus is prolonged, cardiac hypertrophy can decompensate toward heart failure, with compromised pump function [49, 75]. However, this general pattern may not always be consistent. Indeed, some experimental models of heart failure have been reported to lack a compensated period before the full-blown stage of heart failure [76]. In the present study, ventricular hypertrophy did not develop and cellular morphology was normal following chronic verapamil treatment. However, the compromised cardiac intrinsic functions in VPL rats are evident at molecular, subcellular, cellular, organ, and whole animal levels. Considering depression of myocardial intrinsic contractility is an important mechanism for developing heart failure [50], our animal model supports that a compensated period of hypertrophy is not necessary in the progression to heart failure.

4.5.5   Conclusions

The present study further explored the impact of chronic DHPR blockade on protein phosphorylation-dependent regulation of SR function by CaMKII and PKA. It is reasonable to speculate that DHPR blockade depresses basal contractility by reducing CICR that would have preserved more SR and cardiac contractile reserve. Surprisingly, the results reported here show chronic, yet partial blockade of DHPRs by verapamil

attenuates cardiac contractile reserve. Since the cardiac functional reserve determines the risk of heart failure and prognosis in patients with cardiovascular diseases [65] [66], our finding provides mechanistic insights for the risk associated with long-term treatment with DHPR blockers in patients.

In conclusion, chronic, partial DHPR blockade hyper-phosphorylates SR Ca^{2+} cycling proteins, increases activities of CaMKII and PKA, reduces SR functional capacity, and consequently attenuates contractile reserve of the heart. These pathogenic abnormalities occur in the absence of cardiac hypertrophy and contribute to the SR functional remodeling ensued from long-term verapamil treatment.

4.6   References

1.   Bers DM. Cardiac excitation-contraction coupling. *Nature*. 2002;415:198-205

2.   Zhou J, Xu A, Jiang M, Jones DL, Sims SM, Narayanan N. Chronic L-type calcium channel blockade with verapamil causes cardiac ryanodine receptor remodeling and predisposition to heart failure in the rat. *Circ Heart Fail*. 2010

3.   Zhou J, Xu A, Jones D, Sims SM, Narayanan N. Impaired expression and function of cardiac ryanodine receptors underlie predisposition to heart failure following long-term verapamil treatment. . *Acta Physiol Sin.* 2008;60 65~66

4.   Zhou J, Sims SM, Narayanan N. Depressed Ca^{2+} cycling by cardiac sarcoplasmic reticulum (SR) following chronic blockade of L-type Ca^{2+} channels. *Journal of Molecular and Cellular Cardiology*. 2006;40:914-914

5.   Zhou J, Xu A, Chakrabarti S, Jones DL, Sims SM, Narayanan N. Remodelling of cardiac sarcoplasmic reticulum calcium pump and diastolic dysfunction ensue chronic L-type calcium channel blockade in the rat. *Circ Heart Fail*. 2010

6.   Eisenberg MJ, Brox A, Bestawros AN. Calcium channel blockers: an update. *Am J Med*. 2004;116:35-43

7.   Black HR, Elliott WJ, Grandits G, Grambsch P, Lucente T, White WB, Neaton JD, Grimm RH, Jr., Hansson L, Lacourciere Y, Muller J, Sleight P, Weber MA, Williams G, Wittes J, Zanchetti A, Anders RJ. Principal results of the Controlled Onset Verapamil Investigation of Cardiovascular End Points (CONVINCE) trial. *Jama*. 2003;289:2073-2082

8.   MacLennan DH, Kranias EG. Phospholamban: a crucial regulator of cardiac contractility. *Nat Rev Mol Cell Biol*. 2003;4:566-577

9.   Wehrens XH, Marks AR. Altered function and regulation of cardiac ryanodine receptors in cardiac disease. *Trends Biochem Sci*. 2003;28:671-678

10.   Meissner G. Ryanodine receptor/Ca^{2+} release channels and their regulation by endogenous effectors. *Annu Rev Physiol*. 1994;56:485-508

11.   Huke S, Bers DM. Ryanodine receptor phosphorylation at Serine 2030, 2808 and 2814 in rat cardiomyocytes. *Biochem Biophys Res Commun*. 2008;376:80-85

12.   Eisner DA, Kashimura T, O'Neill SC, Venetucci LA, Trafford AW. What role does modulation of the ryanodine receptor play in cardiac inotropy and arrhythmogenesis? *J Mol Cell Cardiol*. 2009;46:474-481

13.   Currie S. Cardiac ryanodine receptor phosphorylation by CaM Kinase II: keeping the balance right. *Front Biosci*. 2009;14:5134-5156

14.   Kadambi VJ, Kranias EG. Phospholamban: a protein coming of age. *Biochem Biophys Res Commun*. 1997;239:1-5

15.   Xu A, Netticadan T, Jones DL, Narayanan N. Serine phosphorylation of the sarcoplasmic reticulum Ca^{2+}-ATPase in the intact beating rabbit heart. *Biochem Biophys Res Commun*. 1999;264:241-246

16.   Narayanan N, Xu A, Virdee I. Interplay of Phospholamban in Calmodulin Control of Sarcoplasmic Reticulum Calcium Pump Function. *J Mol Cell Cardiol*. 2007;42:s37

17.   Narayanan N, Xu A. Phosphorylation and regulation of the Ca^{2+}-pumping ATPase in cardiac sarcoplasmic reticulum by calcium/calmodulin-dependent protein kinase. *Basic Res Cardiol*. 1997;92 Suppl 1:25-35

18.   Netticadan T, Xu A, Narayanan N. Divergent effects of ruthenium red and ryanodine on Ca^{2+}/calmodulin-dependent phosphorylation of the Ca^{2+} release channel (ryanodine receptor) in cardiac sarcoplasmic reticulum. *Arch Biochem Biophys*. 1996;333:368-376

19.   Wehrens XH, Lehnart SE, Huang F, Vest JA, Reiken SR, Mohler PJ, Sun J, Guatimosim S, Song LS, Rosemblit N, D'Armiento JM, Napolitano C, Memmi M, Priori SG, Lederer WJ, Marks AR. FKBP12.6 deficiency and defective calcium release channel (ryanodine receptor) function linked to exercise-induced sudden cardiac death. *Cell*. 2003;113:829-840

20.   Wehrens XH, Lehnart SE, Reiken SR, Marks AR. Ca^{2+}/calmodulin-dependent protein kinase II phosphorylation regulates the cardiac ryanodine receptor. *Circ Res*. 2004;94:e61-70

21.   Jiang M, Xu A, Tokmakejian S, Narayanan N. Thyroid hormone-induced overexpression of functional ryanodine receptors in the rabbit heart. *Am J Physiol Heart Circ Physiol*. 2000;278:H1429-1438

22.   Jones DL, Narayanan N. Defibrillation depresses heart sarcoplasmic reticulum calcium pump: a mechanism of postshock dysfunction. *Am J Physiol*. 1998;274:H98-105

23.   Sathish V, Xu A, Karmazyn M, Sims SM, Narayanan N. Mechanistic basis of differences in Ca^{2+}-handling properties of sarcoplasmic reticulum in right and left ventricles of normal rat myocardium. *Am J Physiol Heart Circ Physiol*. 2006;291:H88-96

24.   Jiang MT, Moffat MP, Narayanan N. Age-related alterations in the phosphorylation of sarcoplasmic reticulum and myofibrillar proteins and diminished contractile response to isoproterenol in intact rat ventricle. *Circ Res*. 1993;72:102-111

25. Hawkins PT, Michell RH, Kirk CJ. A simple assay method for determination of the specific radioactivity of the gamma-phosphate group of ^{32}P-labelled ATP. *Biochem J*. 1983;210:717-720

26. Hawkins C, Xu A, Narayanan N. Sarcoplasmic reticulum calcium pump in cardiac and slow twitch skeletal muscle but not fast twitch skeletal muscle undergoes phosphorylation by endogenous and exogenous Ca2+/calmodulin-dependent protein kinase. Characterization of optimal conditions for calcium pump phosphorylation. *J Biol Chem*. 1994;269:31198-31206

27. Xu A, Narayanan N. Effects of aging on sarcoplasmic reticulum Ca^{2+}-cycling proteins and their phosphorylation in rat myocardium. *Am J Physiol*. 1998;275:H2087-2094

28. Satoh H, Delbridge LM, Blatter LA, Bers DM. Surface:volume relationship in cardiac myocytes studied with confocal microscopy and membrane capacitance measurements: species-dependence and developmental effects. *Biophys J*. 1996;70:1494-1504

29. Colyer J. Control of the calcium pump of cardiac sarcoplasmic reticulum. A specific role for the pentameric structure of phospholamban? *Cardiovasc Res*. 1993;27:1766-1771

30. Osada M, Netticadan T, Tamura K, Dhalla NS. Modification of ischemia-reperfusion-induced changes in cardiac sarcoplasmic reticulum by preconditioning. *Am J Physiol*. 1998;274:H2025-2034

31. Toyofuku T, Curotto Kurzydlowski K, Narayanan N, MacLennan DH. Identification of Ser38 as the site in cardiac sarcoplasmic reticulum Ca^{2+}-ATPase that is phosphorylated by Ca^{2+}/calmodulin-dependent protein kinase. *J Biol Chem*. 1994;269:26492-26496

32.   Xu A, Narayanan N. Ca^{2+}/calmodulin-dependent phosphorylation of the Ca^{2+}-ATPase, uncoupled from phospholamban, stimulates Ca^{2+}-pumping in native cardiac sarcoplasmic reticulum. *Biochem Biophys Res Commun*. 1999;258:66-72

33.   Xu A, Narayanan N. Reversible inhibition of the calcium-pumping ATPase in native cardiac sarcoplasmic reticulum by a calmodulin-binding peptide. Evidence for calmodulin-dependent regulation of the V(max) of calcium transport. *J Biol Chem*. 2000;275:4407-4416

34.   Xu A, Hawkins C, Narayanan N. Phosphorylation and activation of the Ca^{2+}-pumping ATPase of cardiac sarcoplasmic reticulum by Ca^{2+}/calmodulin-dependent protein kinase. *J Biol Chem*. 1993;268:8394-8397

35.   Ishida A, Shigeri Y, Taniguchi T, Kameshita I. Protein phosphatases that regulate multifunctional Ca^{2+}/calmodulin-dependent protein kinases: from biochemistry to pharmacology. *Pharmacol Ther*. 2003;100:291-305

36.   Ikeda Y, Hoshijima M, Chien KR. Toward biologically targeted therapy of calcium cycling defects in heart failure. *Physiology (Bethesda)*. 2008;23:6-16

37.   Maier LS, Zhang T, Chen L, DeSantiago J, Brown JH, Bers DM. Transgenic CaMKIIdeltaC overexpression uniquely alters cardiac myocyte Ca^{2+} handling: reduced SR Ca^{2+} load and activated SR Ca^{2+} release. *Circ Res*. 2003;92:904-911

38.   Wehrens XH, Lehnart SE, Reiken SR, Deng SX, Vest JA, Cervantes D, Coromilas J, Landry DW, Marks AR. Protection from cardiac arrhythmia through ryanodine receptor-stabilizing protein calstabin2. *Science*. 2004;304:292-296

39.   Haghighi K, Kolokathis F, Pater L, Lynch RA, Asahi M, Gramolini AO, Fan GC, Tsiapras D, Hahn HS, Adamopoulos S, Liggett SB, Dorn GW, 2nd, MacLennan DH, Kremastinos DT, Kranias EG. Human phospholamban null results in lethal

dilated cardiomyopathy revealing a critical difference between mouse and human. *J Clin Invest*. 2003;111:869-876

40.   Simmerman HK, Jones LR. Phospholamban: protein structure, mechanism of action, and role in cardiac function. *Physiol Rev*. 1998;78:921-947

41.   Yurukova S, Kilic A, Volker K, Leineweber K, Dybkova N, Maier LS, Brodde OE, Kuhn M. CaMKII-mediated increased lusitropic responses to beta-adrenoreceptor stimulation in ANP-receptor deficient mice. *Cardiovasc Res*. 2007;73:678-688

42.   Couchonnal LF, Anderson ME. The role of calmodulin kinase II in myocardial physiology and disease. *Physiology (Bethesda)*. 2008;23:151-159

43.   Vafiadaki E, Papalouka V, Arvanitis DA, Kranias EG, Sanoudou D. The role of SERCA2a/PLN complex, Ca^{2+} homeostasis, and anti-apoptotic proteins in determining cell fate. *Pflugers Arch*. 2009;457:687-700

44.   Hawkins C, Xu A, Narayanan N. Comparison of the effects of fluoride on the calcium pumps of cardiac and fast skeletal muscle sarcoplasmic reticulum: evidence for tissue-specific qualitative difference in calcium-induced pump conformation. *Biochim Biophys Acta*. 1994;1191:231-243

45.   Maier LS, Bers DM. Calcium, calmodulin, and calcium-calmodulin kinase II: heartbeat to heartbeat and beyond. *J Mol Cell Cardiol*. 2002;34:919-939

46.   DeSantiago J, Maier LS, Bers DM. Frequency-dependent acceleration of relaxation in the heart depends on CaMKII, but not phospholamban. *J Mol Cell Cardiol*. 2002;34:975-984

47.   Schouten VJ. Interval dependence of force and twitch duration in rat heart explained by Ca^{2+} pump inactivation in sarcoplasmic reticulum. *J Physiol*. 1990;431:427-444

48.   Hoit BD. Excitation-contraction coupling in the MLP knockout mouse. *J Mol Cell Cardiol*. 2006;40:335-338

49.   Liao R, Force T. Not all hypertrophy is created equal. *Circ Res*. 2007;101:1069-1072

50.   Oka T, Komuro I. Molecular mechanisms underlying the transition of cardiac hypertrophy to heart failure. *Circ J*. 2008;72 Suppl A:A13-16

51.   Marx SO, Reiken S, Hisamatsu Y, Jayaraman T, Burkhoff D, Rosemblit N, Marks AR. PKA phosphorylation dissociates FKBP12.6 from the calcium release channel (ryanodine receptor): defective regulation in failing hearts. *Cell*. 2000;101:365-376

52.   Vest JA, Wehrens XH, Reiken SR, Lehnart SE, Dobrev D, Chandra P, Danilo P, Ravens U, Rosen MR, Marks AR. Defective cardiac ryanodine receptor regulation during atrial fibrillation. *Circulation*. 2005;111:2025-2032

53.   Coronado R, Morrissette J, Sukhareva M, Vaughan DM. Structure and function of ryanodine receptors. *Am J Physiol*. 1994;266:C1485-1504

54.   Xiao B, Zhong G, Obayashi M, Yang D, Chen K, Walsh MP, Shimoni Y, Cheng H, Ter Keurs H, Chen SR. Ser-2030, but not Ser-2808, is the major phosphorylation site in cardiac ryanodine receptors responding to protein kinase A activation upon beta-adrenergic stimulation in normal and failing hearts. *Biochem J*. 2006;396:7-16

55.   Ai X, Curran JW, Shannon TR, Bers DM, Pogwizd SM. Ca^{2+}/calmodulin-dependent protein kinase modulates cardiac ryanodine receptor phosphorylation and sarcoplasmic reticulum Ca^{2+} leak in heart failure. *Circ Res*. 2005;97:1314-1322

56.   Yano M, Ono K, Ohkusa T, Suetsugu M, Kohno M, Hisaoka T, Kobayashi S, Hisamatsu Y, Yamamoto T, Noguchi N, Takasawa S, Okamoto H, Matsuzaki M. Altered stoichiometry of FKBP12.6 versus ryanodine receptor as a cause of abnormal Ca^{2+} leak through ryanodine receptor in heart failure. *Circulation*. 2000;102:2131-2136

57.   Bers DM. Macromolecular complexes regulating cardiac ryanodine receptor function. *J Mol Cell Cardiol*. 2004;37:417-429

58.   Xiao B, Jiang MT, Zhao M, Yang D, Sutherland C, Lai FA, Walsh MP, Warltier DC, Cheng H, Chen SR. Characterization of a novel PKA phosphorylation site, serine-2030, reveals no PKA hyperphosphorylation of the cardiac ryanodine receptor in canine heart failure. *Circ Res*. 2005;96:847-855

59.   Yang D, Zhu WZ, Xiao B, Brochet DX, Chen SR, Lakatta EG, Xiao RP, Cheng H. Ca^{2+}/calmodulin kinase II-dependent phosphorylation of ryanodine receptors suppresses Ca^{2+} sparks and Ca^{2+} waves in cardiac myocytes. *Circ Res*. 2007;100:399-407

60.   Seidler T, Hasenfuss G, Maier LS. Targeting altered calcium physiology in the heart: translational approaches to excitation, contraction, and transcription. *Physiology (Bethesda)*. 2007;22:328-334

61.   Wegener AD, Simmerman HK, Lindemann JP, Jones LR. Phospholamban phosphorylation in intact ventricles. Phosphorylation of serine 16 and threonine 17 in response to beta-adrenergic stimulation. *J Biol Chem*. 1989;264:11468-11474

62.   Zhang T, Maier LS, Dalton ND, Miyamoto S, Ross J, Jr., Bers DM, Brown JH. The deltaC isoform of CaMKII is activated in cardiac hypertrophy and induces dilated cardiomyopathy and heart failure. *Circ Res*. 2003;92:912-919

63.   Hoch B, Meyer R, Hetzer R, Krause EG, Karczewski P. Identification and expression of delta-isoforms of the multifunctional Ca^{2+}/calmodulin-dependent protein kinase in failing and nonfailing human myocardium. *Circ Res*. 1999;84:713-721

64.   Asahi M, McKenna E, Kurzydlowski K, Tada M, MacLennan DH. Physical interactions between phospholamban and sarco(endo)plasmic reticulum Ca^{2+}-ATPases are dissociated by elevated Ca^{2+}, but not by phospholamban phosphorylation, vanadate, or thapsigargin, and are enhanced by ATP. *J Biol Chem*. 2000;275:15034-15038

65.   Montgomery H. Cardiac reserve: linking physiology and genetics. *Intensive Care Med*. 2000;26 Suppl 1:S137-144

66.   Tan LB. Evaluation of cardiac dysfunction, cardiac reserve and inotropic response. *Postgrad Med J*. 1991;67 Suppl 1:S10-20

67.   Tan LB, Bain RJ, Littler WA. Assessing cardiac pumping capability by exercise testing and inotropic stimulation. *Br Heart J*. 1989;62:20-25

68.   Tan LB, Littler WA. Measurement of cardiac reserve in cardiogenic shock: implications for prognosis and management. *Br Heart J*. 1990;64:121-128

69.   Netticadan T, Temsah RM, Kawabata K, Dhalla NS. Sarcoplasmic reticulum Ca^{2+}/Calmodulin-dependent protein kinase is altered in heart failure. *Circ Res*. 2000;86:596-605

70.   Damiani E, Sacchetto R, Margreth A. Variation of phospholamban in slow-twitch muscle sarcoplasmic reticulum between mammalian species and a link to the substrate specificity of endogenous Ca^{2+}-calmodulin-dependent protein kinase. *Biochim Biophys Acta*. 2000;1464:231-241

71.   Ogrodnik J, Niggli E. Increased Ca^{2+} leak and spatiotemporal coherence of Ca^{2+} release in cardiomyocytes during beta-adrenergic stimulation. *J Physiol*. 2010;588:225-242

72.   Morimoto S, J OU, Kawai M, Hoshina T, Kusakari Y, Komukai K, Sasaki H, Hongo K, Kurihara S. Protein kinase A-dependent phosphorylation of ryanodine receptors increases Ca^{2+} leak in mouse heart. *Biochem Biophys Res Commun*. 2009;390:87-92

73.   Eisner DA, Kashimura T, Venetucci LA, Trafford AW. From the ryanodine receptor to cardiac arrhythmias. *Circ J*. 2009;73:1561-1567

74.   Vinogradova TM, Lakatta EG. Regulation of basal and reserve cardiac pacemaker function by interactions of cAMP-mediated PKA-dependent Ca^{2+} cycling with surface membrane channels. *J Mol Cell Cardiol*. 2009;47:456-474

75.   Benitah JP, Alvarez JL, Gomez AM. L-type Ca^{2+} current in ventricular cardiomyocytes. *J Mol Cell Cardiol*. 2010;48:26-36

76.   Benitah JP, Kerfant BG, Vassort G, Richard S, Gomez AM. Altered communication between L-type calcium channels and ryanodine receptors in heart failure. *Front Biosci*. 2002;7:e263-275

CHAPTER FIVE

SYNOPSIS: MAJOR FINDINGS, CONCLUSIONS, AND FUTURE

PERSPECTIVE

5.1.   Summary of Major Findings

My thesis had 3 specific aims. Here I will summarize the findings arising from my studies.

Aim 1 To determine whether chronic DHPR blockade alters expression and function of RyRs and DHPRs.

This part of my research demonstrated that chronic VPL treatment leads to the following changes.

1)   Altered DHPR/RyR stoichiometry, with down-regulation of RyRs, down-regulation of FKBP12, and up-regulation of DHPRs. This divergent change in DHPR and RyR expression indicates a disarray of the molecular arrangement of DHPRs and RyRs.

2)   Uncompromised I_{Ca}, but remodeled intrinsic gating properties of RyR channels that manifests as high frequency, long duration and large amplitude of diastolic Ca^{2+} sparks, abundant hyperactive spark sites, and increased incidence of Ca^{2+} waves .

3)   Remodeled cardiac electrophysiological properties which manifested as an increased incidence of premature ventricular contraction, susceptibility to arrhythmia, and prolonged nodal conduction.   These electrophysiological alterations observed at organ and whole animal levels agree with impaired intermolecular signaling and local control mechanism between DHPR and RyR observed at molecular and cellular levels.

Conclusion 一   Chronic, yet partial blockade of DHPRs deranges DHPR/RyR stoichiometry, remodels intrinsic functional properties of RyR despite uncompromised I_{Ca}, and consequently leads to impaired intermolecular signaling and spatio-temporal dyssynchrony of E-C coupling events culminating in predisposition to arrhythmias and heart failure.

Aim 2   To determine whether chronic DHPR blockade alters expression and function of cardiac SR Ca^{2+} pump (SERCA2a).

This part of my research demonstrated that chronic VPL treatment leads to the following changes.

1)   Down-regulated SERCA2a and up-regulated PLN. These protein level alterations indicate DHPR Ca^{2+} signals can regulate Ca^{2+} cycling through changing Ca^{2+} cycling proteins levels.

2)   Depressed SERCA2 function manifested as reduced rate of ATP-dependent Ca^{2+} uptake by cardiac SR vesicles, altered myocyte $[Ca^{2+}]_i$ handling, with slower and smaller Ca^{2+} transients, increased diastolic $[Ca^{2+}]_i$, and decreased SR Ca^{2+} content. These changes provide molecular and cellular mechanisms for cardiac diastolic as well as systolic dysfunction.

3)   Depressed both cardiac systolic and diastolic function*s in vivo* and in isolated, perfused hearts and cardiomyocytes.   Though verapamil inhibits cardiac contractility by reducing CICR, we observed the depression of cardiac contractility when verapamil was absent in isolated, purfused hearts and cells.

This observation demonstrates that an intrinsic suppression of basal heart contractility is part of adaptation to chronic, partial DHPR blockade.

Conclusion ― Chronic, yet partial blockade of DHPRs depresses the expression and function of cardiac SERCA2, leading to diastolic and systolic dysfunction culminating in heart dysfunction.

Aim 3   To determine whether chronic DHPR blockade alters physiological mechanisms for protein phosphorylation-dependent regulation of SR/cardiomyocyte Ca^{2+} cycling.

This part of my research demonstrated that chronic VPL treatment leads to the following changes.

1)   Hyper-phosphorylated SR Ca^{2+} cycling proteins paradoxically associated with reduced contractility and relaxation.

2)   Increased activity of CaMKII and PKA, but reduced stimulatory effects of CaMKII and PKA on SR Ca^{2+} transport.

3)   Attenuated inotropic but not chronotropic effect of β-adrenergic stimulation, owing to molecular remodeling.

4)   Myocardial intrinsic contractile properties are compromised in the absence of ventricular hypertrophy.

Conclusion ― Chronic, yet partial blockade of DHPRs causes hyper-phosphorylation of cardiac RyR and PLN, increased CaMKII and PKA activity, and paradoxically reduced basal contractile function and inotropic response to β-adrenergic stimulation of the heart.

Overall conclusions — The heart adapts to chronic, partial DHPR blockade with molecular and functional remodelling of the RyR, SERCA, and protein phosphorylation-dependent regulation of SR/cardiomyocyte Ca^{2+} cycling. Consequent spatio-temporal dyssynchrony of E-C coupling events, depletion of SR Ca^{2+} store, contractile dysfunction, and blunted inotropic response to β-adrenergic stimulation underlie the increased risk of heart failure associated with long-term verapamil treatment.

Figure 5.1 summarizes the cardiac adaptation to chronic, yet partial DHPR blockade at molecular and cellular levels.

A. Normal cardiomyocyte E-C coupling.
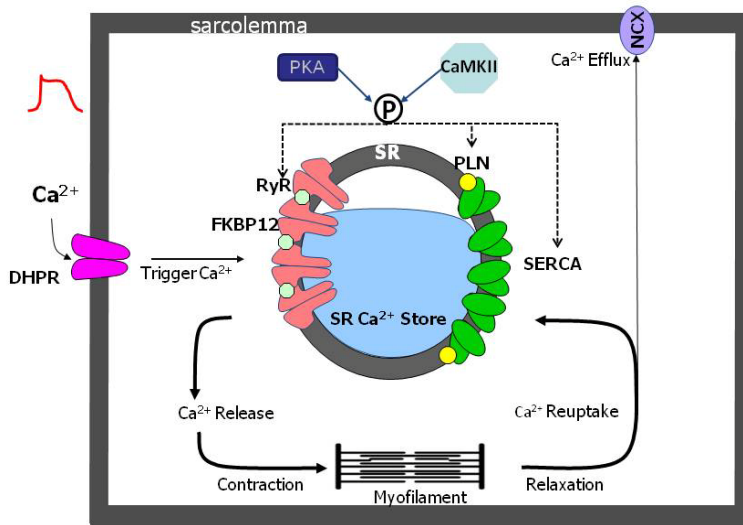
B. Effects of chronic,yet partial blockade of DHPRs on cardiac E-C coupling.
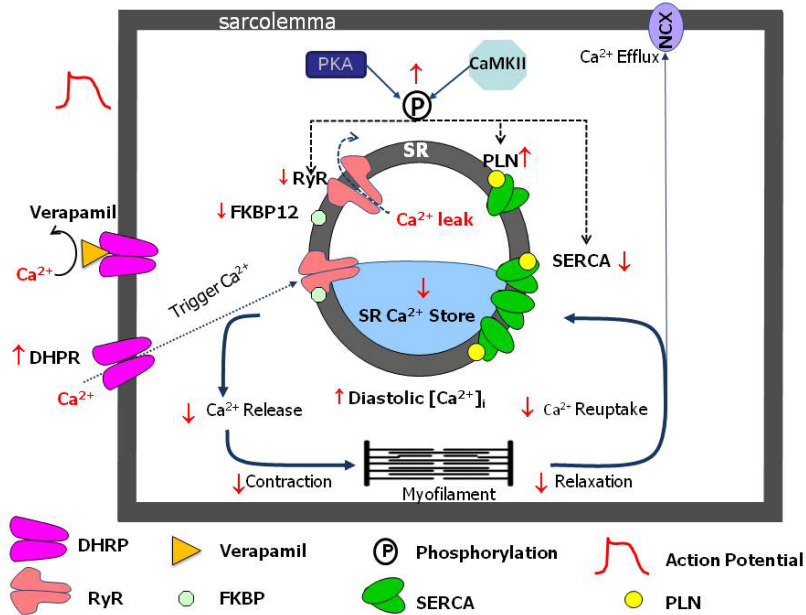
Figure 5.1 Normal cardiomyocyte E-C coupling and effects of chronic, yet partial blockade of DHPRs on cardiac E-C coupling. A, Ca^{2+} transport and key molecular players of Ca^{2+} handling in normal cardiac E-C coupling. B, The consequences of chronic, yet partial blockade of DHPRs in E-C coupling: impaired local control mechanism between DHPRs and RyRs, aberrant Ca^{2+} signaling from RyR, depressed SERCA function, reduced SR Ca^{2+} content, and activated CaMKII & PKA system. Arrows indicate the direction of quantitative changes in either expression of protein, level of phosphorylation, volume of Ca^{2+} movement, or intensity of contractility.

5.2.   Significance of the Study

Physiological and pharmacological significance — My studies are the first to study the cardiac SR adaptation to the chronic, partial DHPR blockade. These adaptive changes reveal a novel mechanism where DHPR Ca^{2+} signal regulates cardiac E-C coupling through alterations of the expression and function of SR Ca^{2+} cycling proteins. Furthermore, these adaptive changes also provide insights for the highly coordinated communication among Ca^{2+} cycling proteins in cardiac E-C coupling.

Clinical relevance — The dosage regimen in our animal model is calculated as a equivalent to a four-year course of verapamil for human at 7−24 mg/d·kg, p.o. The calculation process is as follows. The maximal oral dose of verapamil used clinically in humans is 480 mg/day [1]. According to the guidelines for human equivalent calculation from US Food and Drug Administration (http://www.fda.gov/cber/gdlns/dose.htm) and bioavailability of verapamil (10–35%) [1], the rat dose (625 μg/h/kg subcutaneously) in our study is equivalent to a human dose of 7−24 mg/d·kg, p.o that is 1~3 times of maximal dose for a 60 kg person. The average life span of pet rat is 21.6 months and average human lifespan is 77.1 years. Thus roughly, each rat month is equivalent to 4 human years (http://www.ratbehavior.org/RatYears.htm).   Therefore, the findings from this animal model can relate to similar clinical setting.

Though not the first-line drug choice, verapamil can be prescribed for long-term management of mild to moderate essential hypertension [1, 2]. Verapamil hydrochloride immediate release tablets have been studied in 4826 patients in controlled and uncontrolled trials.   The most serious adverse reactions reported with verapamil

treatment are sudden death, heart failure, A-V block, hypotension and rapid ventricular response [3]. Though above unwanted cardiovascular events can be partially explained by reduced nodal conduction and short QT syndrome caused by I_{Ca} inhibition [4, 5], the discovery of SR functional remodeling from this research work provides a novel mechanism for these adverse effects. My in-depth mechanistic study of DHRP blockade will help clinicians to better understand and manage the risk of long-term treatment with DHPR blockers.

Experimental design — The assessment of an animal model has often focused on a limited number of physiological variables, providing piecemeal aspects of functionalities or mechanisms of the model. Our experiments assessed the cardiac adaptation at a wide range of levels, ranging from intramolecular, intermolecular, molecular, cellular, organ, to entire animal levels. This approach enables logical integration of microscopic mechanisms into macroscopic functional changes, and provides a comprehensive, mechanistic perspective of the impact of chronic DHPR blockade on the heart.

5.3.   Limitations of the Research and Suggestions for Future Studies

Animal model—It is possible that in this model, the heart would not only adapt to the cardiac DHPRs blockade, but also other organ's DHPR blockade. It is possible that the verapamil dose in our model blocked DHPRs of peripheral blood vessels, resulting in hypotension and reflex sympathetic activation. To examine this possibility, future studies could monitor the blood pressure on day1 and day 28 in control and VPL rats. However, we do not think this is a major concern, because verapamil preferentially blocks DHPRs at the myocardium and does not produce reflex tachycardia and hypotension at clinically used doses [4]. The dose in our animal model was estimated to be equivalent to the clinically used dose in humans. Thus, theoretically it will not lead to reflex sympathetic activation due to DHPRs blockade in peripheral blood vessels. Besides, even if a reflex sympathetic activation did occur in our model, it would not affect the significance of this study which focuses on mechanisms for long-term risk of verapamil treatment. In preliminary studies, we have investigated the effect of chronic nifedipine treatment on the heart. On the 15th day and 30th day, the nifedipine group did not show any significant change in RyRs density, whereas the verapamil group did show down-regulation of RyRs. This may be due to the fact that nifedipine preferentially blocks DHPRs in blood vessels but not in the myocardium at the clinically used dose. Our results with nifedipine also indicate that the changes of RyRs in the verapamil model are most likely due to direct cardiac DHPR blockade.

Study of Ca^{2+} sparks—We showed that diastolic Ca^{2+} sparks in control ventricular myocytes are more rapid and less frequent (1−2 sparks/second/cell) than those of VPL cells. It is possible our fast imaging system did not detect some brief, small

sparks from the control group and undervalued Ca^{2+} spark frequency in control rats. In future studies, we can trigger sparks to make the control sparks more evident with physiological or pharmacological interventions, such as gradually increasing extracellular Ca^{2+} or applying ryanodine to myocytes. The control and VPL group then could be compared under same interventional conditions. In addition, the temporal resolution for imaging Ca^{2+} sparks was 56 frames/second in the present study. Considering control sparks are brief with low amplitude, the rising phase of control sparks often finished within 3−5 sampling point time. This temporal resolution makes it a challenge to calculate the rising rate of sparks.

Sympathetic activities in VPL rats — We did not assess the changes of sympathetic activity in response to VPL treatment. A compensatory increase in sympathetic activity may occur, depending on the extent of cardiac functional reduction. During full-blown heart failure, circulating catecholamine levels are markedly elevated [6]. Thus circulating catecholamine levels reflect the degree of cardiac dysfunction and systemic risks for adverse cardiovascular events [7]. In future studies, arterial plasma catecholamine concentrations on day 28 in control and VPL rats can be examined using HPLC method as described previously [8]. However, sympathetic nerve activity is not uniformly regulated among organs, and the largest compensatory increase in sympathetic nerve activity occurs in the target organ [9]. Thus the measurement of circulating hormones may not reflect the regional changes of sympathetic tone in the heart. Therefore, sympathetic activity shall include measurements of arterial plasma catecholamines as well as heart tissue catecholamine measurement in our future studies.

Functional stage in development of heart dysfunction ーOur results convincingly reveal that depression of heart contractile function ensued from chronic, yet partial DHPR blockade. However, the lack of pulmonary edema indicated that VPL rats were not in a decompensated stage of heart failure. Therefore, we need further evidence to assess heart functional stage and explore whether VPL rats can progress into a full-blown (decompensated stage) heart failure. Heart failure arises from the inability of ventricles to efficiently pump blood throughout the circulation [10, 11]. As heart failure evolves, neurohumoral mechanisms are activated to help maintain the cardiac output to meet the body's demand. These compensatory changes include increased sympathetic activity, reduced cardiac vagal activity, and activation of angiotensin-aldosterone system, vasopressin, catecholamines, and B-Type Natriuretic Peptide (BNP) [12, 13]. Thus in the future, we could further explore the neurohumoral changes to assess cardiac functional stage in VPL rats. For example, BNP and N-terminal pro-BNP (NT-proBNP) are established biomarkers for heart failure diagnosis and estimating prognosis [14-16]. A future study could also examine BNP and NT-proBNP levels in blood in VPL rats according to methods described previously [14-16].

We could also use microCT scan to record cardiac cycle *in vivo* in the future. This technique could provide visual, diagnostic data in assessing heart functional stage (ejection fraction, the size of ventricular wall and cavities, dynamic changes of ventricular wall and cavity, etc.). Depressed heart contractile function in VPL rats can reduce coronary supply and consequently lead to ischemic heart diseases, arrhythmias, and heart failure.

Intermolecular interactions and intramolecular events in E-C coupling — The present research examined adaptive changes in regulation of RyR and SERCA2 by protein kinases. Future studies could address the potential impact of chronic DHPR blockade on intermolecular interactions between the molecular players controlling SERCA and RyR function as outlined below. Where possible, the ensuing intramolecular events from intermolecular interactions could also be monitored.

1)   PLN-SERCA2 interaction. Given the down-regulation of SERCA and up-regulation of PLN in the VPL rats, there exists the distinct possibility that a quasi-irreversible PLN-SERCA interaction contributes significantly to the diastolic dysfunction observed in VPL rats. To explore this possibility, SR vesicles and cardiac homogenates from control and VPL rats could be used to determine the relative size of PLN-associated and PLN-free SERCA pools according to the co-immunoprecipitation protocols we have used previously [17]. In addition, this protocol could also address the relative effectiveness of Ca^{2+}, CaM, PLN/SERCA phosphorylation to dissociate PLN-SERCA complexes, which are physiologically relevant.

2)   CaM-SERCA2 interaction. Studies from our laboratory demonstrated that cardiac SR contains appreciable amounts of firmly bound CaM and this SR-associated CaM is essential for SERCA2 function [18]. Functional inactivation of SR-bound CaM using a CaM-binding peptide (CaM BP) results in complete suppression of SERCA2 function which is readily reversed by exogenous CaM [18]. Currently ongoing studies suggest that the mechanism for CaM regulation of SERCA2 involves direct interaction of CaM with SERCA2 resulting in activation of the rate-limiting step (phosphoenzyme decomposition) in the SERCA2 catalytic cycle. Furthermore, this CaM regulation of

SERCA2 is seen in the presence but not in the absence of PLN in the SR. It appears that Ca^{2+}-bound CaM serves as a molecular trigger that activates SERCA2 by disrupting PLN-SERCA interaction. This novel mechanism for the CaM regulation of SERCA function provides an exciting new dimension to our understanding of the molecular events underlying E-C coupling and cardiac muscle physiology. Impairments in this CaM control of SERCA2 function could result in diastolic and systolic dysfunction leading to heart failure. In view of this, studies outlined below could be carried out to investigate potential impact of chronic DHPR blockade on CaM-SERCA2 interaction and its functional consequences. Cardiac SR vesicles from control and VPL rats could be used to determine the effects of CaM BP, Ca^{2+} and CaM on SERCA2-CaM interaction, SERCA2 Ca^{2+} pump function as well as on the evolution of SERCA2 conformational states during the catalytic and Ca^{2+} transport cycle.

3) RyR-FKBP interaction. We have observed nearly similar degree of diminished protein levels for both RyR and FKBP 12 in hearts from the VPL compared to control rats. Native SR vesicles as well as cardiac homogenates from control and VPL rats could be used to determine the relative amounts of FKBP-RyR complexes in control *vs*. VPL rats. In addition, the influence of RyR phosphorylation status on FKBP-RyR interaction could be monitored. The experimental procedures for these studies would be similar to those outlined for PLN-SERCA interaction. FKBP association with RyR is thought to stabilize RyR in a sub-conductance state and thereby minimize diastolic Ca^{2+} leak. Therefore, diminished FKBP-RyR interaction in VPL, if encountered, could constitute a molecular lesion giving rise to the higher incidence of arrhythmias observed in the VPL rats.

Phosphatases and dephosphorylation of SR Ca^{2+} cycling protein — We observed that SR Ca^{2+} cycling protein became hyper-phosphorylated. This hyper-phosphorylation is interpreted as a result of increased activity of protein kinases (PKA and CaMKII) in the present study; but hyper-phosphorylation also can result from decreased activity of phosphatases and reduced dephosphorylation. Thus, the status of protein phosphatases and dephosphorylation of SR Ca^{2+} cycling proteins need to be clarified in our future studies.

5.4. References

1.   Libby P, Bonow R, Mann D, Zipes D, Braunwald E. *Braunwald's Heart Disease: A Textbook of Cardiovascular Medicine*. Natasha Andjelkovic; 2008.

2.   Fauci A, Kasper D, Longo D, Braunwald E. *Harrison's Internal Medicine*. McGraw-Hill Companies; 2010.

3.   Repchinsky C. *Compendium of Pharmaceuticals and Specialties*. 2010.

4.   Goodman LS, Gilman AG, Hardman JG, Limbird LE. *Goodman & Gilman's the pharmacological basis of therapeutics*. New York ; London: McGraw-Hill Medical Publishing Division; 2001.

5.   Antzelevitch C, Pollevick GD, Cordeiro JM, Casis O, Sanguinetti MC, Aizawa Y, Guerchicoff A, Pfeiffer R, Oliva A, Wollnik B, Gelber P, Bonaros EP, Jr., Burashnikov E, Wu Y, Sargent JD, Schickel S, Oberheiden R, Bhatia A, Hsu LF, Haissaguerre M, Schimpf R, Borggrefe M, Wolpert C. Loss-of-function mutations in the cardiac calcium channel underlie a new clinical entity characterized by ST-segment elevation, short QT intervals, and sudden cardiac death. *Circulation*. 2007;115:442-449

6.   Esler M, Kaye D. Measurement of sympathetic nervous system activity in heart failure: the role of norepinephrine kinetics. *Heart Fail Rev*. 2000;5:17-25

7.   Li G, Xu J, Wang P, Velazquez H, Li Y, Wu Y, Desir GV. Catecholamines regulate the activity, secretion, and synthesis of renalase. *Circulation*. 2008;117:1277-1282

8.   Johnson MD, Smith PG, Mills E, Schanberg SM. Paradoxical elevation of sympathetic activity during catecholamine infusion in rats. *J Pharmacol Exp Ther*. 1983;227:254-259

9.   Hjemdahl P. Physiological aspects on catecholamine sampling. *Life Sci*. 1987;41:841-844

10.   Lim HW, Molkentin JD. Calcineurin and human heart failure. *Nat Med*. 1999;5:246-247

11.   Olson TM, Michels VV, Thibodeau SN, Tai YS, Keating MT. Actin mutations in dilated cardiomyopathy, a heritable form of heart failure. *Science*. 1998;280:750-752

12.   Negrao CE, Middlekauff HR. Adaptations in autonomic function during exercise training in heart failure. *Heart Fail Rev*. 2008;13:51-60

13.   Price JF, Thomas AK, Grenier M, Eidem BW, O'Brian Smith E, Denfield SW, Towbin JA, Dreyer WJ. B-type natriuretic peptide predicts adverse cardiovascular events in pediatric outpatients with chronic left ventricular systolic dysfunction. *Circulation*. 2006;114:1063-1069

14.   Maisel AS, Krishnaswamy P, Nowak RM, McCord J, Hollander JE, Duc P, Omland T, Storrow AB, Abraham WT, Wu AH, Clopton P, Steg PG, Westheim A, Knudsen CW, Perez A, Kazanegra R, Herrmann HC, McCullough PA. Rapid measurement of B-type natriuretic peptide in the emergency diagnosis of heart failure. *N Engl J Med*. 2002;347:161-167

15.   Januzzi JL, Jr., Camargo CA, Anwaruddin S, Baggish AL, Chen AA, Krauser DG, Tung R, Cameron R, Nagurney JT, Chae CU, Lloyd-Jones DM, Brown DF, Foran-Melanson S, Sluss PM, Lee-Lewandrowski E, Lewandrowski KB. The N-terminal Pro-BNP investigation of dyspnea in the emergency department (PRIDE) study. *Am J Cardiol*. 2005;95:948-954

16.   Tang WH, Francis GS, Morrow DA, Newby LK, Cannon CP, Jesse RL, Storrow AB, Christenson RH. National Academy of Clinical Biochemistry Laboratory

Medicine Practice Guidelines: clinical utilization of cardiac biomarker testing in heart failure. *Clin Biochem*. 2008;41:210-221

17.   Sathish V, Xu A, Karmazyn M, Sims SM, Narayanan N. Mechanistic basis of differences in Ca^{2+}-handling properties of sarcoplasmic reticulum in right and left ventricles of normal rat myocardium. *Am J Physiol Heart Circ Physiol*. 2006;291:H88-96

18.   Xu A, Narayanan N. Reversible inhibition of the calcium-pumping ATPase in native cardiac sarcoplasmic reticulum by a calmodulin-binding peptide. Evidence for calmodulin-dependent regulation of the V(max) of calcium transport. *J Biol Chem*. 2000;275:4407-4416

APPENDIX A

Ethics Approval of the Animal Use

Western

January 8, 2007

This is the Original Approval for this protocol
A Full Protocol submission will be required in 2011

Dear Dr. Naryanan:

Your Animal Use Protocol form entitled:
Studies on the Regulation of Sarcoplasmic Reticulum Ca2+ Transport in Heart Muscle
Funding Agency CIHR - Grant # MOP-9553; HSFO - Grant #PRG-5071

has been approved by the University Council on Animal Care. This approval is valid from **January 8, 2007 to January 31, 2008**. The protocol number for this project is **#2007-10-01 and replaces #2003-014-01.**

1. This number must be indicated when ordering animals for this project.
2. Animals for other projects may not be ordered under this number.
3. If no number appears please contact this office when grant approval is received.
    If the application for funding is not successful and you wish to proceed with the project, request that an internal scientific peer review be performed by the Animal Use Subcommittee office.
4. Purchases of animals other than through this system must be cleared through the ACVS office. Health certificates will be required.

ANIMALS APPROVED FOR 1 YR.

Species	Strain	Other Detail	Pain Level	Animal # Total for 1 Year
Mouse	C57BL6,CaM BP-Tg and WT	1,3,6, & 12 months M/F	C	600
Mouse	C57BL6,SERCA2aS38A -TG and WT	1,3,6, & 12 months M/F	C	600
Mouse	C57BL6,PLKKO-TG and WT	1,3,6, & 12 months M/F	C	600
Rabbit	NZW	3 kg Male	C	60
Rat	Wistar	250 gm Male	C	300

STANDARD OPERATING PROCEDURES
Procedures in this protocol should be carried out according to the following SOPs. Please contact the Animal Use Subcommittee office (661-2111 ext. 86770) in case of difficulties or if you require copies.
SOP's are also available at http://www.uwo.ca/animal/acvs
310 Holding Period Post-Admission
320 Euthanasia
321 Criteria for Early Euthanasia/Rodents
322 Criteria for Early Euthanasia/Mammals/Non-rode

REQUIREMENTS/COMMENTS
Please ensure that individual(s) performing procedures on live animals, as described in this protocol, are familiar with the contents of this document.

c.c. Approved Protocol   - N. Narayanan, W. Lagerwerf
Approval Letter   - W. Lagerwerf

The University *of* Western Ontario
Animal Use Subcommittee/University Council on Animal Care
Health Sciences Centre • London, Ontario • CANADA - N6A 5C1
Phone: 519-661-2111 ext. 86770 • Fax: 519-661-2028 • www.uwo.ca/animal

APPENDIX B

Expanded Methods Section

Chemicals. Reagents for electrophoresis were obtained from Bio-Rad Laboratories (Mississauga, ON); [3H] ryanodine was obtained from PerkinElmer (Boston, MA); Monoclonal antibodies against RyR-CRC, DHPR, FKBP12, and calsequestrin were obtained from Affinity BioReagents (Golden, CO). Polyclonal antiphosphoserine-2809 RyR, antiphosphoserine-16 PLN, and antiphosphothreonine-17 PLN antibodies were obtained from Badrilla (Leeds, UK). Polyclonal antiphosphothreonine-286 CaM kinase II was purchased from Cell Signaling Technology (Danvers, MA). Anti-CaMK II polyclonal antibody was a generous gift from Dr. H. A. Singer (Weis Center for Research, Danville, PA). [32P] was purchased from Amersham (Oakville, ON), $^{45}CaCl_2$ was from New England Nuclear (Mississauga, ON). All other chemicals were purchased from Sigma Chemical (St. Louis, MO) or BDH Chemicals (Toronto, ON).

Preparation of SR Membranes and Muscle Homogenates. SR membrane vesicles were isolated from the myocardium of VPL and control rats according to the procedure described previously[1].Briefly, ventricular tissue was minced, and homogenized (Polytron, Brinkman Instruments, Westbury, NY, USA) with three 15-s bursts at 30-s intervals at a setting of 5.5 in 6 volumes (based on tissue weight) of ice-cold buffer (10 mmol/L NaHCO$_3$, pH=6.8). The homogenate was centrifuged at 1,000 g for 10 min at 4°C. The supernatant was decanted and kept on an ice slurry. The pellet was resuspended in 4 volumes of ice-cold buffer and centrifuged as described above. The supernatant was decanted and combined with the first supernatant, and the pellet was discarded. The combined supernatant was centrifuged at 8,000 g for 20 min at 4°C. The supernatant was collected, and the pellet was discarded. KCl was added to the supernatant (44 mg/ml, 0.6

mol/L final concentration), swirled until dissolved, left on ice for 25 min, and then centrifuged at 40,000 g for 1 h at 4°C. After isolation, the SR vesicles were suspended in 10 mmol/L Tris maleate (pH 6.8) containing 100 mmol/L KCl and stored at –80°C after quickly freezing in liquid nitrogen. Protein concentration was determined by the method of Lowry et al. [2] with bovine serum albumin used as the standard. The relative purity of myocardial SR vesicles from control and VPL rats did not differ as judged from essentially similar protein profiles revealed by SDS-PAGE. In addition to SR membranes, whole ventricular muscle homogenates from control and VPL rats were used in some experiments. For these experiments, the muscle tissue was homogenized (Polytron) with three 15-s bursts at 30-s intervals at a setting of 5.5 in 10 volumes (based on tissue weight) of buffer (10 mmol/L Tris HCl, 100 mmol/L KCl, pH 6.8). The homogenates were filtered through four layers of cheese cloth.

Immunoblotting. Western immunobloting techniques were used for detection and estimation of the relative amounts of RyR in SR membrane vesicles, and RyR, DHPR, FKBP12 in cardiac muscle homogenates from control and VPL rats. The SR vesicles (25 µg protein/lane) were first subjected to SDS-PAGE using 6% (for RyR), 10% (for DHPR, SERCA2, CaMKII), or 15% (for FKBP12, PLN) gels. The fractionated proteins were transblotted to nitrocellulose membranes. The membranes were probed with antibodies specific for cardiac RyR (monoclonal, dilution 1:2,500), DHPR α subunit (monoclonal, dilution 1:1,000), FKBP12 (polyclonal, 1µg/ml), calsequestrin (polyclonal, dilution 1:1000), SERCA2 (anti-87, polycolonal, dilution 1:1,000), δ-CaMKII (polyclonal, dilution 1:1000), phosphothreonine-286 CaMKII (polyclonal, dilution 1:2000),

phosphoserine-2809 RyR (polyclonal, dilution 1:5000), phosphoserine-16 PLN (polyclonal, dilution 1:5000), and phosphothreonine-17 PLN (polyclonal, dilution 1:5000).. A peroxidase-linked goat anti-rabbit IgG or goat anti-mouse IgG at a dilution of 1:5,000 was used as the secondary antibody. Protein bands were visualized using the enhanced chemiluminescence detection system (Amersham ECL[TM], Buckinghamshire, UK). The images of the protein bands were optimized, captured, and analyzed by a video documentation system (ImageMaster, Pharmacia Biotech, San Francisco, CA). The western blotting detection system was determined to be linear with respect to the amount of SR/homogenate protein in the range 10-40 µg using this camera-based densitometry system.

Measurement of High-Affinity [^{3}H] Ryanodine Binding. High-affinity ryanodine binding was assayed as described by Jiang et al.[3]. In brief, SR vesicles (25 µg) isolated from control and VPL rats were incubated at 37°C for 60 min in a buffered medium (total volume 100 µl) containing 150 mmol/L KCl, 200 mmol/L HEPES (adjusted to pH 7 with KOH), 1.25-80 nmol/L of [^{3}H]ryanodine, 0.1 mmol/L EGTA, and variable amounts of CaCl$_2$ to obtain free [Ca^{2+}] ranging from 0.05 to 6.1 µmol/L as calculated by the computer program of Fabiato [4]. The binding reaction was terminated by filtration through 0.22 µm GS Millipore filters and washed sequentially with 4 ml of washing buffer [150 mmol/L KCl, 200 mmol/L HEPES (adjusted to pH 7 with KOH)] and then twice with 4 ml each of ice-cold 10% ethanol. Specific binding of ryanodine was determined as the difference between total counts and nonspecific counts (measured in the presence of 10 µmol/L of unlabeled ryanodine).

Determination of Ca^{2+} uptake. SR membrane vesicles were isolated from control and VPL rats according to the procedure described previously [1]. Following isolation, the SR vesicles were suspended in 10 mM Tris-maleate (pH= 6.8) containing 100 mM KCl. Protein concentration was determined by the method of Lowry *et al.* [2] using bovine serum albumin as a standard. The relative purity of the SR vesicles from RV and LV myocardium of control and VPL-treated rats did not differ as judged from essentially similar protein profiles revealed by SDS-polyacrylamide gel electrophoresis (SDS-PAGE). ATP-dependent, oxalate-facilitated Ca^{2+} uptake by cardiac SR vesicles was determined using the Millipore filtration technique as described previously [5]. The standard incubation medium for Ca^{2+} uptake (total volume 250 µl) contained 50 mM Tris-maleate (pH 6.8), 5 mM MgCl$_2$, 5 mM NaN$_3$, 120 mM KCl, 0.1 mM EGTA, 5 mM potassium oxalate, 5 mM ATP and 0.1 mM ^{45}CaCl$_2$ (~8,000 cpm/nmol, 8.2 µM free Ca^{2+}), 0.025 mM ruthenium red and cardiac SR vesicles (7.5 µg protein). In experiments where Ca^{2+} concentration was varied, the EGTA concentration was held constant at 0.1 mM and the amount of total ^{45}CaCl$_2$ added was varied to yield the desired free Ca^{2+} according to the computer program of Fabiato [4]. The Ca^{2+}-uptake reaction was initiated by the addition of SR to the rest of the assay components, preincubated for 3 min at 37°C. The data on Ca^{2+} concentration-dependence of Ca^{2+} uptake were analyzed by nonlinear regression analysis (SigmaPlot) and fitted to the equation

$$v = V_{max}[Ca^{2+}]^n / (K^n_{0.5} + [Ca^{2+}]^n)$$

where v is the measured Ca^{2+} uptake activity at a given Ca^{2+} concentration, V_{max} the maximum activity, $K_{0.5}$ the Ca^{2+} concentration giving half V_{max}, and n is equivalent to the Hill coefficient.

To evaluate the effect of SR-associated, endogenous CaMKII on Ca^{2+} uptake, assays were performed in the absence of CaM and in the presence of 3 μM CaM. The Ca^{2+} uptake reaction was initiated by either the addition of SR or ATP to the rest of the assay components preincubated for 3 min at 37°C.

Cardiomyocyte Isolation. Myocytes from control and VPL rats were isolated as previously described [6]. Briefly, hearts were mounted on a Langendorff apparatus and perfused with Ca^{2+}-free Tyrode solution containing (in mmol/L) 120 NaCl, 5.4 KCl, 1 $MgCl_2$, 0.33 NaH_2PO_4, 10 HEPES, and 10 glucose at pH 7.4. After a brief equilibration period, 1.16 mg/ml type II collagenase (Worthington Biochemical, Lakewood, NJ) and 0.1 mg/ml protease type XIV were added to the buffer, and the heart was perfused for 10 min in a recirculating manner. Collagenase was washed out with buffer containing 0.2 mmol/L Ca^{2+}, and the left ventricle of the heart was anatomically separated and diced with scissors. After incubation at 37°C, tissues were filtered through a nylon mesh and allowed to settle. The cells were exposed to a series of sedimentation and resuspension steps in buffer containing increasing concentrations of Ca^{2+} (0.2–1.8 mmol/L). Cell yield was assessed microscopically, and the density was diluted to ~10^5 cells/ml; 50–60% of isolated cells were healthy and rod-shaped.

Imaging and Measurement of Ca^{2+} Sparks. A custom-built wide-field digital fluorescence imaging system (Photon Technology International Inc; PTI Inc, NJ, USA) with a Cascade Photometrics 650 cooled charge-coupled (CCD) camera (653 x 492 pixels; Roper Scientific Inc., Tucson, AZ) and ImageMaster Software (version 5; PTI

Inc., London, ON) was used to acquire images of isolated cardiomyocytes from control and VPL rats at 67 Hz (67frames/s). To optimize the speed of acquisition, the region acquired was limited to that surrounding only a single cell. With the X60 lens, each pixel represented an area of 196 x 196 nm. Cells were loaded with the Ca^{2+} indicator dye fluo-4-AM (5 µmol/L, with 0.05% pluronic acid) for 40 min at room temperature. Cells were then allowed to settle for 10 min on a 1 ml glass-bottomed perfusion chamber mounted on a Nikon inverted microscope (Nikon Eclipse TE2000-U) equipped with a plan apochromatic X60 water immersion lens (NA 1.2) and a blue excitation filter cube with an emission bandpass of 535 ± 40 nm. Cells were perfused with normal Tyrodes solution containing (in mmol/L) 1.8 $CaCl_2$, 120 NaCl, 5.4 KCl, 1 $MgCl_2$, 0.33 NaH_2PO_4, 10 HEPES, and 10 glucose at pH 7.4 at a rate of 1 to 3 ml per min. Then, cells were field-stimulated at 0.5 Hz via platinum electrodes until the Ca^{2+} transient reached a steady state. Subsequently, the stimulation was stopped to observe resting Ca^{2+} sparks and waves within ~23s. Excitation of fluo-4 was provided by the 488 nm line of a multi-line argon laser and cell exposure to the laser was controlled by a shutter. Image processing was performed off-line using ImageMaster 5. The acquired images were Gaussian filtered using three-by-three pixels and baseline Ca^{2+} images were subtracted pixel by pixel using the equation $\Delta F/Fo\ (\%) = 100x\ [F(x,y,t) - Fo(x,y)]/ Fo(x,y)$, where F(x,y,t) was the fluorescence at each pixel in the time series and Fo was an image of the "baseline" level given by the average of ~50 consecutive images of the cell at rest and in the absence of sparks. The change in fluorescence, $\Delta F/Fo\ (\%)$ is a relative measure of free intracellular Ca^{2+} concentration. To create the plots of $\Delta F/Fo$ with time, areas of interest of 10 x 10 pixels (3.6 μm^2) were located at the centre of each spark site. The size of the area of

interest was chosen since, on average, it surrounded the entire event at the time at which each spark event was initiated. The root mean square (rms) noise of the image was less than 2%, and an increase in fluorescence was considered to be Ca^{2+} spark when it was equal to or greater than 5% and lasted for at least 5 frames (79 ms), as described earlier [7]. The frequency of sparks was measured from the change in fluorescence ($\Delta F/Fo$ (%)) with time plots using the threshold detection routine in pClamp (version 9.0, Axon Instruments). Images immediately preceding the beginning of sparks were used as the baseline level, Fo. The beginning of the spark was identified as that image having a change in fluorescence > 5% above baseline.

Measurement of free intracellular Ca^{2+} concentration ($[Ca^{2+}]_i$). Isolated cardiomyocytes were loaded by incubation with 1 μM fura-2 acetoxymethyl ester for 30 min at 35°C and then allowed to settle onto a glass coverslip that comprised the bottom of a perfusion chamber (~0.75 ml vol). The chamber was mounted on a Nikon inverted microscope and continuously perfused with bathing solution at 2-3 ml/min at room temperature. Cells were considered viable if they demonstrated a characteristic rod shape without blebbing and contracted reversibly after electrical pacing with a pair of platinum electrodes. Cells were illuminated with alternating 345- and 380-nm light using a Deltascan system (Photon Technology International), with the 510-nm emission detected using a photometer, as previously described [8]. $[Ca^{2+}]_i$ was calibrated according to the methods of Grynkiewicz *et al* [9], with $[Ca^{2+}]_i = (K_d(R-R_{min})/(R_{max}-R)) Sf_2/Sb_2$, where R_{min} and R_{max} are the ratio of fluorescence intensity at 345/380, and R_{min} and R_{max} are the ratios with Ca^{2+}-free and saturated conditions, respectively. Sf_2/Sb_2 is the ratio of

fluorescence values for Ca^{2+}-free/Ca^{2+}-bound indicator measured at 380 nm. We used a dissociation constant (K_d) of 225 nM for binding of Ca^{2+} to fura-2 [9] and a viscosity factor of 0.6. Data were corrected for background fluorescence. The calculation of $[Ca^{2+}]_i$ involves a number of assumptions, and factors such as inhomogeneity of Ca^{2+} within cells introduce uncertainty in the values. However, the time-course of $[Ca^{2+}]_i$ transients is not influenced by the calibration.

To examine the frequency-dependent changes of twitch $[Ca^{2+}]_i$ transients, myocytes were stimulated at frequencies from 0.25 Hz to 2 Hz. The cell stimulation at any frequency lasted for 60 s was then stopped for 30 s before resumed to next higher frequency.

To study the time to restore the steady-state of twitch $[Ca^{2+}]_i$ transients following caffeine-induced depletion of SR Ca^{2+} store, myocytes were continuously stimulated at 0.5 Hz and 10 mM caffeine was applied for 30 s by pressure ejection from a micropipette (10 mm) when myocyte twitches had reached steady state.

The SR Ca^{2+} load in myocytes was assessed by rapid application of 10 mM caffeine to induce SR Ca^{2+} release. Cells were first stimulated at 0.25 Hz. When cell twitches stabilized, the stimulation stopped and 20 s later 10 mM caffeine was applied for 30 s.

Measurement of Contractile Performance of the Isolated Cardiomyocytes. Isolated cardiac myocytes from control and VPL rats were transferred to a continuously perfused glass-bottomed chamber mounted on a Nikon inverted microscope (Nikon Eclipse TE2000-U) equipped with a plan apochromatic X60 water immersion lens (NA 1.2). The

chamber was perfused with normal Tyrodes solution at 1 to 3 ml per min. Myocyte contraction was induced once per two second (0.5 Hz) by platinum field electrodes placed in the cell chamber. Bright field images of a single cell were continuously acquired at 67 frames/s with a Cascade Photometrics 650 CCD camera (653 x 492 pixels; Roper Scientific Inc., Tucson, Arizona, USA). Myocyte dimensions were calibrated with a hemocytometer grid placed on the microscope stage. Myocyte length was measured using ImageMaster Software (versions 5, PTI Inc.) Myocytes were selected for study according to the following criteria: a rod-shaped appearance with clear striations and no membrane blebs, no spontaneous contractions.

Langendorff heart perfusion for hemodynamic studies. Hearts were rapidly excised and rinsed in ice-cold normal Tyrodes solution. The aorta was then cannulated and connected with the Langendorff apparatus to start perfusion with normal Tyrodes solution at a constant flow rate of 10 ml min^{-1} at 35±1°C. A water-filled latex balloon, connected to a pressure transducer (COBE, Lakewood, CO, USA), was inserted through the mitral valve into the left ventricle to allow isovolumic contractions and to continuously record mechanical parameters. The balloon was progressively filled with water up to 80 μL to obtain an initial left ventricular end diastolic pressure of 5–8 mmHg [10]. The normal Tyrodes solution for perfusion consisted of s (in mM) 1.8 $CaCl_2$, 120 NaCl, 5.4 KCl, 1 $MgCl_2$, 0.33 NaH_2PO_4, 10 HEPES, and 10 glucose and was adjusted to pH 7.4 with NaOH and the solution was equilibrated at 37°C by 100% O_2. Haemodynamic parameters were assessed using a BioPAC M1000 data acquisition

system and analysed using AcqKnowledge® Ver.3.7 software (BioPAC Systems, Goleta, CA, USA).

Cardiac Electrophysiological Study of Isolated Hearts and Whole Animals. Rats from control and VPL groups were anesthetized with a mixture of Ketamine (70mg/kg) and Xylazine (3.5 mg/kg) and then had standard limb lead ECG recordings for a baseline observation of 10 minutes. Subsequently, the hearts were quickly removed, were mounted on a Langendorff apparatus and perfused at $35\pm1°C$ with normal Tyrodes buffer containing (in mmol/L) 1.8 $CaCl_2$, 120 NaCl, 5.4 KCl, 1 $MgCl_2$, 0.33 NaH_2PO_4, 10 HEPES, and 10 glucose at pH 7.4. Pair of electrodes were placed on the right atrial appendage and ventricular apex to record bipolar epicardial electrocardiograms. Next, the atrioventricular (AV) interval, sinus cycle length, sinus node recovery time (SNRT), SNRT corrected for spontaneous sinus cycle length (cSNRT), Wenckebach cycle length (WCL), and electrical stimulation threshold to induce ventricular arrhythmias were determined as described previously[11]. The AV interval was measured as the time from the last paced stimulus to the onset of the QRS complex. The SNRT was measured as the time from the last paced stimulus to the onset of the next spontaneous P wave. To control for differences in sinus rate, SNRT was normalized to resting heart rate by subtracting the sinus cycle length from the SNRT (cSNRT = SNRT – sinus cycle length). Sinus cycle length was determined from at least 60 consecutive cycles after the pacing period when normal sinus rhythm resumed. A 60-s period was allowed to elapse between each successive pacing bouts. The WCL was determined using 10 ms incremental decreases in atrial pacing cycle length. The WCL was defined as the minimum cycle length that

failed to conduct through the AV node as indicated by the absence of the QRS. Missed

ventricular contractions were detected by both the ECG and the arterial pressure

waveform. The electrical stimulation threshold to induce ventricular arrhythmias was

determined as previously described[11]. A Grass S88 stimulator (Grass Instrument Inc.,

Quincy, Mass) delivered trains of pulses through the ventricular stimulating electrodes

(50 Hz; 10 ms pulse duration). The intensity of the trains was increased in ~10 µA

increments every 10 s. The electrical stimulation threshold to induce ventricular

arrhythmias was determined as the minimum current that caused ventricular arrhythmias.

Ventricular arrhythmias were identified on the ECG as rapid, wide QRS complexes with

concomitant decreases in arterial pressure. Normal sinus rhythm appeared on termination

of the stimulation without the use of defibrillation shocks.

References:

1. Jones DL, Narayanan N. Defibrillation Depresses Heart Sarcoplasmic Reticulum Calcium Pump: A Mechanism of Postshock Dysfunction. *Am J Physiol*. 1998;274:H98-105

2. Lowry OH, Rosebrough NJ, Farr AL, Randall RJ. Protein Measurement with the Folin Phenol Reagent. *J Biol Chem*. 1951;193:265-275

3. Jiang M, Xu A, Tokmakejian S, Narayanan N. Thyroid Hormone-Induced Overexpression of Functional Ryanodine Receptors in the Rabbit Heart. *Am J Physiol Heart Circ Physiol*. 2000;278:H1429-1438

4. Fabiato A. Computer Programs for Calculating Total from Specified Free or Free from Specified Total Ionic Concentrations in Aqueous Solutions Containing Multiple Metals and Ligands. *Methods Enzymol*. 1988;157:378-417

5. Narayanan N. Effects of Adrenalectomy and in Vivo Administration of Dexamethasone on Atp-Dependent Calcium Accumulation by Sarcoplasmic Reticulum from Rat Heart. *J Mol Cell Cardiol*. 1983;15:7-15

6.   Ebihara Y, Karmazyn M. Inhibition of Beta- but Not Alpha 1-Mediated Adrenergic Responses in Isolated Hearts and Cardiomyocytes by Nitric Oxide and 8-Bromo Cyclic Gmp. *Cardiovasc Res*. 1996;32:622-629

7.   ZhuGe R, Sims SM, Tuft RA, Fogarty KE, Walsh JV, Jr. Ca^{2+} Sparks Activate K^+ and Cl^- Channels, Resulting in Spontaneous Transient Currents in Guinea-Pig Tracheal Myocytes. *J Physiol*. 1998;513 (Pt 3):711-718

8.   Sathish V, Xu A, Karmazyn M, Sims SM, Narayanan N. Mechanistic Basis of Differences in Ca^{2+}-Handling Properties of Sarcoplasmic Reticulum in Right and Left Ventricles of Normal Rat Myocardium. *Am J Physiol Heart Circ Physiol*. 2006;291:H88-96

9.   Grynkiewicz G, Poenie M, Tsien RY. A New Generation of Ca2+ Indicators with Greatly Improved Fluorescence Properties. *J Biol Chem*. 1985;260:3440-3450

10.   Cerra MC, De Iuri L, Angelone T, Corti A, Tota B. Recombinant N-Terminal Fragments of Chromogranin-a Modulate Cardiac Function of the Langendorff-Perfused Rat Heart. *Basic Res Cardiol*. 2006;101:43-52

11.   Rodenbaugh DW, Collins HL, Nowacek DG, DiCarlo SE. Increased Susceptibility to Ventricular Arrhythmias Is Associated with Changes in Ca^{2+} Regulatory Proteins in Paraplegic Rats. *Am J Physiol Heart Circ Physiol*. 2003;285:H2605-2613

APPENDIX C

Movie 1. Ca^{2+} sparks in myocyte isolated from control rat

Movie 1 is available online at the following webpage link.

http://ir.lib.uwo.ca/cgi/preview_article.cgi?article=1113&context=etd

Movie 1. **Ca^{2+} sparks in myocyte isolated from control rat.** Ventricular myocytes were isolated and with fluo-4 dye and monitored using a high-speed digital fluorescence imaging system. This movie was acquired at 67 frames per second and plays in real time. Cell was stimulated by field electrodes at 0.5 Hz, initiating global rise of Ca^{2+} accompanied by contraction. When Ca^{2+} transients reached a steady state, stimulation was stopped (only last three transients are illustrated). After several seconds delay some brief, highly localized Ca^{2+} sparks were evident in the myocyte and no Ca^{2+} waves were evident. The image is 127 x 24 µm.

APPENDIX D

Movie 2. Increased incidence of Ca^{2+} sparks in myocyte from verapamil-treated rat

Movie 2 is available online at the following webpage link.

http://ir.lib.uwo.ca/cgi/preview_article.cgi?article=1113&context=etd

Movie 2. **Increased incidence of Ca^{2+} sparks in myocyte from verapamil-treated rat.** Ventricular myocytes were isolated from rat chronically treated with verapamil, then loaded with fluo-4 dye and monitored using fluorescence imaging. This movie was acquired at 67 frames per second and plays in real time. Cell was stimulated by field electrodes at 0.5 Hz, initiating global rise of Ca^{2+} accompanied by contraction. When Ca^{2+} transients reached a steady state, stimulation was stopped (only last three transients are illustrated). Many Ca^{2+} spark sites were apparent, with frequent events, and the sparks were larger and of longer duration. In this cell a Ca^{2+} wave was also generated at the peak of Ca^{2+} spark activity. The image is 127 x 24 µm.

CURRICULUM VITAE

EDUCATION

Doctor of Philosophy, Physiology   2010

> The University of Western Ontario (UWO), London, Ontario, Canada

- Completed Ph.D. thesis: Cardiac Adaptation to Chronic Blockade of Voltage-gated, L-type calcium Channels in the Sarcolemma.

Bachelor of Medicine, Clinical Medicine   1999

> Tongji Medical College, Huazhong University of Science and Technology (HUST), Wuhan, China

- Achieved top 5% of the graduating class.

APPOINTMENTS

Junior Lecturer (faculty position)   1999 – 2004

> Department of Pharmacology, Tongji Medical College, HUST, China

- HUST was ranked 5th among China's top universities in 2004

  (http://www.chinadaily.com.cn/english/doc/2005-02/21/content_418027.htm).

- Completed a project titled "pharmacological and toxicological effects of Anthoplerin-Q on cardiovascular system" with a first-authored paper in a peer-viewed journal in English.

- Co-investigated and fulfilled a commercial contract of pre-clinical study of rhodiola rosea on fatigue & anoxia endurance in mice.

- Gained expertise in group randomization, cardiovascular pharmacodynamic studies, preparation of standard operating procedures (SOPs) of Good Laboratory Practice (GLP) etc.

- Ran a national conference with a net gain over the budget and expenses.

- Participated in the establishment of departmental Good Laboratory Practice laboratories(GLP); prepared GLP standard operating procedures (SOPs).

- Winner of a national competition and earned the honor as a representative of Chinese Young Pharmacologists to attend The XIVth World Congress of Pharmacology in USA, 2002.

TEACHING EXPERIENCE

Teaching Assistant in Physiology   2004 - 2009

   Schulich School of Medicine & Dentistry, UWO, London, Canada

- Taught physiology to medical science students.

- Earned George W. Stavraky Teaching Excellence Award, UWO, Canada, 2006.

Junior Lecturer in Pharmacology   1999 – 2004

   Tongji Medical College, HUST, Wuhan, China

- Effectively lectured pharmacology to medical students with average rating 4.6/5 over 4 years.

- Achieved a promotion to **course manager** of pharmacology in 2003.

- Redeveloped course Pharmacology for undergraduate program resulting in improved student performance, reduced teaching workload, and increased efficiency of using teaching resources.

CLINICAL EXPERIENCE

Residency in Respiratory Medicine   2001 - 2002

   Union Hospital, Tongji Medical College, HUST, China

- Effectively communicated with patients and earned trusts from the patients and colleagues.

Medical Internship   1997 - 1999

   Tongji Hospital, Tongji Medical College, HUST, China

- Completed clinical rotations with distinction in internal medicine, surgery, obstetrics and gynecology, pediatrics, geriatrics, psychiatry, ophthalmology, etc

GRANTS

Principal Investigator, Tongji Medical College Young Investigator Fund (¥10,000).2001-2002

Title of project:Effects of Anthoplerin-Q on cardiac electrophysiology and hypertrophy.

AWARDS AND HONORS

2008   **Student Travel Award,** Canadian Physiological Society

2007   **Best Graduate Student Poster Presentation in the Cardiovascular and Pulmonary Research,** 2nd Annual Research Day of Physiology & Pharmacology, UWO, Canada

2007   **Research Excellence Award,** 20th annual Western Research Forum, UWO, Canada

2006   **George W. Stavraky Teaching Award in Physiology,** UWO, Canada

2005   **Graduate Student Teaching Award** (Nominee), UWO, Canada

2004-2009   **Western Graduate Research Scholarship,** UWO, Canada

2003   **Teaching Excellence Award,** Tongji Medical College, HUST, China

2002   **Travel Award,** The XIVth World Congress of Pharmacology, San Francisco, USA

2002   **Research Excellency Award,** Chinese Pharmacological Society

1994-1999   **People's Scholarship for Medical Students,** Tongji Medical College, China

PUBLICATIONS

Zhou J, Xu A, Jiang M, Jones DL, Sims SM, Narayanan N. Chronic L-type calcium channel blockade with verapamil causes cardiac ryanodine receptor remodeling and predisposition to heart failure in the rat. *Circ. Res.* 2010 (submitted).

Zhou J, Xu A, Chakrabarti S, Jones DL, Sims SM, Narayanan N. Remodelling of cardiac sarcoplasmic reticulum calcium pump and diastolic dysfunction ensue chronic L-type calcium channel blockade in the rat. *Circ Heart Fail.* 2010 (to be submitted).

Zhou J, Xu A, Jones DL, Sims SM, Narayanan N. Impact of chronic L-type calcium channel blockade on phosporylation-dependent regulation of cardiac sarcoplasmic reticulum function in the Rat. *Circ Heart Fail.* 2010 (to be submitted).

Xu A, Jiang M, **Zhou J**, Jones DL, Sims SM, Narayanan N. Unique, novel and obligatory role of calmodulin in sarcoplasmic reticulum calcium pump function and cardiac muscle relaxation. *Nat. Cell Biol.* 2010 (submitted).

Zhou J, Xu A, Jones DL, Sims S, Narayanan N. Impaired expression and function of cardiac ryanodine receptors underlie predisposition to heart failure following long-term verapamil treatment. *Acta Physiol Sin.* 60 (suppl.1):65~66, 2008

Zhou J, Xu A, Sims S, Narayanan N. Depressed Ca^{2+} cycling by cardiac sarcoplasmic reticulum (SR) ensues chronic blockade of L-type Ca^{2+} channels. *J Mol Cell Cardiol.* 40:914, 2006

Zhou H, Wang F, Cheng L, Fu L, **Zhou J ,** Effects of tetrandrine on calcium and potassium currents in isolated rat hepatocytes. *World J Gastroenterol.* 9(1):134-136, 2003.

Wang F, Zhou H, Cheng L, Zhao G, **Zhou J,** Jiang M, Yao W. Effects of palmatine on potassium and calcium currents in isolated rat hepatocytes. *World J Gastroenterol.* 9(2):329-333, 2003.

Zhou J, Fu L, Xiang G, Jiang M, Yao W. Effects of Anthopleurin-Q on myocardial hypertrophy in rats and physiologic properties of isolated atria in guinea pigs. *Acta Pharmacol Sin.* 23:924-929, 2003.

Zhou J, Fu L, Jiang M, Yao W. Dose-dependent effects of Anthopleurin-Q on myocardial hypertrophy in rats and physiologic properties isolated atria in guinea pigs. *Pharmacologist.* 44 (suppl.1):A144~A145, 2002

Zhou J, Guo L. Chapter12, Section 10 and 11. In: Tutorials and Lab Experiments in Medical Science of Organism Function, edited by Hu H. Bejing: Science Publishing House, 2002. ISBN:7-03-010194-4/R.842

Zhou J. Chapter 21 Section1, 2, 4, 5. In: Practical Cardiovascular Receptorology, edited by Liu Z.   Beijing: Science Publishing House, 2001.ISBN:7-03-009284-8/R.687.

SCIENTIFIC CONFERENCE PRESENTATION

The Joint Conference of Physiological Sciences, Beijing, China, 2008

The International Society for Heart Research Meeting, Toronto, Canada, 2006

The XIVth World Congress of Pharmacology, San Francisco, USA, 2002

AFFILIATIONS

Canadian Physiological Society

American Heart Association

Chinese Pharmacological Society